2020-05-19

Quality of Experience Enhancement Architecture For Video Delivery On WiFi

Osunkunle, Isaac

UNIVERSITY OF CALGARY

Quality of Experience Enhancement Architecture For Video Delivery On WiFi

by

Isaac Osunkunle

A THESIS

SUBMITTED TO THE FACULTY OF GRADUATE STUDIES

IN PARTIAL FULFILLMENT OF THE REQUIREMENTS FOR THE

DEGREE OF DOCTOR OF PHILOSOPHY

GRADUATE PROGRAM IN ELECTRICAL AND COMPUTER ENGINEERING

CALGARY, ALBERTA

MAY, 2020

Abstract

WiFi has become a widely used medium for delivery of video content. At the same time, there is a proliferation of WiFi capable devices such as mobile phones and portable computers with the capability of consuming video content using WiFi as the access technology. Due to the proliferation of such devices, there is a probability of reduced video Quality of Experience (QoE) due to wireless channel impairments. Wireless channel impairments are a challenging problem for WiFi which uses the license free ISM band. Even though most devices using the WiFi frequencies will adhere to the Carrier Sense Multiple Access with Collision Avoidance (CSMA/CA) protocol, there are other devices which do not use this protocol and thus cause interference. Another issue that impairs the wireless channel is reduced Signal to Interference plus Noise Ratio (SINR) due to the access point (AP) to user equipment (UE) distance, or obstruction. Also, when the number of users in a radio range increase, there is an increased probability of collisions. These impairment mechanisms will consequently reduce the video QoE served to a user. The QoE is reduced because of the need for retransmissions, which reduces the channel throughput. Also, because of impairments, the modulation and coding scheme (MCS) selected by the rate adaptation algorithm for WiFi is restricted to combinations which are more robust against these impairments. To improve the QoE served to a user, this research pursues two main approaches: (1) Evaluate methods of estimating QoE for streaming video (2) Use a Rate Adaptation (RA) algorithm in conjunction with Application Layer Forward Error Correction (AL-FEC) to improve air efficiency. This research utilizes a mathematical model which considers the reduced video resolution during impairments, and effects of stalled video, on the QoE. To reduce the effects of retransmissions, and increase the air efficiency, this study investigates the use of Application Layer Forward Error Correction (AL-FEC), in coordination with Rate Adaptation. FEC schemes are investigated, and a theoretical and experimental evaluation of a AL-FEC scheme is validated, for each MCS selection. Further, a scheme is proposed whereby the

wireless channel is regarded as the lowest bandwidth of the path between the video source and consumer. The video source will signal to the WiFi AP for the desired MCS, based on the AL-FEC capabilities, and AL-FEC success rate at the user. The desired MCS is determined by the user and sent via a feedback channel to the video source. The rate adaptation algorithm is evaluated using a Markov model to estimate the gains achieved when using AL-FEC aware Rate Adaptation. Finally an end-to-end algorithm is proposed which selects the optimal AL-FEC scheme based on the current channel conditions. The QoE is compared for critical insight into the gains obtained when using the AL-FEC aware Rate Adaptation Algorithm, and AL-FEC, in order to improve the user Quality of Experience.

Acknowledgments

I would like to thank my supervisor, Prof. Abraham Fapojuwo for his invaluable guidance and support throughout the course of my research work. His patience and passion for my success has greatly assisted in the production of this research. Also, I will like to thank my supervisory committee, including Prof. Laleh Behjat, and Prof. John Nielsen, for the guidance related to my research work.

I am thankful to my wife for the support provided to me over the course of my study. I am very appreciative of her patience and sacrifices made over the years to ensure the success of my study. Thanks to my loving children as well who allowed their dad to study when they wanted to play. I will like to appreciate my manager at my place of work, for the support provided over the years. My research peers at the Wireless Networking Research Laboratory have been a part of this journey with interesting research discussions over the years. Thanks to Dr Ismail Kamal, Dr Kazi Ashrafuzzaman, Dr. Jaya Rao, Dr. Xiaobin Yang, Jonathan Kwan, Hai Wang, Okechukwu Ochia, Simon Windmuller, Akash Melethil and Dr. Fatemeh Ghods.

Finally, I thank everyone that has had an impact in my research directly or indirectly.

To my family

Table of Contents

[1] Sections 3.4 and 3.5 of this Chapter appear in a published conference paper - "Osunkunle I. Improving 802.11 video transport air efficiency with AL-FEC. In 2017 IEEE International Conference on Wireless for Space and Extreme Environments (WiSEE) 2017 Oct 10 (pp. 31-36). IEEE."

List of Figures and Illustrations

List of Tables

List of Symbols

τ ..... Probability that a station transmits in a WiFi slot time

$\bar{P}$ ..... Average Received Power

N_o ..... Noise Power Spectral Density in W/Hz

W ..... Channel Bandwidth

T_{SLOT} ..... Slot Time

T_{L-SIG} ..... Non-HT/legacy SIGNAL field duration

T_{SIFS} ..... Short inter-frame spacing duration

T_{DIFS} ..... Distributed Interframe spacing duration

m_{STBC} ..... Space time block code

N_{ES} ..... Number of encoded streams

T_{L_STF} ..... Non-HT/legacy short training sequence

T_{L_LTF} ..... Non-HT/legacy long training sequence

T_{SYM} ..... Regular GI symbol interval

$T_{LEG\_PREAMBLE}$ Legacy preamble duration

$T_{VHT\_PREAMBLE}$ Very High Throughput preamble duration

$T_{VHT-SIG-A}$ ... VHT SIGNAL A field duration

$T_{VHT-SIG-B}$ ... VHT SIGNAL B field duration

T_{VHT_STF} ..... Very High Throughput signal short training field duration

T_{VHT_LTF} ..... Very High Throughput signal short training field duration

T_{SYML} ..... Long GI symbol interval

T_{SYMS} ..... Short GI symbol interval

N_{SYM} ..... The number of symbols in the Data field

N_{VHTLTF} ..... The number of VHT-LTF symbols

$N_{SERVICE}$ ..... Number of bits in the SERVICE field

N_{Tail} ..... Number of tail bits per BCC encoder

N_{DBPS} ..... Number of data bits per symbol

R ..... Binary Convolutional Coding Rate

N_{BPSCS} ..... Number of coded bits per subcarrier per spatial stream

N_{SD} ..... Number of complex data numbers per frequency segment

N_{SP} ..... Number of pilot values per frequency segment

N_{CBPS} ..... Number of coded bits per symbol for user

N_{ES} ..... The number of BCC encoders

GI ..... Guard interval

List of Abbreviations

ACK ..... Acknowledgment

ACKTimeout Acknowledgment Time Out

AVC ..... Advanced Video Coding

AP ..... Access Point

ARQ ..... Auto Repeat Request

AWGN ..... Additive White Gaussian Noise

BER ..... Bit Error Rate

BPSK ..... Binary Phase Shift Keying

BSC ..... Binary Symmetric Channel

CBR ..... Constant Bit Rate

CCK ..... Complementary Code Keying

CRC ..... Cyclic Redundancy Check

CSMA/CA .. Carrier Sense Multiple Access With Collision Avoidance

CTS ..... Clear To Send

DASH ..... Dynamic Streaming Over Hypertext Transport Protocol

DCF ..... Distributed Coordination Function

DIFS ..... DCF Inter-frame Space

DIR ..... Diffuse Infrared

DSSS ..... Direct Sequence Spread Spectrum

FEC ..... Forward Error Correction

FER ..... Frame Error Rate

FHSS ..... Frequency Hopping Spread Spectrum

HSDPA ..... High Speed Downlink Packet Access

HDD ..... Hard Decision Decoding

MAC ..... Media Access Control

MIMO ..... Multiple-input Multiple-output

MPEG ..... Moving Picture Experts Group

MTU ..... Maximum Transmission Unit

NACK ..... Negative Acknowledgment

OSI ..... Open Systems Interconnection

OFDM ..... Orthogonal Frequency Division Multiplexing

PAM ..... Pulse Amplitude Modulation

PCF ..... Point Coordination Function

PEC ..... Packet Erasure Channel

PER ..... Packet Error Rate

PHY ..... Physical

PIFS ..... PCF Inter-frame Space

PLCP ..... Physical Layer Convergence Procedure

PSDU ..... Physical Layer Service Data Unit

QAM ..... Quadrature Amplitude Modulation

QoS ..... Quality Of Service

QoE ..... Quality of Experience

QPSK ..... Quadrature Phase Shift Keying

RSSI ..... Received Signal Strength Indicator

RTP ..... Real-time Transport Protocol

RTS ..... Request To Send

SDD ..... Soft Decision Decoding

SIFS ..... Short Inter-frame Space

SNR ..... Signal To Noise Ratio

SVC ..... Scalable video coded

TCP ..... Transmission Control Protocol

TDMA ..... Time Division Multiple Access

UDP ..... User Datagram Protocol

VoIP ..... Voice Over Internet Protocol

WLAN ..... Wireless Local Area Network

Chapter 1

Introduction

1.1 Context and Motivation

With advances in the compute capabilities of mobile devices [1], there has been an increase in Internet traffic from an insignificant percent, to currently more than half of all web delivery in the last 10 years. This trend is shown in Figure 1.1[1]. Mobile devices are much more conveniently operated while using a wireless connection. Thus the volume of traffic transferred over mobile devices have increased significantly, both using licensed and unlicensed spectra. Thus, the ever increasing demand for higher throughput on end user devices has driven improvements in the wireless technologies used for mobile service delivery. This research focuses on the Carrier Sense Multiple Access with Collision Avoidance (CSMA/CA) protocol, which operates in the license free industrial scientific, and medical (ISM) frequency bands. Of the traffic types consumed by mobile devices, video traffic is often the traffic type with the highest bandwidth requirements. Video delivery requires a high bandwidth because of the volume of information in a single screen, which changes at the refresh rate of the video recorder. Early research on the human visual capacities, and technical limitations led to a decision to utilize 60 Hz as the refresh rate with the National Television System Committee (NTSC) standard, and 24Hz for film reproduction.

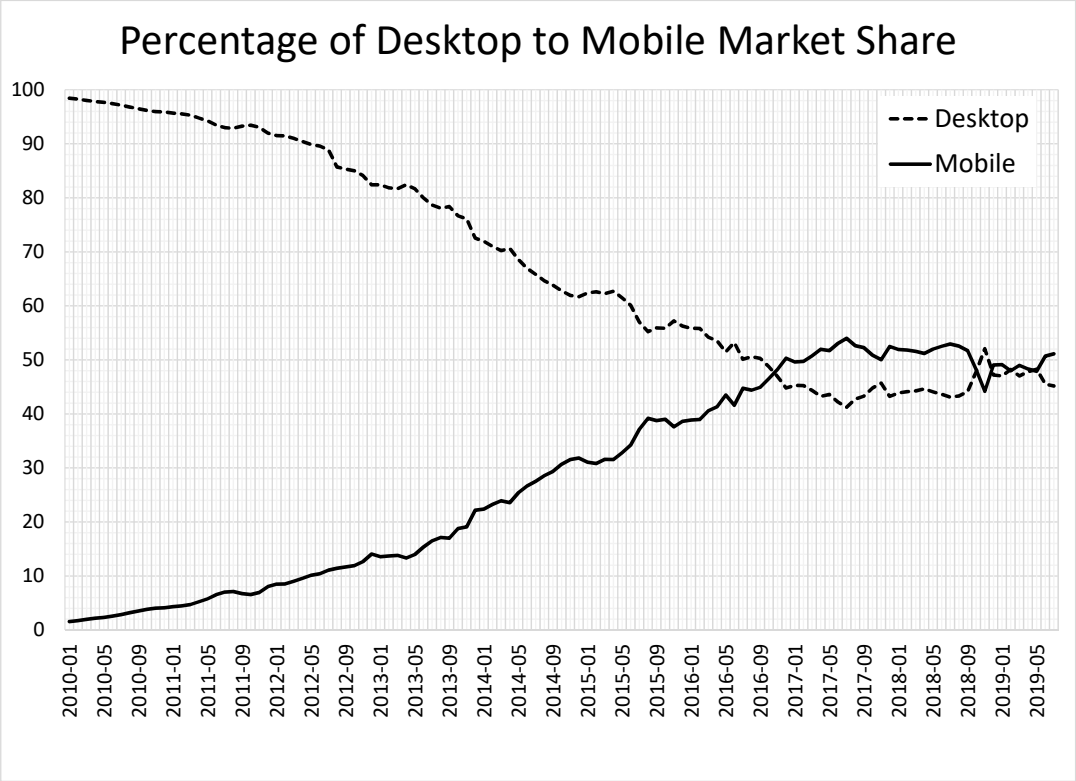

Figure 1.1: Percentage of Desktop Compare to Mobile Internet Traffic

To reduce the bandwidth usage, video streams are compressed for example using the H.264 or H.265 standards [2][3]. These compression standards utilize multiple techniques to reduce the data rate from for example 3 Gbps to 8 Mbps.

The encoding process used by H.264/Advanced Video Coding (AVC) and is shown in Figure 1.2. The encoder begins by splitting the image into macroblocks, to which a discrete cosine transform (DCT) is applied. DCT coefficients are then quantized. Other steps in the H.264/AVC standard include inter-frame prediction and entropy coding.

The output of the H.264/AVC compression is a much lower bit rate, however, the compressed bit stream is very sensitive to packet errors. Thus a reliable protocol must be used to transport H.264/AVC.

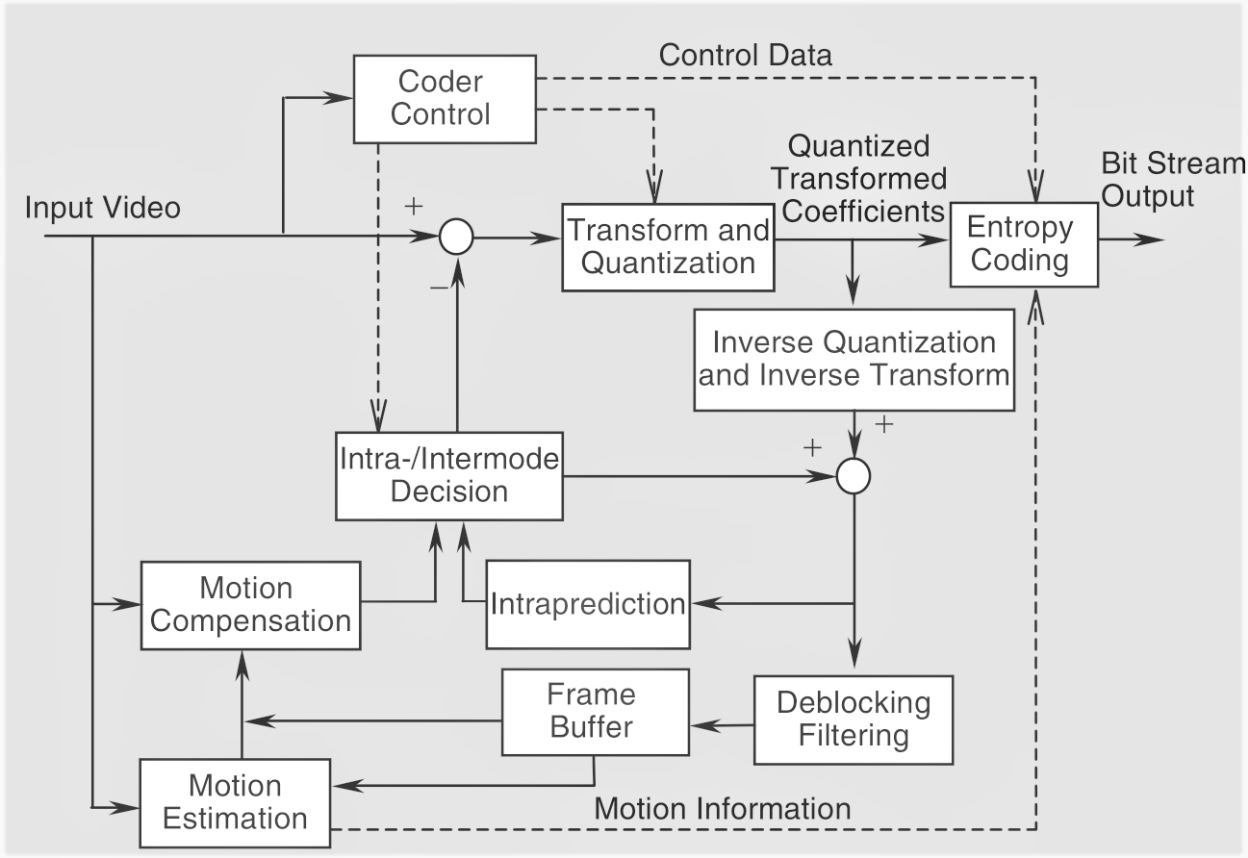

Figure 1.2: H.264/AVC block diagram [4]

H.264/AVC compression rates and complexity are specified with profiles such as Constrained Baseline Profile, Baseline Profile, Main Profile, High Profile and so on. Another parameter that determines the quality of H.264/AVC bit-stream is the level specification which can range from "1" - for a video resolution of 128x96 pixels at 30.9 frames per second (FPS) to "6.2" with a resolution of 8192x4320 pixels at 120.9 frames per second.

When the compression is increased, there is a perceptual loss in video quality as observed by the user. This loss in compression, and other artifacts that occur during playback, are not pleasurable to the user, thus to quantify this loss, the Quality of Experience (QoE) measure has been defined. To deliver a satisfactory Quality of Experience, it is of importance to use the highest quality video profile and level for the bit stream delivery.

Transport protocols have evolved in recent times to reliably handle video delivery. Initially, video on demand was a mechanism that downloaded the complete video resources in the form of files before playing. However, video streaming, which downloads sections of the video, begins playing while continuing to download, is the dominant method of video delivery currently. Also, video resources are often transported over the Hypertext Transfer Protocol (HTTP), with video delivery protocols such as Dynamic Streaming over HTTP (DASH). Streaming over HTTP has become the dominant method for video delivery over the Internet. This is because streaming over HTTP does not require any special hardware or software for the infrastructure. A standard HTTP web server is used to deliver the files, which will have been encoded and segmented onto storage. An index file and play list will be sent to the video playing device, and the streaming protocol then requests the file it requires dynamically during the video play out.

Mobile wireless device throughput has also increased with advances in radio access technologies. Thus a mobile device in modern times will have multiple wireless radios, for example radios for (a) WiFi (IEEE 802.11), (b) Long Term Evolution (LTE), (c) Bluetooth, and (d) Near Field communications. Users normally have to pay for wireless service over LTE, while WiFi access is usually free. However, WiFi radio range is in tens of meters, while

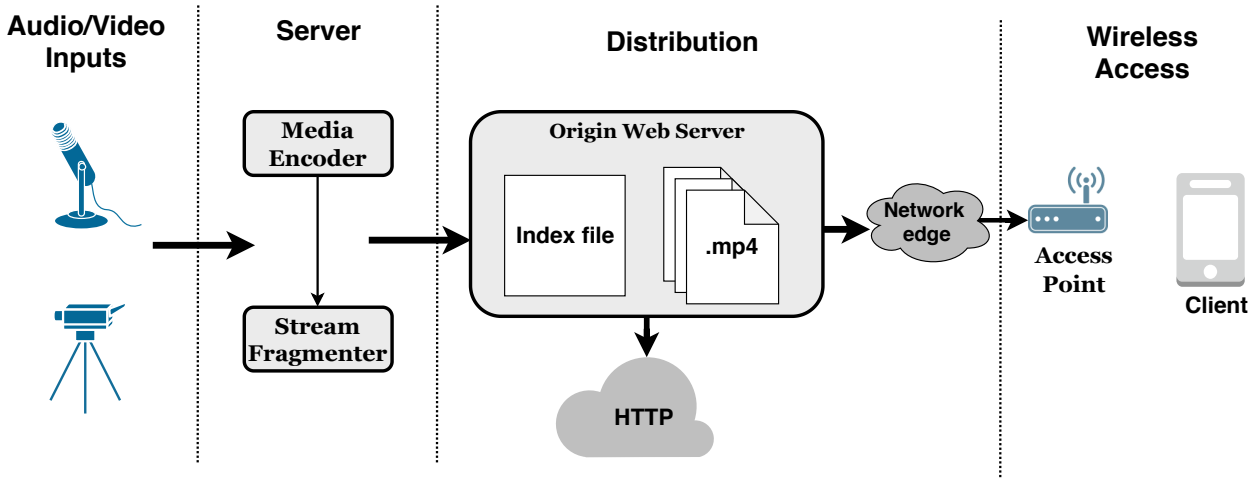

Figure 1.3: Streaming Architecture with HTTP Transport[5]

the LTE range will be hundreds of meters. After crossing the wireless interface, the back haul connection to the Internet from a user device is usually a wired connection from a user's home device – such as a cable modem, or a LTE backhaul fiber connection.

The wireless interface is usually the lowest capacity portion in the end to end video delivery architecture. This wireless channel is dynamic, with a possibility for large changes in effective throughput. Thus multiple dynamic events occur when the throughput is restricted due to channel impairments. These events include rate adaptation changes, and video stream quality changes. The video stream being delivered may also experience a stall.

1.2 Problem Statement

This thesis focuses on the problem of changing and unpredictable QoE delivered to a video user under dynamic wireless channel conditions, using the IEEE 802.11 standard.

Even though the IEEE802.11 standard uses the ISM band, which does not guarantee packet delivery due to the possibility of interference, there is a possibility to increase the probability of a better QoE delivered to clients.

As shown in Figure 1.3, the client-server architecture[5] passes over the Internet, with the last hop being the wireless channel. This wireless channel is often the lowest capacity in

the network link between the client and server. Impairments are caused by multiple reasons, such as lower SINR with increasing distance, multi-path fading, frame collisions, interference sources which do not perform carrier sense before transmission, or sources which transmit continuously. Also, the probability of a collision increases as the number of clients increase, and also, when conditions for the hidden node, and exposed node problems occur in WiFi.

This thesis considers a feedback architecture, whereby the user can signal to the video source, for the ability to support more efficient MCS combination from the last hop. A control algorithm is required for the overall functionality, whereby the MCS selection is optimized based on channel conditions and AL-FEC capability of the video consuming device.

This thesis considers a model for the QoE estimation which works with two parameters (1) The frequency of video stalling, and (2) The resolution of the video stream.

1.3 Objectives

The objectives of this thesis are as follows:

1. Improve QoE served to subscribers on WiFi, with minimal changes to the link layer.
2. Provide a robust dynamic QoE estimate when users are consuming video services over HTTP streaming protocols.
3. Leverage hardware capabilities of end user to perform objectives (1) and (2).

1.4 Contributions

This thesis develops a QoE estimation model based on the frequency of video stalling, and the resolution of video frames. This QoE estimation model is used to evaluate the end-to-end performance of the video streaming architecture. To improve the QoE, the following research activities have been contributed:

- Proposed AL-FEC mechanism for QoE improvement modeled as a concatenated FEC system (Chapter 3, Section 3.3.3).
- Analytical expression for frame error probability with AL-FEC - Packet error probability after AL-FEC is an important indicator for the QoE served to the subscriber (Chapter 4).
- AL-FEC aware Rate Adaptation Algorithm - A mathematical Markov based model is investigated for improving the Rate Adaptation, depending on the capability of the end user (Chapter 4, Section 4.7).
- AL-FEC enabled video streaming architecture (Chapter 5, Section 5.3).
- Analytical expression for QoE - This analytical expression is used to estimate the QoE based on the received video quality and the number of stalled frames (Chapter 5).

1.5 Thesis Outline

This thesis is organized into six chapters. Chapter 2 reviews previous approaches to improving QoE for wireless users. Chapter 3 outlines the AL-FEC approach proposed for the QoE improvement mechanism, and also presenting initial results of AL-FEC on a unidirectional WiFi channel. The mechanism for controlling the WiFi rate adaptation using the AL-FEC enabled architecture is presented in Chapter 4. A method of measuring QoE is presented in Chapter 5. Also, the research results of QoE improvement is shown in Chapter 5. The thesis conclusion is in Chapter 6, with statements on research findings, the research significance, limitations and suggestions for further research.

Chapter 2

Literature Review

Ever since digital video was introduced, a high Quality of Experience for video delivery has been an important requirement. Thus over the years, there have been increasing improvements in video compression techniques and standards such as the H.264 and H.265 video compression techniques. These compression techniques have been increasing delivered video quality, while at the same time reducing the required data rate. An additional challenge exists when the subscribers devices are wireless. This is because the error rate on wireless channels are orders of magnitude higher than on wired connections. Wired losses are mostly due to congestion, while wireless losses are due to channel impairments such as interference, path loss, shadow fading, Rician and Rayleigh fading. The IEEE functional requirements for IEEE802.3 requires an error rate for Ethernet as 1×10^{-8} [6] per octet of MPDU length, while for wireless IEEE802.11 standards require a rate adaptation change when the error rate exceeds 10% [7].

2.1 Approaches to QoE Improvement

To mitigate the reduction of QoE when using the wireless channel as the delivery method, multiple approaches have been applied. These can be classified into: (1) Human Visual Approach - which includes Video Error Concealment[8][9][10][11], Video Codec Optimization

and Video Bit Rate Reduction; and (2) Wireless channel approach - which includes (a) Video Cross-Layer Optimization[12] [13] and (b) Video Forward Error Correction.

2.1.1 Video Error Concealment

Video Error Concealment[8][9][10][11], is an approach to QoE improvement, which utilizes information in-between video frames, to conceal errors in which are in some frames.

2.1.2 Video Codec Optimization

Video Codec Optimization is an approach by which options in the video codec used for delivery are adjusted to deliver an optimum QoE under the current wireless channel conditions. This is primarily driven by standards such as the H.264 and H.264 [2][3].

2.1.3 Video Bit Rate Reduction

The Motion Pictures Experts Group (MPEG), have been introducing codec standards regularly over recent years, such as the H.264 and H.265 standards. These codec standards build upon state-of-the art research regarding the video codec with the ability to reduce video bit rate, while at the same time increase the video quality.

2.1.4 Forward Error Correction

QoE improvements can be achieved by applying Forward Error correction (FEC) to video packets before delivery. Protocols such as FECFRAME [14] have been proposed. The FEC algorithm used can be rate-less codes such as Fountain Codes and Raptor Codes, or block codes such as Reed-Solomon codes, Low Density Parity Check Codes (LDPC) and so on.

2.1.5 Video Cross-Layer optimization

Video Cross-Layer optimization [12] [13], is an approach to QoE improvement, whereby all the protocol layers are jointly optimized for video QoE delivery.

This thesis is based on the wireless channel approach. This is because the proposed QoE improvement, is achieved using a combination of the wireless channel Modulation and Coding Scheme(MCS) selection for the PHY rate, and a Forward Error Correction (FEC) code. Initially, the application layer PHY rate selection inspects the current data link layer PHY rate selection. The data link layer rate selection is driven by the data link rate adaptation algorithm such as Auto Rate Fallback (ARF). Using the current PHY rate, the AL-FEC rate algorithm determines if a PHY rate, which has a more complex modulation scheme and thus a higher throughput, and error rate which exceeds the required 10% by the IEEE802.11 standard, can be supported with AL-FEC. Thus the AL-FEC will recover from the additional errors which will ensure the residual error rate is less than 10%. Thus, the goal of this approach is to work in conjunction with the data link rate adaptation algorithm.

The QoE architecture and algorithm proposed has minimal requirements on the existing WiFi MAC protocol. This thesis work begins by investigating the end-to-end video delivery path. The main QoE improvement mechanism is the joint AL-FEC and rate adaptation selection.

Related methods which have been proposed for cross layer QoE improvement include approaches using cross layer video transmission rate control over LTE networks [15], whereby parameters including video sending rate, quantization parameter, and MCS are reduced based on the channel conditions, however, FEC is not considered as a mechanism to improve QoE. Another approach using Systematic Raptor and Rate-compatible punctured convolutional (RCPC) Codes was proposed by [16], whereby unequal error protection (UEP) is applied to video packets traversing the wireless network, however [16] does not consider controlling modifying the wireless rate adaptation process. Another research approach utilized

rate distortion [17] as a QoE optimization criteria, and thereby presented a quantization distortion model.

This research work improves related works in the following areas:

1. Improve QoE with minimal changes to state-of-the-art video streaming architectures such as HTTP live stream

2. Opportunistically select a higher MCS in order to improve wireless throughput

3. Recover from packet errors using AL-FEC, without disrupting other application behavior on the user's device - this is possible because the MCS is selected per packet. Thus the application serving video on the user's device is the only one which will receive AL-FEC encoded packets. Other applications, which are not AL-FEC enabled, can continue to operate as designed.

4. Leverage TCP reliability as a mechanism for packet re-transmits

5. Utilize parameters obtained from the link layer rate adaptation algorithm as input to the AL-FEC rate selection process.

Another important research area is the development of robust methods estimating the QoE have been proposed.

This research work first considers the wireless channel in WiFi networks as a superchannel[18]. A superchannel is the aggregation of a wireless channel and FEC code into a single unit. This approach was proposed by Forney [18] in the use of code concatenation. The motivation for the superchannel designation is the mandatory FEC usage with the IEEE 802.11 WiFi specification[19]. Whereby Convolutional code or LDPC must be used by the PHY layer. Expected residual error rates on the PHY are estimated based on the binary convolutional code. Next, AL-FEC is applied to the superchannel, which is considered as a component of the concatenated FEC system, and the residual error evaluated based on the performance of the AL-FEC code.

2.2 WiFi PHY and MAC Efficiency

Shannon's limit for the Additive White Gaussian Noise(AWGN) channel capacity is given by $C = B \cdot log_2\left(1 + \frac{S}{N}\right)$, where C is the capacity, B is the bandwidth, signal power is denoted by S, noise power represented by N, and $\frac{S}{N}$ represents signal to noise ratio gives the theoretical capacity for WiFi channels. However, due to licensing and government regulations, the channel is band limited. Also the power used by WiFi is limited. Thus, in the presence of AWGN the capacity can be written as [20]:

$$C_{AWGN} = B \cdot log_2\left(1 + \frac{P}{N_o B}\right) [bits/s] \tag{2.1}$$

where

- description $\frac{P}{N_o B}$ is the received signal to noise ratio
- N_o is the noise power spectral density
- P is the average received power
- B is the signal bandwidth

Using Orthogonal Frequency Division Multiplexing (OFDM), and modulation methods such as 256QAM in WiFi and Long Term Evolution (LTE), the throughput on the wireless channel can approach the channel capacity [21].

However, because of the overhead of the CSMA protocol, the entire throughput of the channel is not available for subscribers. Thus to estimate the real user throughput on the wireless channel, we can use the MAC efficiency [22]

$$\eta_{MAC} = \frac{MTP}{R_{DATA}} \tag{2.2}$$

Where MTP is the maximum throughput, and R_{DATA} is the PHY rate.

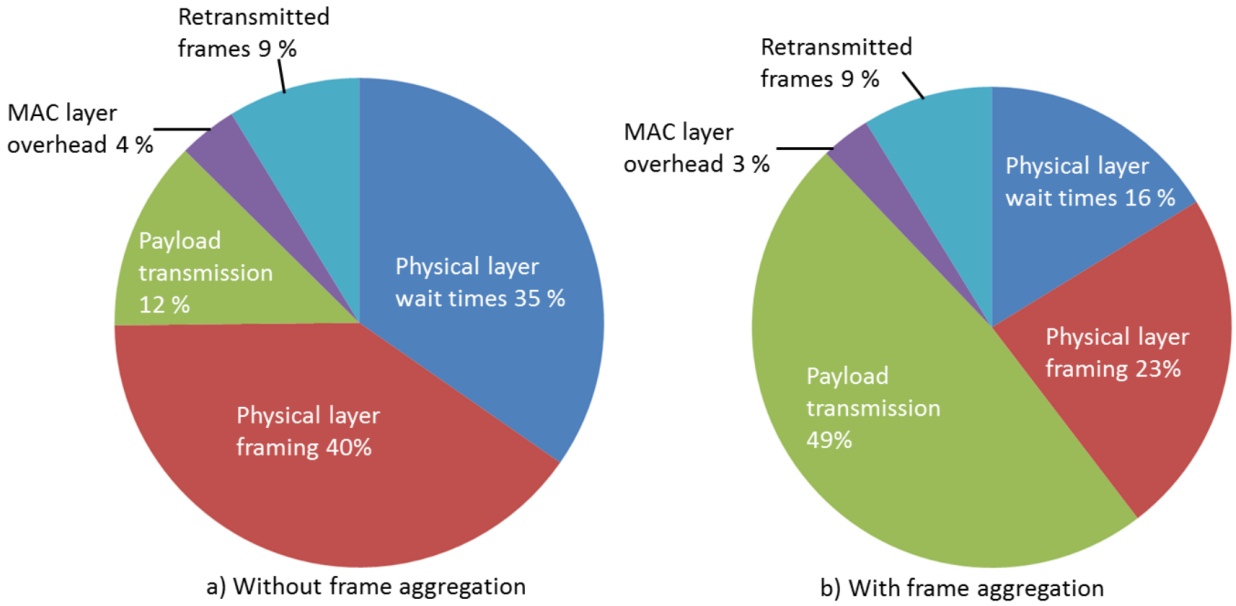

Figure 2.1: MAC efficiency for WiFi [23]

As an example, the MAC efficiency for WiFi can be as low as 12% without frame aggregation, while increasing to 49% with frame aggregation[23]. This is illustrated in Figure 2.1, which shows 9% of frame retransmissions due to packet errors, packet losses, or interference. Packet losses cause the CSMA protocol to go into a back-off state, where every station waits for its backoff period, before retransmission. The air time utilization can be obtained from the IEEE802.11ac-2013 standard Amendment 4 which specifies the transmit time $TXTIME$ to be [24]:

$$\begin{aligned} TXTIME = {} & T_{LEG\_PREAMBLE} + T_{L-SIG} + T_{VHT-SIG-A} + T_{VHT\_PREAMBLE} \\ & + T_{VHT-SIG-B} + T_{SYML} + \left\lceil \frac{T_{SYMS} \times N_{SYM}}{T_{SYML}} \right\rceil \end{aligned} \tag{2.3}$$

$$T_{LEG\_PREAMBLE} = T_{L\_STF} + T_{L\_LTF} \tag{2.4}$$

$$T_{VHT\_PREAMBLE} = T_{VHT\_STF} + N_{VHTLTF} \times T_{VHT\_LTF} \tag{2.5}$$

$$N_{SYM} = m_{STBC} \times \left\lceil \frac{8 \times DATA\_LENGTH + N_{SERVICE} + N_{tail} \times N_{ES}}{m_{STBC} \times N_{DBPS}} \right\rceil \tag{2.6}$$

The description and values of the parameters in the equations above are in Table 2.1

The parameters used for this example are shown in Table 2.2, and were selected based on the IEEE802.11ac-2013 standard - shown in Table 2.3

$$
\begin{aligned}
N_{SYM} &= 1 \times \left\lceil \frac{8 \times 1034 + 16 + 6 \times 1}{1 \times 1080} \right\rceil \\
&= 8 \\
TXTIME &= 8\mu s + 8\mu s + 4\mu s + 8\mu s + 4\mu s + 2 \times 4\mu s + 4\mu s + 4\mu s \times \left\lceil \frac{3.6\mu s \times 8}{4\mu s} \right\rceil \\
&= 76\mu s
\end{aligned}
$$

Table 2.1: IEEE 802.11n and 802.11ac parameters

Symbol	**Description**	**802.11n**	**802.11ac**
T_{SLOT}	Slot Time	$9\mu s$	$9\mu s$
T_{L-SIG}	Non-HT/legacy SIGNAL field duration	$4\mu s$	$4\mu s$
T_{SIFS}	Short inter-frame spacing duration	$16\mu s$	$16\mu s$
T_{DIFS}	Distributed Inter-frame spacing duration	$34\mu s$	$34\mu s$
m_{STBC}	Space time block code	1	1
N_{ES}	Number of encoded streams	1	1-2
T_{L_STF}	Non-HT/legacy short training sequence	$8\mu s$	$8\mu s$
T_{L_LTF}	Non-HT/legacy long training sequence	$8\mu s$	$8\mu s$
T_{SYM}	Regular GI symbol interval	$4\mu s$	$4\mu s$
$T_{LEG\_PREAMBLE}$	Legacy preamble duration	$8\mu s$	$8\mu s$
$T_{VHT\_PREAMBLE}$	Very High Throughput preamble duration	$1\mu s$	$1\mu s$
$T_{VHT-SIG-A}$	VHT SIGNAL A field duration	$8\mu s$	$8\mu s$
$T_{VHT-SIG-B}$	VHT SIGNAL B field duration	$8\mu s$	$8\mu s$
T_{VHT_STF}	Very High Throughput signal short training field duration	-	$4\mu s$
T_{VHT_LTF}	Very High Throughput signal short training field duration	-	$4\mu s$
T_{SYMS}	Short GI symbol interval	-	-
N_{SYM}	The number of symbols in the Data field	-	-
N_{VHTLTF}	The number of VHT-LTF symbols	-	-
$DATA\_LENGTH$	Length of payload in bytes	-	-
$N_{SERVICE}$	Number of bits in the SERVICE field	-	-
N_{Tail}	Number of tail bits per BCC encoder	-	-
N_{DBPS}	Number of data bits per symbol	-	-

Table 2.2: Selected VHT parameters

Parameter	**Value**
Modulation	64QAM
Code Rate	5/6
Bandwidth	40MHz
Spatial Streams	2
Data Bits Per Symbol	1080
Data Length	1034 bytes

Table 2.3: IEEE 802.11 VHT Parameters 40MHz Bandwidth[24]

VHT-MCS Index	**Modulation**	***R***	N_{BPSCS}	N_{SD}	N_{SP}	N_{CBPS}	N_{DBPS}	N_{ES}	**Data rate (Mb/s)**	
									800 ns GI	**400 ns GI**
0	BPSK	1/2	1	108	6	216	108	1	27.0	30.0
1	QPSK	1/2	2	108	6	432	216	1	54.0	60.0
2	QPSK	3/4	2	108	6	432	324	1	81.0	90.0
3	16-QAM	1/2	4	108	6	864	432	1	108.0	120.0
4	16-QAM	3/4	4	108	6	864	648	1	162.0	180.0
5	64-QAM	2/3	6	108	6	1296	864	1	216.0	240.0
6	64-QAM	3/4	6	108	6	1296	972	1	243.0	270.0
7	64-QAM	5/6	6	108	6	1296	1080	1	270.0	300.0
8	256-QAM	3/4	8	108	6	1728	1296	1	324.0	360.0
9	256-QAM	5/6	8	108	6	1728	1440	1	360.0	400.0

2.3 Adopted Mathematical Tools

Markov modeling enables tractable mathematical analysis of the dynamic behavior of the carrier sense multiple access with collision avoidance (CSMA/CA)[25][26], used by WiFi devices. Alternative models that can be considered for CSMA/CA performance include (1)

Gibbs Fields [27][28], (2) Constrained Random Walks[29], (3) Self Avoiding Walks [30][31], and (4) Levy Processes [32]. However, Markov Modeling provides an estimate of the throughput with good accuracy. Thus it is the most widely adopted method.

The model proposed by Bianchi [25] makes an assumption that the probability p of a packet collision, is independent of the state of the station. The model considers a number n of stations in the WiFi service area. These stations are assumed to be in saturation mode, thus each has a packet ready for transmission. Each station is defined to be in a back off stage $s(t)$ at time t. Using the one-step transition probabilities, and also the fact that a transmission occurs when the back-off time counter is equal to zero, the probability that a station transmits τ is derived[25].

$$\tau = \sum_{i=0}^{m} b_{i,0} = \frac{b_{0,0}}{1-p} = \frac{2(1-2p)}{(1-2p)(W+1) + pW(1-(2p)^m)} \tag{2.7}$$

where

- m is the maximum back-off stage
- $i \in (0, m)$ is the back-off stage
- W is the minimum contention window size
- $W_i = 2^i W$ is the contention window size at backoff stage i
- $b_{i,k} = \lim_{t\to\infty} P\{s(t) = i, b(t) = k\}, \quad i \in (0, m), k \in (0, W_i - 1)$ is the stationary distribution of the Markov chain.
- p is the probability of a packet collision
- W is the contention window size

The probability of a packet collision is also derived as the probability of at least one of the

$n-1$ stations transmits. This is given by

$$p = 1 - (1 - \tau)^{n-1} \tag{2.8}$$

The values of τ and p are determine by numerical methods. Subsequently the throughput S of the channel is determined as a ratio of the expected value of the time for a successful transmission to the total time of a renewal interval:

$$S = \frac{E\left[\text{time used for successful transmission in an interval}\right]}{E\left[\text{length of renewal interval}\right]} \tag{2.9}$$

The Bianchi model determines the throughput for a single MCS value. In this research work, another Markov model is used to determine the current MCS used by a subscriber. The Markov model for Rate Adaptation analysis proposed by Choi *et al.* [33] is used to model the behavior of the Auto Rate Fallback (ARF) rate adapation algorithm. This is shown in Chapter 4.

The Ebbinghaus forgetting curve is utilized for estimating the QoE in Chapter 5. This is similar to the approach by Zhengfang *et al.* [34].

2.4 Quality of Experience (QoE) of Delivered Video

Video Quality of Experience is a measure of satisfaction of a subscriber when viewing the video content. The International Telecommunication Union (ITU) has published a standards regarding QoE as the recommendation ITU-T G.1080 [35], with a focus on IPTV.

To evaluate the QoE of a delivered video, two approaches are usually considered: (1) Objective QoE measurement, and (2) Subjective QoE measurement [36].

Because QoE is the perception of the user, QoE may be influenced by user expectations and context. Thus QoE is always subjective depending on the user's personality. Because of the subjectivity of QoE, group data is used to determine the QoE. With the group data,

a baseline is can be determined. This baseline from subjective measurements can be used to create a relationship between network parameters and the QoE. Thus subsequent QoE measurements - which are referred to as Objective QoE - can be obtained using network parameters, which depend on the previous mapping from subjective measurements.

The ITU has classified factors which contribute to QoE as shown in Figure 2.2. The factors can be classified into two main parts: (1) Human components, and (2) Network Quality of Service components.

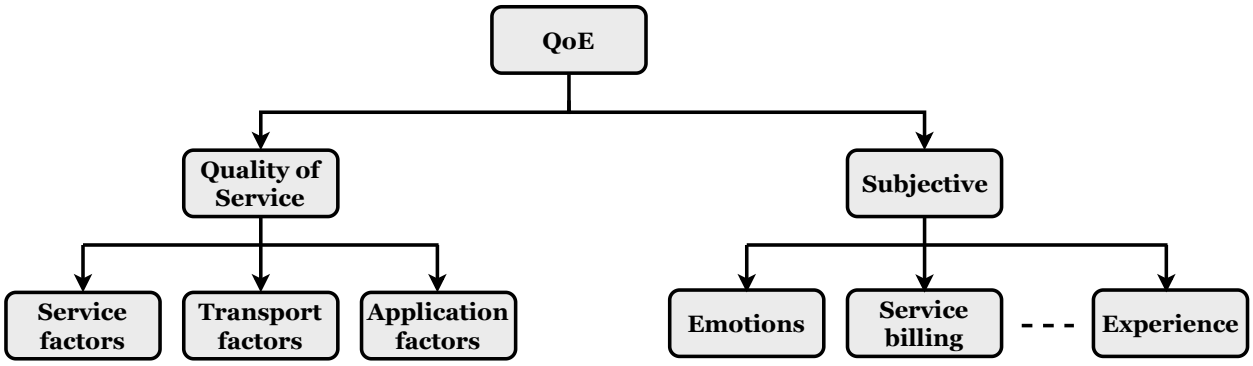

Figure 2.2: ITU-T G.1080 QoE reference [35]

2.4.1 Subjective QoE Measurement

The subjective method, which is performed by humans is an expensive method of QoE estimation. Recommended procedures for Subjective QoE measurement can be found in ITU recommendation ITU-R BT.500-11 [36]. There are two classes of subjective assessment in general: (1) Quality assessment, and (2) Impairment assessment. Subjective quality assessments are performed under optimum conditions, while impairment assessments are performed after the video has passed through a transmission channel, which may have added imperfections to the video. To perform subjective assessments, tests are recommended by the ITU [36]. The recommendations include the test environment such as home and laboratory tests, and other factors such as the size of screen, brightness, room illumination and so on.

2.4.2 Objective QoE Measurement

Objective QoE measurements are determined by models defined in terms of network QoS parameters. Network QoS parameters [37][38] which are of interest include:

- **Packet loss**: Packet loss can occur due to imperfections in the medium or channel between the source and recipient of the packet. Packet loss can also occur due to network congestion on network elements, malfunctioning equipment, or wrongly provisioned equipment. When packet loss is experienced, the packets must be recovered, if protected by error correction methods, or re-transmitted. For basic video calling at 1080p, a packet loss of 5% has been reported as the basic minimum acceptable[37][38].

- **Jitter**: Jitter is the uneven and untimely delivery of packets to a destination. Thus packets may arrive too late for presentation, or too many packets appear suddenly, which could cause congestion at the destination. These variations in packet delivery will be experienced as variations in round trip time (RTT). To combat the effects of jitter, playback buffers are utilized in streaming video applications. The effect of the playback buffer is to smooth out the packet delivery to the application on the user device. Thus packets that arrive too early are placed in the buffer. Also, when packets do not arrive on time, those stored in the playback buffer can be presented.

- **Throughput**: Throughput is the measure of packets delivered per time interval, usually measured in bits per second (bps). Higher definition video requires a higher throughput. For example the ITU H.264 specification [39] states the maximum bit rate for 480p video is 1.2Mbps, while the maximum bitrate for 1080p video is 8.16 Mbps. This is because higher definition video contains a higher density of picture information. Throughput is usually measured in two directions: (1) Upload throughput is the speed of packets sent to a server by a consumer, and (2) Download throughput is the speed at which packets are being sent from a server to a consumer.

- **Latency**: Latency is the amount of time elapsed from when a packet leaves a source, until it gets to its destination. Latency includes the time to transfer a packet between network interface buffers, propagation time over media such as fibre optic and the wireless medium, time to re-transmit packets which fail error checks, and the time to decode packets.

Typical values of these network parameters are shown in Table 2.4

Table 2.4: Network parameters for video streaming applications[37]

QoE Parameter	Excellent Quality	Basic Quality
Download throughput	4Mbps	512Kbps
Upload throughput	2Mbps	128Kbps
Latency	50ms	100ms
Jitter	20ms	50ms
Packet Loss	0%	5%

Objective methods which closely track the estimated subjective evaluations have been developed [40]. Network parameters are often used to determine the QoE [40].

2.5 Concatenated FEC System

In order to conform to the IEEE802.11 specifications, whereby a link level FEC is mandated, the overall FEC is modeled as a concatenated FEC system [18][41].

A concatenated FEC system consists of multiple FEC encoding blocks in sequence. Thus the output of the first FEC block is fed to a subsequent FEC block. To decode a concatenated FEC system, the data stream is passed into a series of FEC decode blocks.

The concatenated FEC system provides a tractable mathematical approach to determine the performance of the AL-FEC system. Previous works which have considered AL-FEC as a concatenated FEC system include [42] which considers Fountain codes as the AL-FEC. [42] considers only multicast packets, however, because streaming video protocols are unicast

based on the HTTP protocol, such a system as in [42] will not be directly adaptable for supporting video streaming. [42] also does not consider a mechanism for the subscriber to signal to the server the MCS it desires. Another approach by [43] combines error and erasure correction coding to optimize wireless system performance, however, the study does not consider the IEEE802.11 standard, nor does it consider the rate adaptation process for WiFi. This thesis fills the afore-mentioned gaps.

2.6 AL-FEC

Application Layer Forward Error (AL-FEC), is the mechanism whereby a FEC code is added to packets at the application layer. Historically, FEC has been added only to the link layer. This link layer FEC is normally implemented in hardware, with a very low latency for FEC decode. With the improvements in general purpose CPU capabilities, it has become feasible to add another layer of FEC to the data packets. Video streaming protocols such as Dynamic Streaming over HTTP (DASH), use a playback buffer which can be about 10 seconds or larger depending on the DASH algorithm operation [44]. Thus, when using AL-FEC, the error correction algorithm has less stringent conditions, which is to repair packets with error in an interval of seconds. Comparing to link layer FEC, the acknowledgment time out (ACKTimeout) is in the order of micro seconds [7].

$$ACKTimeout = SIFS + ACK\ Transmission\ Duration + SlotTime \tag{2.10}$$

When a maximum distance separable (MDS) AL-FEC code is unable to recover a packet, a mechanism is required to perform the automatic repeat request (ARQ). Otherwise, if a Fountain Code such as Raptor code is used, then the user must wait until enough packets have been received, which can be used to correct the errors.

This thesis has focused on Reed-Solomon Codes as the AL-FEC layer. These and other codes have been proposed in the FECFRAME standard [14]. Reed-Solomon (RS) codes

were selected, because of the lack of error floor property of RS codes. The error floor is a performance limit of error correcting codes, which are based on sparse graphs. FEC codes with error floors include LDPC, Fountain codes, Turbo codes and Polar codes[45][46].

Previously, Reed-Solomon codes were only used to correct up to $t/2$ symbol errors, where $t = \lfloor \frac{n-k}{2} \rfloor$, and n is the codeword size, and k is the message size. Algorithms for decoding Reed-Solomon codes include the Berlekam-Massey algorithm which is of polynomial time complexity $O(n^3)$. However more recently, other methods have been shown to perform better than the Berlekam-Massey algorithm [47]. For example, using the Guruswami-Sudan list decoding algorithm, with a polynomial time complexity of $O(n^2m^4)$, the error correction performance improves and becomes $t_{GS} = n-1-\lfloor\sqrt{(k-1)n)}\rfloor$ where m is the interpolation multiplicity[48][47].

2.7 WiFi Rate Adaptation

A rate adaptation algorithm design is generally in two classes: (i) Loss-triggered, and (ii) SNR triggered[49]. Loss-triggered algorithms select the MCS based on a threshold count of sequential failure or transmission success. SNR triggered algorithms base the MCS selection on a model of the wireless channel error estimate determined by the current SNR. Vutukuru *et al.* [50] proposed a Cross-Layer Wireless Bit Rate Adaptation referred to as 'SoftRate', which provided throughput gains of up to two times over SampleRate and Robust Rate Adaptation Algorithm (RRAA) [51] , by using SoftPHY hints from the physical layer. Wong *et al.* [51] proposed a robust rate adaptation algorithm (RRAA) which uses short-term loss ratio to control the rate adaptation algorithm. RRAA was shown to outperform Auto Rate Fallback (ARF), Adaptive Auto Rate Fallback (AARF) and Sample rate with possible improvements of up to 143%.

There are multiple WiFi Rate Adaptation algorithms in use, these include:

1. **SoftRate**[50]: SoftRate is a rate adaptation algorithm with the goal of maximizing throughput, while responding to rapidly changing channel conditions. SoftRate imports into the control algorithm, confidence information estimated from the PHY. This confidence information is used to determine the rate selection. SoftRate detects abrupt changes in BER estimates, and classifies these as interference. Thus SoftRate maintains the sending rate for interference conditions and only reduces the rate when channel impairments caused by other factors such as fading or signal attenuation are responsible. SoftRate is a loss-triggered algorithm.

2. **Robust Rate Adaptation Algorithm (RRAA)**: [51] RRAA attempts to maximize wireless throughput by considering conditions such as fading, mobility, and hidden terminals. A hidden terminal is one which is within radio range of two other users, while these users are out of radio range with each other. RAA uses short-term loss ratio to determine its rate selections. RRAA also uses an adaptive Request To Send (RTS) filter to prevent collision losses from triggering a rate decrease. RRAA is a loss-triggered algorithm.

3. **Auto Rate Fallback** (ARF)[52]: This algorithm attempts to achieve the maximum throughput on the WiFi channel. The ARF algorithm modifies the transmit MCS based on the success of packet transmissions. If two consecutive ACK frames are not received correctly, a timer is started and, the second retransmission will be sent at a lower MCS. After 10 successful ACKs have been received, or the timer expires, a probe frame is sent at the next higher rate. If no ACK is received at the higher rate, the next transmit rate is lowered, and the timer is restarted to count down. This thesis research utilizes the ARF as a model for AL-FEC performance. ARF is a loss-triggered rate adaptation algorithm.

4. **Adaptive Auto Rate Fallback (AARF)**: AARF is a throughput optimization algorithm which improves ARF for low latency systems. AARF provides short-term

and long-term adaptation. AARF is a loss-triggered rate adaptation algorithm.

5. **MiSer**[53]: The MiSer rate adaptation algorithm attempts to minimize the local power consumption, not the throughput. MiSer adapts both the transmission rate and power. A lookup table, which contains transmission rate and power pairs, is created from a specific wireless channel. During operation of the device, table lookups are used to determine the optimum rate and power. MiSer is a SNR triggered rate adaptation algorithm.

6. **SampleRate**[54]: The SampleRate algorithm maximizes wireless throughput. Most packets are sent at the bit rates with the highest throughput. SoftRate periodically sends probe packets at other bit rates in order to update the MCS selection table. SoftRate will switch to a another bit rate if it determines the new bit rate has a better throughput than the current value. If SampleRate experiences several successive losses at a certain MCS, it stops probing that bit rate. SampleRate is a loss-triggered rate adaptation algorithm.

7. **Minstrel-Piano**[55]: The Minstrel-Piano rate control algorithm attempts to obtain the maximum throughput on the WiFi channel. A multi-rate-retry chain (MRR) is utilized by Minstrel-Piano. The MRR keeps track of each packet to be sent. There are four different rates in the MRR. For every failed packet transmission, the packet is retried with the next lesser MCS parameter. The MRR MCS values are labeled as (a) Best Throughput, (b) Next best throughput, (c) Best probability of success, and (d) lowest base rate . This MRR chain is updated every 100ms. An Exponential Weighted Moving Average (EWMA) is used to determine the values of the probabilities of each MCS combination. From these probabilities, the MRR MCS combinations are set. To determine the EWMA for each MCS, Minstrel-Piano sends probe packets. The probe packets ensure that each MCS is regularly tested for probability of success. Minstrel-Piano is a loss-triggered rate adaptation algorithm.

2.8 Related Works

Related works include a study of AL-FEC for mobile streaming over LTE by Bouras *et al.*[56]. Bouras *et al.* [56] consider using AL-FEC to protect LTE services sent over Multimedia Broadcast/Multicast Services (MBMS), whereby the same data is sent to multiple users in a geographical area. Bouras *et al.* [56] investigate the benefits of AL-FEC, which is realized using Raptor Codes[57] - for a smooth video streaming experience, with a result showing increases in user satisfaction when the AL-FEC overhead is increased. Wu *et al.* [58] investigated source FEC coding for cloud gaming video. Wu *et al.* [58] developed and analyzed a framework which approximates the loss rate, and controls the FEC coding adaptation. Wu *et al.* [58] show that measurable gains can be achieved when source-FEC coding is applied.

Irrespective of the AL-FEC code used, there can be improvements in the video delivery capability. However, Fornet [18] has suggested using a non-binary outer-code in a concatenated FEC system. Reed-Solomon codes are non-binary codes which are used in this study.

2.9 Proposed Research in the Context of Current State of the Art

There have been multiple approaches used by researchers to improve the QoE of video delivery over the wireless channel. These works include Fan*et al.* [59], where a cross layer scheme based on a Lyapunov optimization framework for H.264/AVC was proposed. [59] focuses on the state of frame buffers at the destination nodes for scheduling packet transmissions in wireless ad-hoc networks. The QoE improvement is achieved by routing and network scheduling of video packets according to the status of frame buffers at the users. Another approach by Ullah *et al.* [60] focuses on cache management and the use of H.264

Scalable Video Codec (SVC). A cooperative interest forwarding and cache decision policy are then executed with a goal to minimize the average delay, and also maximize the cache hit rate. Thakolsri *et al.* [61] proposes a QoE driven cross layer optimization which jointly optimizes the application layer and wireless protocol stack by allocating network resources, and the rate adaptation, in order to minimize temporal video quality fluctuation. Shehada *et al.*[62] proposed a cross-layer optimization framework, which jointly optimizes the application and lower layers of the A greedy algorithm with target of mean utility is used to optimize network resources. A QoE driven cross-layer optimization for High Speed Downlink Packet Access(HSDPA) is evaluated by [63] whereby an algorithm is presented to optimize the delivered QoE for wireless HSDPA subscribers, and [63] compares multiple adaptation algorithm targets such as maximum rate, or maximum Mean Opinion Score (MOS). A scalable video coding (SVC) based streaming scheme with dynamic adaptation with scheduling is proposed by [64] with a result of 13% video quality gain observed for wireless Long Term Evolution (LTE) users.

2.9.1 Present Thesis Compared to the Related Works on Video QoE Estimation

Multiple works to establish Quality of Experience for video have created well known quality assessment algorithms such as Structural Similarity (SSIM), Multiscale Structural Similarity (MSSIM)[65], Peak Signal to Noise Ratio (PSNR), Mean Squared Error (MSE) and so on[66][67]. The popular video delivery frameworks such as HTTP live stream, utilize TCP as a transport protocol. Thus the frame quality of the transported video will be the same as that of the source. However, multiple resolution video streams, will have on average the same QoE parameter difference between the higher and lower resolution streams. Thus a single integer can be used to represent the quality degradation between video streams. This is the proposed method used in this thesis. This QoE evaluation method is objective. In addition, video stall frequencies and initial buffering are dependent on packet loss. Evaluating QoE

Table 2.5: Comparison of similar research works for Video QoE improvement

	Optimization Parameter	**Method**	**Model**	**QoE Evaluation Tools**	**Video delivery method**	**RAN Technology**
This research	Packet failure probability	AL-FEC + RA	Markov	Ebbinghaus	TCP	IEEE802.11
Shu Fan [59]	Video frame delay	Schedule Video Packet according to state of frame buffer	Lyapunov optimization framework	PSNR	Not specific	IEEE802.11
Thakolsri [61]	Minimize temporal fluctuation of video Quality	PHY rate adaptation, video rate adaptation	Utility function	VSSIM	Not specific	HSPA
Shehada [62]	Maximize perceived quality	QoE optimization framework for LTE resource allocation	Objective function	MOS	Not specific	LTE
Thakolsri [63]	Downlink resource optimization	HSDPA link adaptation	Cross layer parameter exchange	MOS	Not specific	HSDPA
Radhakrishnan [64]	Improve video quality	Dynamic adaptaiton of H.264 Scalable Video Codec	CQI feedbacks	PSNR	RTP	LTE
Ullah [60]	Base layer caching of scalable video code	cache management	cooperative Interest forwarding scheme	Average delay	Not specific	LTE

based on the video stalling has been investigated by Mok *et al.* [40]. The stall frequency is also modeled by Duanmu *et al.* [34], which proposes the previous frame quality as the present frame quality during a stall. Duanmu *et al.* [34] also propose using the Ebbinghaus forgetting curve to model the memory of a video stall by a consumer. The results show a good fit to the subjective evaluation methods.

Chapter 3

Application Layer Forward Error Correction

3.1 Introduction [1]

Historically, Forward Error Correction (FEC) has been applied at the link layer of the Open Systems Interconnection (OSI) model [68]. However, with the continual improvement of general purpose processors, and the introduction of specialized computing hardware such as graphics processing units (GPU), it has become of interest to apply FEC at the application layer. Thus Application Layer Forward Error Correction (AL-FEC), is the mechanism by which additional FEC is introduced and managed at the application layer. Compared to Link layer FEC, AL-FEC provides increased flexibility for the packet delivery architecture regarding FEC algorithms. This is because link layer FEC is usually standardized into a set of possible combinations, in order to ensure compatibility between different manufacturer hardware implementation. AL-FEC can be modeled as a system with another layer of FEC. Thus the overall FEC rate will be the product of AL-FEC and link-layer FEC rates [41].

[1] Sections 3.4 and 3.5 of this Chapter appear in a published conference paper - "Osunkunle I. Improving 802.11 video transport air efficiency with AL-FEC. In 2017 IEEE International Conference on Wireless for Space and Extreme Environments (WiSEE) 2017 Oct 10 (pp. 31-36). IEEE."

Table 3.1: Standard OSI and Proposed AL-FEC layers

Standard OSI Model	**Protocol Data Unit**	**Error protection mechanism**	**AL-FEC Network Model**	**AL-FEC Error protection mechanism**
Application	Data	None	Application	Specific to FEC method (Syndrome for Reed-Solomon)
Presentation	Data	None		
Session	Data	None		
Transport	Segment	Checksum		
Network	Packet	Header Checksum	Network	Header Checksum
Data Link	Frame	FCS	Data Link	FCS
Physical	Symbol/Bit	None	Physical	None

The FEC scheme at the application layer can be optimized for the current application, depending on requirements such as the decoding delay, and acceptable loss. Table 3.1 shows the proposed AL-FEC position on the OSI model, and the error protection mechanism used by AL-FEC and standard application Link layer FEC.

In general, AL-FEC will have a higher latency for packet processing. This is because the packet has to traverse higher into the operating system network model. Also, applications such as video streaming utilize a play back buffer, which affords AL-FEC schemes a possibility to perform advanced error recovery while the buffer occupancy is above a specified threshold. There will be moments where the error rate is low, requiring minimal AL-FEC processing. Low error rate moments can have the play out buffer fill up faster than real time. When the error rate is high, AL-FEC is able to restore packets, even though recovery may be slightly less than real-time.

3.2 Application Layer Forward Error Correction (AL-FEC) Cost

Performing AL-FEC requires the use of computing resources on the host device. In this research, the computing resources are regarded as infinite. This is because of the wide variety of possible AL-FEC hardware and algorithms which are available. For example, some clients and servers in specific scenarios may have dedicated hardware for the AL-FEC decode.

3.3 Forward Error Correction

When transmitting digital signals between two different entities, assurances must be made that the information sent from the source is the same as that received. Thus error checking algorithms must be used to validate received information. The Frame Check Sequence (FCS) is used in IEEE 802.11 to validate received frames. This FCS is implemented as a 32 bit Cyclic Redundancy Check (CRC)[7]. If it is determined that the received information is corrupt, the receiver needs to signal the sender to re-transmit the information. Because re-transmissions can be expensive in terms of air resource efficiency, another option is to add redundant information into the packet sent. By utilizing the redundant information, the recipient is able to detect and correct some or all of the errors in the packets received. This is termed as forward error correction (FEC). Adding redundant FEC information requires an increase in bandwidth, thus for bandwidth limited systems, a decision must be made on the FEC gain compared to the extra bandwidth usage, otherwise the transmission time will be longer due to the additional bits of information. FEC is widely used in digital systems, for example reading the contents of a storage device, FEC schemes may be used to recover corruptions. To ensure data integrity in wired and wireless digital systems FEC is normally a standard component of the architecture. FEC codes generate parity information

which transmitted in sequence to the message stream for Systematic Codes. There are two general classes of FEC codes: (1) Block codes, and (2) Convolutional codes. A block code encoder generates parity by performing a mathematical operation on individual data blocks, with no interdependence between each data block[41]. Convolutional codes generate parity information using a sliding window over the data stream. A boolean polynomial function accepts input from multiple positions of the data stream, and generates an output which is transmitted in sequence to the output data stream.

3.3.1 Block Encoder

A block encoder accepts a message which is binary k-tuple $\mathbf{u} = (u_0, u_1, \cdots, u_{k-1})$, with 2^k different messages possible, and outputs codeword, which is an n-tuple $\mathbf{v} = (v_0, v_1, \cdots .v_{n-1})$. There are also 2^k possible codewords, and the code rate, which represents the FEC overhead is $R = \frac{k}{n}$, where $k < n$, and the extra bits $n - k$ are referred to as the parity bits, which have a mathematical relationship to the k message bits.

3.3.2 Convolutional Encoder

A convolutional encoder output is dependent on the previous m message blocks, and the current block $\mathbf{u}$ of size k bits. m is the memory order. The output code sequence $\mathbf{v}$ is of size n bits. The code rate is the ratio $R = \frac{k}{n}$.

The choice of FEC method selected is related to system requirements such as the cost and latency. The IEEE 802.11-2012 specification requires devices to support Convolutional codes and optionally, Low Density Parity Check (LDPC). LDPC codes are block codes, which are based on sparse bipartite graphs. The code rate for each modulation scheme is also specified. FEC codes at the application and link layers can be concatenated, and the application layer FEC can be visualized as a upper level combination. More than one error correction mechanism can be used in series with a communications link, this is termed

concatenated FEC. The concatenated FEC scheme used in this research is shown in Figure 3.1.

To approach channel capacity, a non-binary FEC code is required to be the outer coder [18]. Reed-Solomon error correction code was used for investigating AL-FEC performance in this research work, as this is a well understood non-binary FEC code.

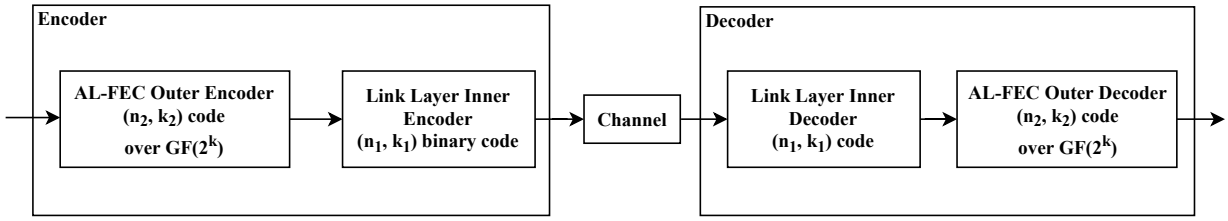

Figure 3.1: Concatenated FEC

3.3.3 Concatenated FEC System

Concatenated FEC was proposed by Forney[18], who showed that concatenation of an arbitrarily large number of codes can yield a probability of error, which decreases exponentially with the overall block length, and decoding complexity increases only algebraically. This is because when using the concatenated FEC system, the inner coder operates only on n_1 sized segments, while the outer coder operates on n_2 sized blocks as shown in Figure 3.1. The overall system can be represented as a system with $(2^{n_2})^{n_1}$ code words [18]. If we assume RS codes are used as inner and outer codes, we have two stages of decode complexity with a total complexity of $O(2n^3)$. If $n = n_1 = n_2$, then without concatenation, the decode complexity will be $O(n^6)$.

The IEEE802.11 standard requires that either convolutional code, or optionally LDPC to protect the wireless link. Also, this research work uses using a Reed-Solomon code to protect the packets, before sending to the convolutional encoder. Thus the overall system FEC blocks can be modeled as a concatenated FEC system.

When two codes are concatenated, the outer code can be designed to greatly reduce the probability of error P_e. If we consider the inner code and channel combination as a reduced

error binary symmetric channel (BSC), then P_e after the outer code is given by [69]

$$P_e \approx N_e(4p)^{\lceil \frac{d_{free}}{2} \rceil} \tag{3.1}$$

where

- P_e is the average probability of error for a vector channel with Additive White Gaussian Noise (AWGN)
- N_e is the average number of neighbors for a signal constellation
- p is the BSC cross over probability
- d_{free} is the free distance of the convolutional inner code

3.3.4 Reed Solomon Error Correction

3.3.4.1 Initial Approach to Reed Solomon Error Correction

An error correction code **E**, now commonly referred to as Reed-Solomon codes, described by Reed and Solomon[70] has been applied to wireless packets in order to obtain air efficiency gains. Reed-Solomon codes are polynomial codes, which operate on finite fields, also known as Galois fields GF. The common representation of a Galois field indicates how many elements it contains. Thus a 2^k element GF is denoted as $GF(2^k)$ where k is the number of binary bits in a message.

Reed-Solomon codes expands the size of the data payload by adding redundant parity bits. Thus introducing redundancy in the data stream. Bandwidth to accommodate this expansion in data size can be obtained by stepping up to the next modulation and coding scheme (MCS) in WiFi. If K is a field of degree n, over the field of two elements Z_2, and K has two distinct digits per element, where n is the total number of digits per element, then K contains 2^n elements. The code E maps m-tuples of K into 2^n-tuples of K. The

multiplicative group of field K is cyclic and is generated by powers of α, and α is the root of a suitable irreducible polynomial over Z_2.

Thus if we denote the field as $K = Z_2(\alpha)$, which is the vector space over Z_2, and we select an irreducible polynomial with root α, the basis of K contains n elements as follows: $1, \alpha, \alpha^2, \cdots, \alpha^{n-1}$. The nonzero elements of K form a multiplicative group, and the elements of K can be represented by[70]

$$0, \beta, \beta^2, \cdots + \beta^{2n-2}, \beta^{2n-1} = 1$$

where β is a generator of a multiplicative cyclic group. Reed-Solomon translates a message with m elements into the expanded and protected form with 2^n elements by evaluating a polynomial

$$P(x) = a_0 + a_1 x + a_2 x^2 + \cdots + a_{m-1} x^{m-1}$$

at each value of its generator multiple β for each message element. Thus the translation is
$(a_0, a_1, \cdots, a_{m-2}, a_{m-1}) \rightarrow$
$(P(0), P(\beta), P(\beta)^2, \cdots, P(\beta)^{2n-2}, P(1))$

After receiving the message

$$P(0), P(\beta), P(\beta)^2, \cdots, P(\beta)^{2n-2}, P(1)$$

it may be decoded by solving simultaneously any m of the 2^n equations. This is because any set of m are linearly independent. Expanding the message received -

$$P(0) = a_0$$

$$P(\beta) = a_0 + a_1 \beta + \cdots + a_{m-1} \beta^{m-1}$$

$$P(\beta^2) = a_0 + a_1 \beta^2 + \cdots + a_{m-1} \beta^{2m-2}$$

$$\vdots$$

$$P(1) = a_0 + a_1 + a_2 + \cdots + a_{m-1}$$

The linear dependence of any m subset of these n can be inferred because the coefficient determinant of any such subset, for example $P(\alpha), \cdots, P(\alpha_m)$ is a Vandermonde determinant whose value is not zero.

$$\begin{vmatrix} 1 & \alpha_1 & \alpha_1^2 \\ 1 & \alpha_2 & \\ 1 & \alpha_3 & \\ \cdots & \cdots & \cdots \\ 1 & \alpha_3 & \end{vmatrix}$$

$$\det = \pi_{j<i}(\alpha_i + \alpha_j) \neq 0$$

If reception is error free, then with the received values of $P(\cdot)$ multiple determinations of the sent message (a_0, $\cdots$, a_{m-1}) can be obtained. The number of these determination is $\binom{2^n}{m}$. If there are any errors in the received packets, the determinations of the values of $(a_0, \cdots, a_{m-1})$ will differ depending on the selected combinations of $P(\cdot)$. For small numbers of errors, a voting mechanism can be used to determine the order of error, and correct the errors. It has been shown[70] that if the number of errors is denoted by s, then

$$s < \frac{2^n - m + 1}{2} \tag{3.2}$$

Thus the code will correct errors of order less than $(\frac{2^n-m+1}{2})$. For m odd, error correction can be performed up to $(s = \frac{2^n-m-1}{2})$ and error detection performance up to $(s = \frac{2^n-m+1}{2})$. When m is even, RS code can correct up to $(s = \frac{2^n-m}{2})$ but will not detect more errors.

3.3.4.2 Generator Polynomial Approach to Reed Solomon Error Correction

The generator polynomial approach for Reed-Solomon implementation is the most common used in industry[71]. This approach evolved as a description of a cyclic code. A cyclic code is one which when cyclically shifted, the resulting value will be another codeword. Thus if the codeword is $c = (c_0, c_1, c_2, ..., c_{n-2}, c_{n-1})$, then $c'(c_1, c_2, c_3..., c_{n-2}, c_{n-1}, c_0)$ is also a codeword. With this approach, a message $m(x) = m_0 + m_1x + \cdots + m_{k-1}$ is encoded by multiplication with a generator polynomial

$$g(x) = g_0 + g_1x + g_2x^2 + \cdots + g_{n-k}x^{n-k} \tag{3.3}$$

Thus

$$c(x) = m(x)g(x) \tag{3.4}$$

The length of cyclic RS codes is given by $q-1$ which is one coordinate less than the number of coordinates in the original RS code approach. Thus the generator polynomial approach to formulate a t error correcting Reed-Solomon code is to determine a generator polynomial which has $2t$ consecutive powers of α as roots. where α is primitive element. Thus

$$g(x) = \prod_{j=1}^{2t}(x - \alpha^j) \tag{3.5}$$

Thus valid code polynomials have degrees from $2t$ to $(q-2)$, where q is the number of codeword coordinates in $GF(2^n)$. The number of code words $q-1$ in the Galois Field GF(q) is one less than that of the original approach to Reed-Solomon which is $GF(q)$

3.4 Reed-Solomon Code Performance

The performance of Reed-Solomon codes can be evaluated by considering the wireless system as shown in Figure 3.2.

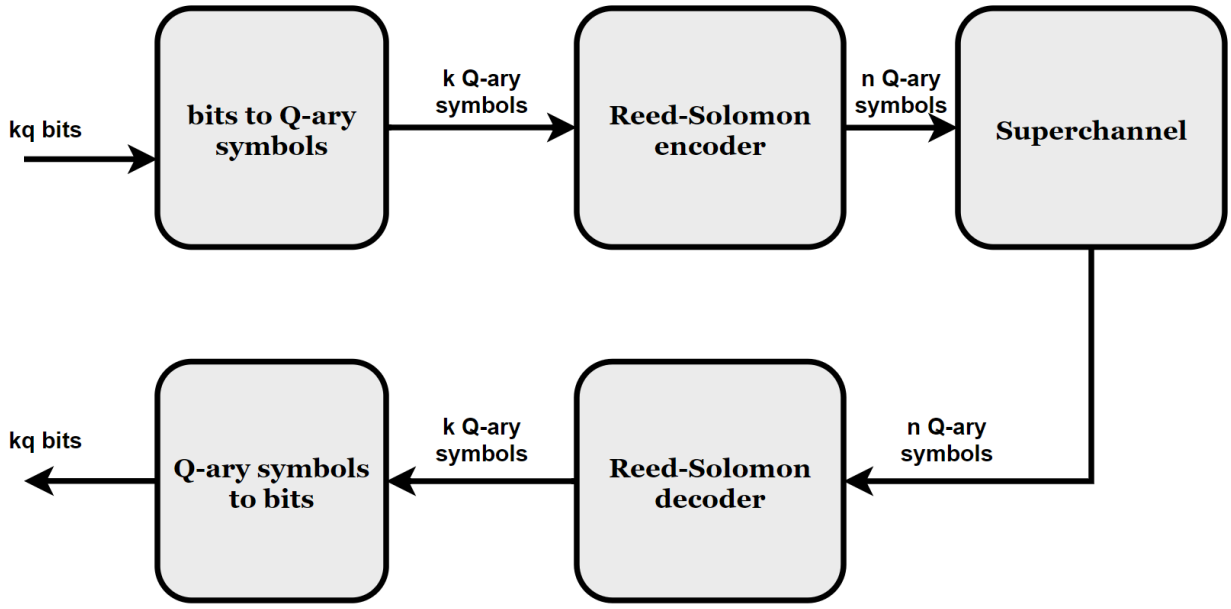

Figure 3.2: Application Layer Reed Solomon Performance Model

Reed-Solomon (RS) codes are Q-ary codes represented by (n, k) with code size n and message size k. A Q-ary code consists of Q elements in a finite field. The symbol size can be represented by $q = log_2 Q$ bits, and block length $n = Q - 1$. The minimum distance is $d = n - k + 1$ and they can correct up to $t = \lfloor \frac{d-1}{2} \rfloor$ symbol errors. The weight distribution of RS codes is [48]:

$$A_j = \binom{n}{j}(Q-1)\sum_{i=0}^{j-d}(-1)^i\binom{j-1}{i}Q^{j-d-i} \tag{3.6}$$

where A_j is the number of codewords of weight j, $j > 0$ and $A_0 = 1$.

Packets are sent from the RS encoder to the superchannel consisting of the M-ary superchannel. A M-ary super channel supports symbols up to 2^M distinct values.

If the probability of error for the M-ary symmetric channel is p, and the probability of a RS codeword in error is defined as P_q, then the probability of a correctly received RS symbol is $1 - P_q$, and the probability of a given incorrect symbol is $\frac{P_q}{Q-1}$.

The probability that the received codeword is correctly decoded is given by[48]:

$$P_{cd} = \sum_{i=0}^{t} \binom{n}{i} P_q^i (1 - P_q)^{n-i} \tag{3.7}$$

Using a bounded distance decoder (BDD), the RS decoder error rate is $1 - P_{cd}$ which can be expressed as [72]:

$$P_{cw} = \sum_{i=t+1}^{n} \binom{n}{i} P_q^i (1 - P_q)^{n-i} = P_{df} + P_{de} \tag{3.8}$$

Where P_{de} is the probability of decoder error and P_{df} is the probability of decoder failure. The probability of decoder error has been shown by Wicker [73] to be:

$$P_{de} = \frac{1}{n} \sum_{j=1}^{n} j A_j P_{de}^j \tag{3.9}$$

Where P_{de}^j is the probability that the decoding sphere of radius t covers a weight j codeword:

$$\begin{aligned} P_{de}^j = & \sum_{v=0}^{t} \sum_{w=0}^{t-v} \binom{n-j}{v} \binom{j}{w} (Q-1)^{w-j} \\ & \times \left(1 - \frac{P_q}{Q-1}\right)^w (1 - P_q)^{n-j-v} P_q^{j+v-w} \end{aligned} \tag{3.10}$$

The probability of symbol errors after decoding Reed-Solomon codes is given by[48][73]:

$$P_{sde} = \frac{1}{n} \sum_{j=1}^{n} j A_j P_{de}^j \tag{3.11}$$

When error statistics are available, and P_j represents the probability of j errors in a codeword. P_j', the probability of receiving a particular j error tuple is defined as:

$$P'_j = \frac{P_j}{\binom{n}{j}(Q-1)^j} \tag{3.12}$$

For the memoryless channel, the probability of j errors are determined empirically.

$$P_j = \binom{n}{j} P_q^i (1-P_q)^{n-i} \tag{3.13}$$

The probability of correct decoding is :

$$P_{cd} = \sum_{j=0}^{t} P_j \tag{3.14}$$

Thus the probability of decoding error, and subsequent symbol error when a decoding failure occurs are given by[48]:

$$P_{de} = \sum_{j=0}^{n} A_j \sum_{v=0}^{t} \sum_{i=0}^{v} P'_{j+i} \sum_{c=0}^{v} \binom{n-j}{c} \binom{j}{b} \times \binom{j-b}{c-i} (Q-1)^c (Q-2)^b \tag{3.15}$$

and the probability of a symbol error for this incorrect decoding is [48]:

$$P_{sde} = \frac{1}{n} \sum_{j=0}^{n} A_j \sum_{v=0}^{t} \sum_{i=0}^{v} P'_{j+i} \sum_{c=0}^{v} \binom{n-j}{c} \binom{j}{b} \times \binom{j-b}{c-i} (Q-1)^c (Q-2)^b \tag{3.16}$$

where $b = v - 2c + i$

3.4.1 Decoding Reed-Solomon Codes

There are multiple algorithmic approaches to decoding Reed-Solomon codes, such as the Peterson-Gorenstein-Zierler decoder[74], the Berlekamp-Massey decoder[75] and the Berlekamp-Welch decoder [76]. In this thesis the method used was the Berlekamp-Massey (BM) decoder. The BM decoder was utilized because of the availability of a tested and validated implemen-

tation for research work, and also the BM decoder is sufficient to validate the AL-FEC performance. In recent times, the Guruswami-Sudan decoder was proposed for improving the decode capability of Reed-Solomon Codes [77]. Using the Berlekamp-Massey decoder, the steps to decoding and error correction are[78]:

1. Calculate the syndrome - if syndrome is zero, there are no errors. The syndrome is the product of the parity check matrix and the received vector.
2. Determine the error locator polynomial using the Berlekamp-Massey algorithm
3. Find the roots of the error locator polynomial using Chien search
4. Determine the magnitude of the errors using the Forney algorithm
5. Correct the errors by subtracting the error magnitude from the received message.

3.4.2 Interleaving

After applying FEC to packets, there is a possibility to improve the FEC performance by shuffling the order of packet transmission. A situation that can occur when transferring packets over the air is when a packet is transmitted error free, while the next packet has errors exceeding the error correction capability of the AL-FEC. To increase the probability of recovering from the burst error in the second packet, the bytes between packets can be interleaved. Two types of interleavers have been identified:

1. Block inter-leavers - the data is organized in an $n_1 \times n_2$ matrix. The data are written column wise and then read row wise. This interleaver requires a memory capacity of $n_1 \times n_2$ symbols. This is illustrated in Figure 3.3.
2. Cross interleaver - this type of interleaver described by Ramsey [79] is implemented by multiplexing the code words over a set of delay lines with different delays. The delay line outputs are then combined and sent on the channel. The receiver performs the inverse operation.

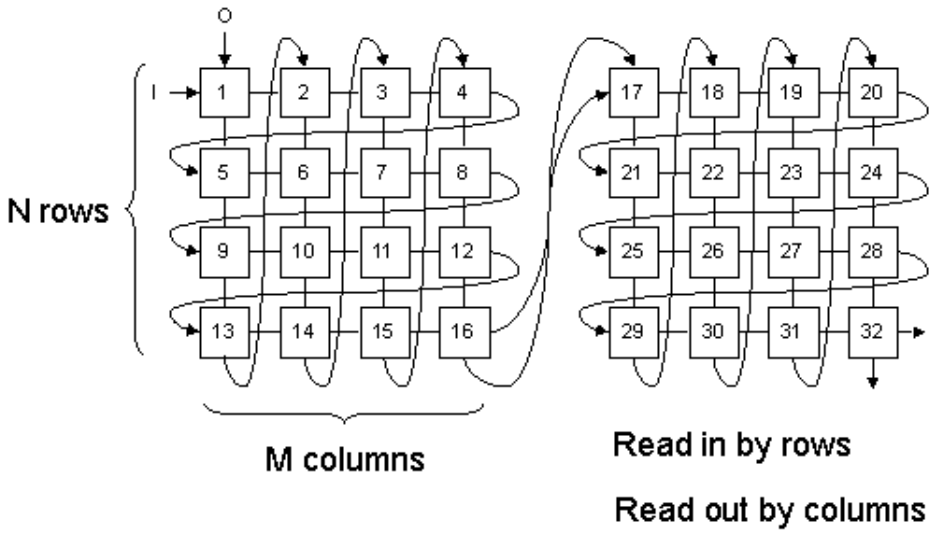

Figure 3.3: Block Inter-leaver

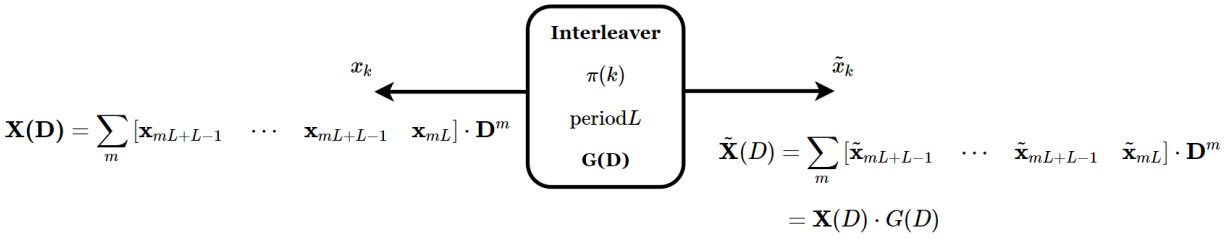

Figure 3.4: Basic Inter-leaver Model

3.4.3 Interleaver Analysis

The interleaver creates a well defined and reversible reordering of blocks of L bits. The reverse process is performed by the de-interleaver. Error bursts can be experienced in the channel due to the following[69]:

1. Non-stationary channel noise
2. Impulse noise
3. OFDM sub carrier errors
4. Incorrect decoder decision - these will span the entire codeword causing a burst of error symbols

The burst errors are effectively broken up into smaller bursts after de-interleaving.

3.4.3.1 Depth of an Interleaver [69]

The depth J of an interleaver is the minimum separation in symbol periods at the output of the interleaver between any two symbols that were adjacent at the input of the interleaver.

3.4.3.2 Interleaver Period

The period L of an interleaver is the shortest bit sequence interval for which the re-ordering algorithm used by the interleaver repeats.

3.4.3.3 Minimum Distance Magnification in Interleaving

For inner channels with an outer hard-decision code of block length equal to the period of interleaving, and only one error burst occurs within $(J-1)\cdot(L-1)$ symbols, then the outer codes free distance is multiplied by the depth J for inner-channel burst errors.

As shown in Figure 3.4 an interleaver creates a re-ordering of its input $\mathbf{x}_k$ to produce an output $\tilde{\mathbf{x}}_k$

$$\tilde{\mathbf{X}} = \mathbf{X}_{\pi(k)} \tag{3.17}$$

where the re-ordering procedure is represented by $\pi(k)$. Due to the periodicity

$$\pi(k) - L = \pi(k - L) \tag{3.18}$$

also, the interleaver depth can be defined using π as

$$J = \min_{k=0,\ldots,L-1} |\pi^{-1}(k) - \pi^{-1}(k-1)| \tag{3.19}$$

Using D as a representation of a delay variable, this delay is considered as equivalent to one interleaver period. Also, a symbol delay is represented as D_{sym} thus,

$$D = D_{sym}^{L} \tag{3.20}$$

The sequence of symbols presented at the input of the interleaver can be represented by a L-dimensional row vector of sequence $\mathbf{X}(D)$. Each element in this sequence is present in one period of the interleaver. Using the time index $k = m \cdot L + i$ where $i = 0, \ldots, L-1$, an interleaver of block index m can be represented as

$$\mathbf{X}_m = \begin{bmatrix} \mathbf{x}_{mL+(L-1)} & \mathbf{x}_{mL+(L-2)} & \cdots & \mathbf{x}_L \end{bmatrix} \tag{3.21}$$

Where successive interleaver input symbols are indexed by m, and

$$\mathbf{X}(D) = \sum_m \mathbf{X}_m D^m \tag{3.22}$$

The interleaver output can be represented by a row of symbols of length L. Thus a "rate 1" convolutional or block code over the symbol alphabet can be used to represent the inter-

leaving process

$$\tilde{\mathbf{X}}(D) = \mathbf{X}(D) \cdot G(D) \tag{3.23}$$

In Equation (3.23), $G(D)$ is an $L \times L$ non singular generator matrix. This matrix has the following constraints: (1) Only 1 entry in each row or column can be non zero, (2) Nonzero entries are of the form D^l where l is an integer.

3.5 802.11 Transmission Errors

For every packet transmitted using the 802.11 protocols there are four possible observations by the intended recipient:

1. The packet is not detected and is completely lost - This implies that the preamble is not detected. This is a complete packet erasure.
2. The packet is detected, reception begins but is interfered by another entity, thus it fails an error check
3. The packet is received, it passes the error check, however it contains an error
4. The packet is received without errors

These losses will cause the 802.11 MAC layer to retransmit the packet, which increases air resource utilization, for example the maximum physical layer service data unit (PSDU) for IEEE 802.11n is 65535 bytes [7], and for 802.11ac, the maximum PSDU is 4,692,480 bytes[7]. This PSDU is transferred in a time period of 5.484 ms in mixed mode on 802.11n and 802.11ac [80]. It is possible to recover the PSDU using an error correction scheme, for observations 2, 3 and 4 stated above. The error correction scheme used in this thesis - Reed-Solomon, was restricted during experimentation to block lengths of 65535 symbols, and each byte corresponds to a symbol. The block length limitation is because the decoding process on a general purpose CPU increases exponentially, thus increasing the risk of not decoding the symbols before the presentation deadline.

3.5.1 Hybrid Auto Repeat Request (HARQ)

In the event of a failed packet transfer, where the protected payload cannot be recovered even after error correction, a retransmission of the packet is required. This is handled automatically by several protocols which maintain reliability at the link layer. The combination of forward error correction and ARQ is referred to as Hybrid ARQ. Hybrid ARQ mechanisms have been classified into Types I and Type II. A Type I hybrid ARQ mechanism retransmits an encoded packet if the receiver is unable to decode the packet. For a Type II Hybrid ARQ, the sender utilizes code combining. Thus the sender uses two sub-codes. If the first packet with the first sub-code is not decodable, the sender re-sends the packet with the second sub-code. If the second sub-code is not decodable, the receiver attempts to decode a combination of the two sub-codes. If this also fails, the receiver then asks for a retransmission.
The number of retries for HARQ will depend on the specific protocol implementation. IEEE 802.11 uses a Type I ARQ, with multi rate retry (MRR), whereby the second packet retry will be sent at a lower MCS. Depending on the rate adaptation algorithm, multiple retries can be sent. SampleRate sends four retries.

Adding AL-FEC to the delivery mechanism will reduce the probability of packet failure. There are two approaches to using ARQ with AL-FEC: (1) Using the multicast channel, which does not send ACK frames on the link layer, and (2) Modifying the IEEE 802.11 frame transmission, to send packets which have been identified without requesting a ACK frame.

3.5.2 Bit Error Rate Estimation for IEEE 802.11n

The block diagram of the experimental system used in this thesis, for WiFi transmission system is shown in Figure 3.5.

In this experimental setup, a H.264 encoded file in an MP4 container is placed on a computer disk. The file is read in segments by the file segmenter, and then passed to the AL-

FEC transmit application. The AL-FEC application performs RS encoding and interleaving on the segments. These segments are then sent to the transmitter. The transmitter encodes the segment as WiFi frames. These frames are passed through a TGn WiFi channel. AWGN is added to the frame to get the desired SINR. The output of the channel, is sent to a the receiver, which performs the IEEE802.11 receive procedures, namely channel estimation and equalization, then decoding. The output of the receiver is the PSDU, which is sent to the AL-FEC receive application. The AL-FEC application de-interleaves the frame bytes, and then passes them to the RS decoder. The output of the RS decoder are combined into segments to make the received video file. The error rate is obtained by comparing the initial video file with the received video file.

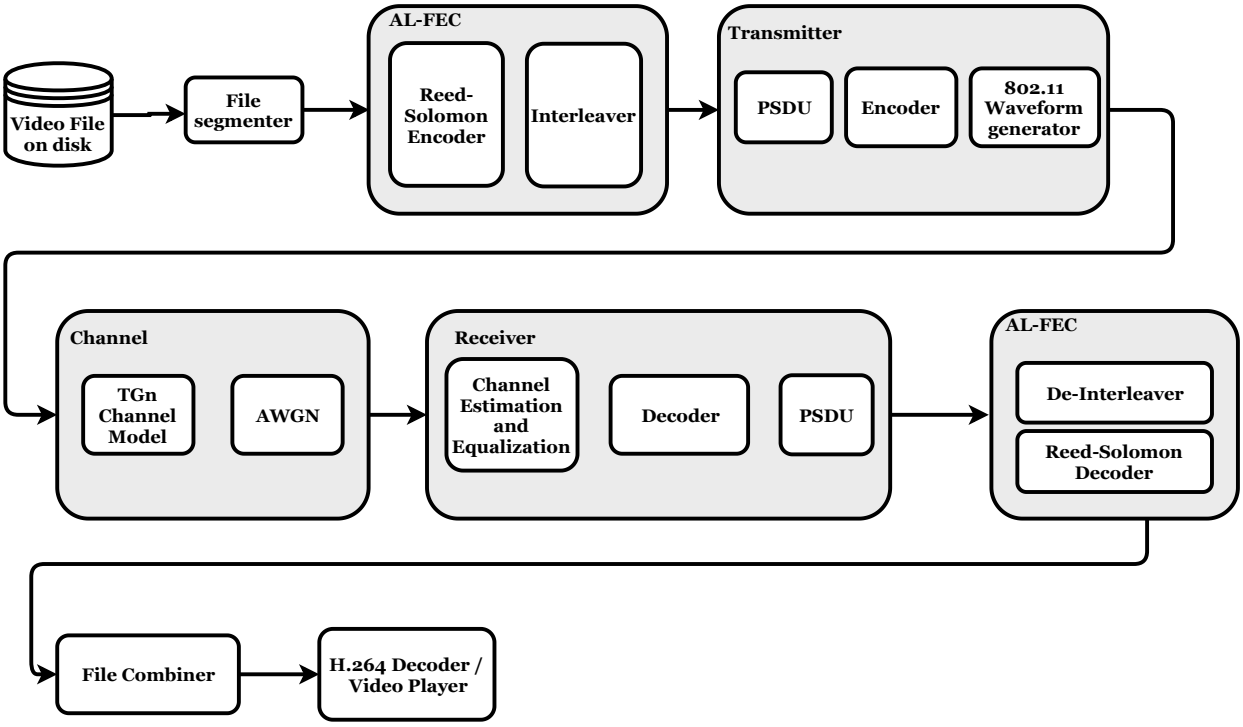

Figure 3.5: Video Transmission System

The packet error rate of packets after going through the WiFi channel must be less than the maximum bit error rate that the AL-FEC encoding scheme can correct. For a maximum distance separable code (MDS) such as Reed-Solomon, the maximum error rate which can be corrected is determined by the coding rate[81]. Individual bytes are interpreted as Reed-

Solomon symbols. For a message with length k and the corresponding code with length n, the code rate is n/k, and the number of parity symbols is $(n-k)/2$. Each group of symbols, or packet transmitted on the air is a code word of length n. To estimate the packet error rate, the WiFi channel has been analyzed based on the performance of multi-carrier OFDM schemes. IEEE 802.11n utilizes multi-carrier orthogonal frequency division multiplexing (OFDM) with 52 data sub-carriers and 4 pilot tones. Between each of these sub-carriers is a carrier separation of 312.5kHz. Each sub-carrier can be modulated with Binary Phase Shift Keying (BPSK), Quadrature Phase Shift Keying (QPSK), 16-level Quadrature Amplitude Modulation (16QAM) or 64-level Quadrature Amplitude Modulation (64QAM). Interference or other types of errors experienced in any sub-carrier will affect each of the other sub-carriers because of the inverse DFT operation which introduces frequency smearing between the sub-carriers. Thus there is no closed-form expression for the expected packet error rate estimate for the OFDM channel. To estimate the packet error probability, i.e. packet error rate, several link quality metric(LQM) methods[82][83] such as (1) Instantaneous SNR, (2) Shannon Capacity Expression, and (3) Exponential Effective Signal to Interference Ratio Mapping (Exp-ESM) method can be used. After determining the LQM, the numerical value of the LQM is used to determine the bit error rate by using a lookup table. For the Exp-ESM method, the LQM which represents the SNR is given by[82]:

$$\gamma_{eff} = -\beta \log\left(\frac{1}{N_u N_s}\sum_{j=1}^{N_u}\sum_{i=1}^{N_s}\exp\left(-\frac{\gamma_i^j}{\beta}\right)\right) \tag{3.24}$$

where γ_i^j denotes the output of the space-time processing stage for stream i on sub-carrier j, N_u is the number of useful data sub-carriers, N_s is the number of independent bit streams, and β is a scalar parameter found by fitting the model over a sufficient set of independent channel realization over a criterion. A suggested criterion is [82]:

$$\beta_{opt} = \min_{\beta}\left(\max_{i,j}(|\gamma_{eff,j} - \gamma_{eff,i})\right) \tag{3.25}$$

where $\gamma_{eff,i}$ is the effective SNR for the ith independent channel trial.

In this study, spatial division multiplexing (SDM) was investigated as the MIMO method. This is because SDM is the most widely supported and deployed Multiple-input Multiple-output(MIMO) technique with 802.11. To determine γ_i^j, the Minimum Mean Squared Error (MMSE) MIMO decoder is considered[82]. A symbol vector dimension N_r x 1 denoted by $y^1 = [y_1^1, ..., y_{N_r}^1]^T$, where T represents the transpose operation, and N_r is the number of receive antennae, is multiplied by a matrix $\mathbf{W}$. If $\mathbf{H}$ is the N_r x N_t channel matrix on a subcarrier, W is obtained as[82]:

$$\mathbf{W} = \mathbf{H^H} \left(\mathbf{HH^H} + \sigma^2 \frac{N_t}{P_t} I_{N_r} \right)^{-1} \tag{3.26}$$

where:

- $\mathbf{H}$ is the channel matrix between the transmitter and receiver
- σ^2 is the noise variance per receive antenna
- N_t number of columns of channel matrix, which is also the number of transmit antennae
- P_t is the transmit power over all antennae
- I is the identity matrix
- N_r number of rows of channel matrix, which is also the number of receive antennae

if the vector of sent symbols is denoted by $\mathbf{s} = [s_1, s_2, ..., s_{N_s}]^t$, where t represents the transpose operation. And the thermal noise is denoted by vector $\mathbf{n}$, the output after MMSE processing can be obtained as [82]:

$$\mathbf{z} = \mathbf{WHs} + \mathbf{Wn} = \text{diag}(\mathbf{WHs}) + (\mathbf{WH} - \text{diag}(\mathbf{WHs})) + \mathbf{Wn} \tag{3.27}$$

Thus the output can be seen to be a combination of the signal $\mathbf{s}$, inter-stream interference $(\mathbf{WH} - \text{diag}(\mathbf{WH}))\mathbf{s}$ and colored noise $\mathbf{Wn}$. The covariance matrices of the overall noise

plus interference is given by [82]:

$$\mathbf{R} = \frac{P_t}{N_t}(\mathbf{WH} - \text{diag}(\mathbf{WH}))(\mathbf{WH} - \text{diag}(\mathbf{WH}))^H + \sigma^2\mathbf{WW}^H \tag{3.28}$$

Thus the γ_i^j in equation 3.24 are the elements of vector $\boldsymbol{\gamma}$ given by:

$$\boldsymbol{\gamma} = \text{diag}\left(\frac{P_t}{N_t}\text{diag}(\mathbf{WH})\text{diag}(\mathbf{WH})^H\text{diag}(\mathbf{R})^{-1}\right) \tag{3.29}$$

The value of β was obtained by simulations [84] and some values from[84] are shown in Table 3.2. The resulting packet error rate evaluation with 2 spatial streams, 64-QAM modulation, FEC Rate 0.75, using Exp-ESM gives a theoretical value of 1×10^{-2} at an SNR of 18dB[82].

Table 3.2: β values for Exp-ESM [84]

Modulation	**Rate**	β
QPSK	1/2	1.75
QPSK	2/3	2.25
16QAM	2/3	6.75
16QAM	3/4	7.5

3.5.3 AL-FEC Scheme

RS Codes recover packets by appending additional parity packets. RS codes operate on blocks of data, thus they are referred to as block codes. RS codes are maximum distance separable codes, which do not exhibit an error floor, thus they are suitable for video applications which are very sensitive to bit errors.

3.5.4 Overall System Forward Error Correction Model

The overall system FEC, which includes: (i) the 802.11 Binary Convolutional Code (BCC) FEC and (ii) Reed-Solomon AL-FEC can be described as a concatenated coding system this

was first devised by Forney [18]. This method delivers good results from a combination of shorter codes. Concatenated codes can be used in multiple levels. In this simulated system, there are two levels -

1. The inner code is the standardized IEEE802.11 BCC code - The BCC encoding layer uses 64-state rate 1/2 code with a generator polynomial in octal form [85]

$$G = [133, 175]$$

or in generator matrix form:

$$G = [D^6 + D^4 + D^3 + D + 1,\ D^6 + D^5 + D^4 + D^3 + D^2 + 1]$$

For the higher 802.11 coding rates - 2/3, 3/4 and 5/6, the rate 1/2 code is punctured [19]

2. For the outer code, Reed-Solomon AL-FEC code is used. This is a code with (n, k) parameters (65535, 63847). These Reed-Solomon values were chosen in order to ensure decoding is completed in the time constraint of displaying a video frame. For a 24 frames per second this will be approximately 40 milliseconds. Error recovery using the Reed-Solomon decoder increases in complexity when the parity symbols are increase.

Thus the overall system coding rate is the product of the coding rate of the inner and outer FEC. The outer code rate is 0.97 and the inner coding rate takes on values of 1/2, 2/3, 3/4 and 5/6 thus the overall coding rates are shown in Table 3.3.

3.6 WLAN Experiment

3.6.1 AL-FEC Constraints

For applications with time constraints, such as video and audio conferencing, there is a requirement to deliver packets before a deadline. For video sent at 24 frames per second, this

Table 3.3: Overall System Coding Rates

Inner FEC	**Outer FEC**	**Overall Rate**
0.5	0.97	0.49
0.67	0.97	0.65
0.75	0.97	0.73
0.83	0.97	0.81

means that the error correction must be completed with minimal impact on the time budget of approximately 40 milliseconds.

Another AL-FEC constraint is the complexity of the FEC algorithm. In order to decode within the deadline, the coding computational requirements have to be within realistic capacities of the general purpose CPU used. For Reed-Solomon FEC, the complexity increases with the increase in number of roots of the generator polynomial. For a commodity CPU used for this test, Intel Core i7-6500U, at 2.5GHz , this limits the real-time error correction capability to the order of ten thousand bytes of consecutive errors per second [86].

3.6.2 IEEE 802.11 Wireless Channel Models

The IEEE 802.11 standards specify the channel models to be used for WiFi perfomance analysis. These are the $TGxx$ models, where the xx represents for example n [87], ac and ax. The TGn model was used in the AL-FEC experimental procedure.

3.6.3 Experimental Procedure

To observe the performance of AL-FEC over a range of modulation and coding schemes, the following experimental procedure was executed. Also, because the Hybrid Auto Repeat Request (HARQ) of WiFi does not allow packets which have uncorrectable errors to be sent upwards on the OSI stack to the application layer, the HARQ mechanism is not implemented.

A video file was encoded with Reed-Solomon, and then interleaved, before being sent

on the wireless channel. Both Reed-Solomon encoding and interleaving are performed by applications on the source host. The WLAN experimental setup, unlike 802.11 hardware devices, did not implement ARQ. Thus the behavior of the 802.11n packet transmission with the experiment is similar to that of a broadcast channel, which does not perform ARQ. The received packets were de-interleaved and then decoded to recover the original video signal. This is shown in Figure 3.5. In an 802.11 system, the end user device typically has a Maximum Transmission Unit (MTU) of 1500 bytes for network interfaces. Thus the operating system of the user's device will split the PSDU into MTU sized chunks. In the case of failed packets after AL-FEC, an application layer protocol will request for the non-recoverable packets. The re-transmission process will be handled at the application layer, specifically with the Transmission Control Protocol (TCP).

To validate the AL-FEC performance behavior, a video file containing 10 seconds of video at a resolution of 320x180 pixels, and a frame rate of 24 frames per second was tested. This file had a size of 464426 bytes. The video file was then encoded with a Reed-Solomon code (65535, 63487). Thus the maximum number of errors in a 65535 block that can be corrected is $(n - k)/2 = 1024$. This Reed-Solomon error correction encoding and decoding was realized in the C programming language and executed on an Intel Core i7 6500 CPU running at 2.5GHz. To improve the error correction performance, an inter-leaver is used after Reed-Solomon encoding. The interleaver redistributes symbols across blocks before transmission. When there are burst errors on the channel, such as a PSDU is completely lost, the de-interleaving process will redistribute these errors across the blocks. Thus error recovery performance is improved with the interleaving process.

Table 3.4 shows the symbol error counts before and after FEC application. This table show MCS values from MCS10 to MCS15. These correspond to two spatial streams and MCS 8, and 9 have been omitted because the errors were not significant. It can be seen that for the more complex modulations, such as 64QAM, the error rates are higher as expected, however, AL-FEC is able to reduce the residual errors to low percentages starting at SNR

30dB.

3.7 WLAN with AL-FEC Experiment Results

The AL-FEC scheme was tested with multiple modulation and coding scheme (MCS) values ranging from 2 to 23. MCS 0 and 1 were omitted because the data rates at these MCS values are relatively low, with throughputs 6.5 and 13 Mbps respectively when using a 20MHz channel without a short guard interval (SGI). For each MCS value, a Physical Layer Service Data Unit (PSDU) packet size is selected. The PSDU used in the experiments ranged from 1000 to 8000 bytes. The upper limit is constrained by the decoding time required for Reed-Solomon error correction algorithm.

Using a fixed MCS and PSDU length, the SNR was increased in steps of 10 from 20 to 50dB. The noise characteristic used was additive white Gaussian. A video file with size 464426 bytes is then encoded with Reed-Solomon, which increases the file size to 524280 bytes. The encoding is performed in blocks, with parity appended to each block, and the blocks are interleaved, then stored on disk for transmission through the simulated WiFi channel. Using a PSDU length of 3000 bytes, 175 blocks are required to transfer the complete video file. For shorter PSDU lengths, the number of required blocks increases. This increase is because a smaller section of the video file is transmitted with smaller PSDU sizes. Measurements inspected without FEC indicate that as the modulation order increases, there is an increasing rate of error on the channel. This is expected because the probability of incorrect decoding increases as the modulation complexity increases. After passing through the channel, the video file is then de-interleaved and decoded with the Reed-Solomon FEC. In several instances using AL-FEC, the transmission can be completely recovered, even though there were receive errors. The best performing MCS selections have a low order modulation schemes, such as BPSK, and QPSK. The coding rate of the Reed-Solomon AL-FEC used for simulations is 0.97. This value was selected as a trade-off between decode complexity, and

Table 3.4: Error Performance of AL-FEC scheme (a) Modulation and BCC coding combinations (b) Number of symbol errors without FEC (c) Number of symbol errors after FEC (d) Residual error percentage after FEC [88]

(a) Modulation and BCC Coding combinations

Inner Code Rate	3/4	1/2	3/4	2/3	3/4	5/6
Modulation	QPSK	16-QAM	16-QAM	64-QAM	64-QAM	64-QAM
MCS Index	10	11	12	13	14	15

(b) Number of symbol errors Before FEC

MCS Index	10	11	12	13	14	15
SNR 20	65643	114895	288468	432345	489126	497451
SNR 30	3577	6237	21747	49521	93482	63296
SNR 40	648	109	2721	2728	8740	3661
SNR 50	391	28	2721	2710	1380	2724

(c) Number of symbol errors after FEC

MCS	10	11	12	13	14	15
SNR 20	58737	101623	255799	383491	433204	441033
SNR 30	0	0	19523	44322	82955	56399
SNR 40	0	0	0	0	7626	0
SNR 50	0	0	0	0	0	0

(d) Residual Error Percentage

MCS	10	11	12	13	14	15
SNR 20	11.20	19.38	48.79	73.15	82.63	84.12
SNR 30	0.00	0.00	3.72	8.45	15.82	10.76
SNR 40	0.00	0.00	0.00	0.00	1.45	0.00
SNR 50	0.00	0.00	0.00	0.00	0.00	0.00

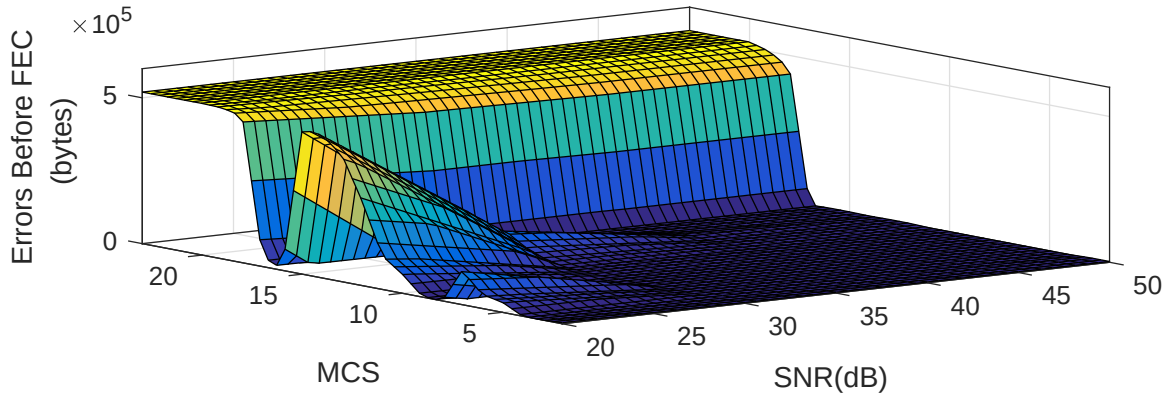

(a) Byte Errors Before FEC, PSDU 3000 bytes

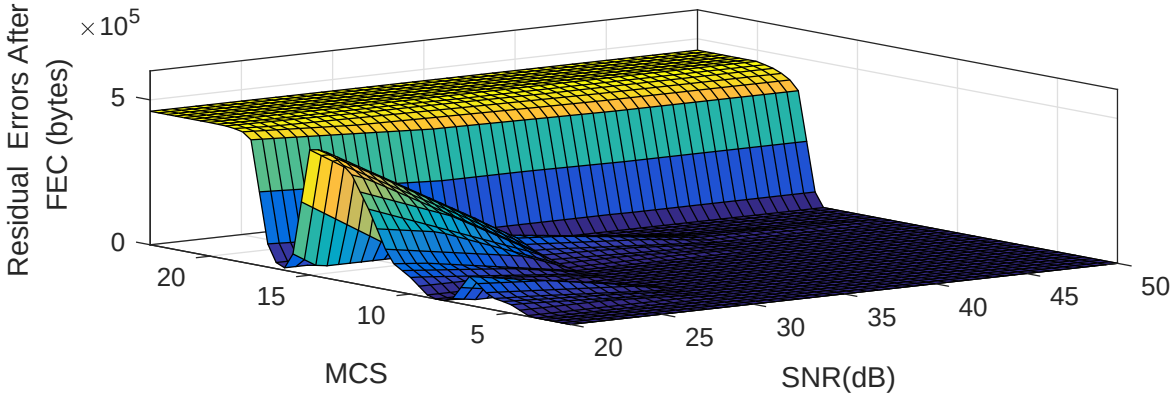

(b) Residual Errors After FEC, PSDU 3000 bytes

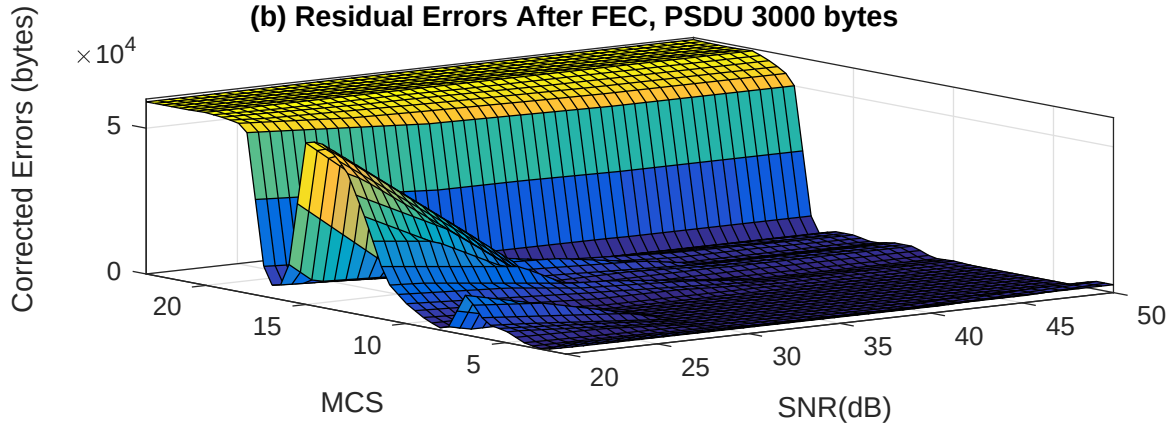

(c) Corrected Errors PSDU 3000 bytes

Figure 3.6: Errors with PSDU 3000 bytes for MCS range $2 \rightarrow 23$, and SNR Range $20 \rightarrow 50dB$ (a) Before FEC (b) After FEC and (c) Number of Corrected Errors [88]

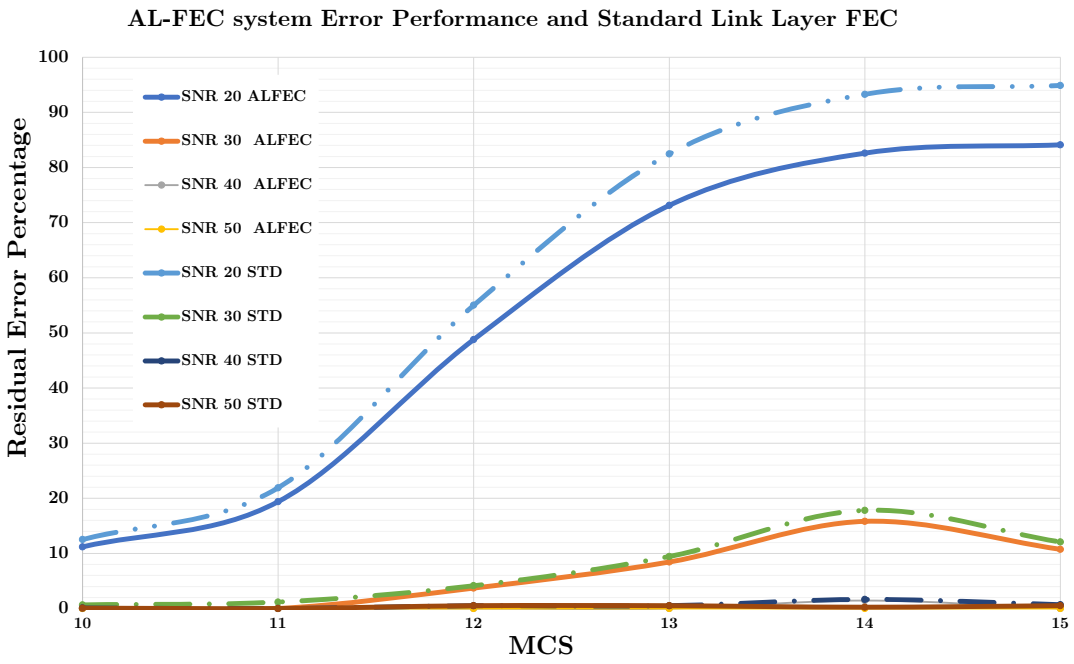

Figure 3.7: A Concatenated FEC system has a lower residual error percentage after error correction.

bandwidth expansion after AL-FEC encoding.

As shown in Figure 3.6(a), the number of errors increases with an increasing MCS for the 802.11n channel. This increasing errors are reflective of the increasing probability of decode error, when high order modulations are used. However, dips are seen in the MCS axis at MCS values of 8 and 16. These MCS values use a low order modulation of BPSK, with spatial streams of 2 and 3, respectively. The number of error reduces as the SNR is increased, except for MCS 18 to 23, where the error rate is high. The high error rate MCS 18 to 23 have 3 spatial streams and QSPK, 16-QAM and 64-QAM modulations.

Residual symbol errors after AL-FEC recovery are shown in Figure 3.6(b), and corrected errors after AL-FEC are shown in Figure 3.6(c). With an increasing MCS, thus increasing the number of spatial streams, order of modulation, and coding rate simultaneously, it is observed that the error correction performance reduces.

A closer look at the error performance is shown for selected MCS values in Table 3.4. Also shown in Table 3.4(d) is the error percentage after recovery when using MCS 10 to 15. Tables 3.4(b) and (c) show the number of symbol errors before and after AL-FEC. The total file size in used is 524280 bytes.

The error performance Table 3.4 also shows that a user can receive packets with MCS 11(64-QAM, BCC rate 1/2, PHY rate 52Mbps) instead of using MCS 10 (QPSK, BCC rate 1/2, PHY rate 39Mbps). Both at SNR 30 dB thereby clearly offsetting the 3% bandwidth overhead required by AL-FEC. Thus as will be shown in Chapter 4, when AL-FEC is in use, higher MCS selections can be used in many instances, which will improve the air efficiency, and instantaneous throughput. The end-to-end MCS selection algorithm is always seeking to make selections to higher MCS indices, whose error rates can be minimized with AL-FEC.

The residual error performance after AL-FEC is also shown in Figure 3.7, where it can be seen that at every MCS combination, there is a reduction in received errors at the application layer.

The maximum decode time for the 10 second video under different simulation conditions

was 5 seconds, thus the AL-FEC mechanism is able to correct errors within the deadline for the application to present the video frames without exceeding a play-out buffer. The decode time was measured by sending the output of the receiver to the RS decoder while setting a timer, on completing the FEC recovery, the timer was stopped.

3.8 TCP with Application AL-FEC

If the packet is not successfully decoded after executing the error correction algorithm the packet must be re-sent. Application Layer Forward Error Correction requires the lower layers of the OSI to send packet which are not error free, up on the stack to the application layer, in order for the AL-FEC to attempt the decode on these error-ed packets. This thesis proposes modifying the IEEE802.11 receive mechanism to allow packets which fail CRC to be sent up to the application stack. To achieve the AL-FEC efficiency gains, Automatic Repeat Request (ARQ) must be handled by the application layer.

This thesis investigated multiple reliable protocols: (1) Negative Acknowledgment Oriented Multicast (NORM) protocol [89] , (2) QUIC Protocol [90], and (3) Transmission Control Protocol (TCP) variant TCP-CUBIC[91].

TCP was selected for AL-FEC reliable transfer due to its performance and being a well understood protocol.

Performance improvements when using AL-FEC with TCP transport has been investigated by [92]. Several parameters determine the effectiveness of AL-FEC for video transport over TCP. These include the latency of the decoding, and the ARQ mechanism if decode fails.

3.8.1 FEC Latency

Because of the computational complexity of FEC algorithms, there exists a latency between when the corrupt packets are presented, and when the FEC algorithm is able to deliver an

error free output packet. If an ARQ system is in place, the FEC result must be present before the ARQ timer expires. In the case of IEEE 802.11, the link layer FEC is often convolutional code, which is implemented in hardware, and can meet the timing requirement. When AL-FEC is in operation, the timing output usually will not be sufficient for operation at the link layer, because the packet must travel up the networking stack to the application layer, get corrected, and sent back down to the PHY layer. Thus to implement ARQ with AL-FEC, an application layer protocol must control the repeat request event, this is fulfilled by TCP in this thesis.

3.8.2 Application Layer ARQ

Packet decode times can be relatively long when using AL-FEC compared to link layer FEC. Thus to handle retransmissions, an application layer repeat request mechanism is required. This repeat request mechanism has the flexibility of being tuned to the system in operation. The TCP protocol is responsible for this ARQ, because TCP will perform retransmissions when packets are not acknowledged.

3.8.3 TCP based Reliable Delivery With AL-FEC

Because the probability of packet error is reduced when using AL-FEC, the congestion control behavior of TCP is different [93].

The TCP congestion window [94] is a variable in the TCP state machine that limits the maximum amount of data that a sender can transmit before receiving an acknowledgment.

TCP congestion window size is a function of packet loss and is given by [95]:

$$W_{TCP} = \sqrt{\frac{8}{3p}} \tag{3.30}$$

Where p is the packet loss.

In case of packet losses, there can be significant gain in the throughput when AL-FEC

is applied. Also, consideration must be made regarding the AL-FEC block length and TCP window size.

The throughput of a TCP connection in packets per second can be expressed as [92][96]:

$$T = \min\left\{\frac{1}{RTT}\sqrt{\frac{3}{2p_{loss}}}, \mu\right\} \tag{3.31}$$

where RTT is the smoothed round trip time, μ is the most restrictive path in the link, which is the wireless channel in our study, and p_{loss} is the probability that the TCP packet is lost.

The most restrictive path in the link μ can be represented by [97][98]:

$$\mu = \frac{W_{max}}{RTT} \tag{3.32}$$

where W_{max} represents the maximum window size.

When AL-FEC is enabled, with a a FEC scheme of k-size messages and n-size code words (n, k), the throughput can be expressed as [96][99]:

$$T = \min\left(\frac{1}{RTT}\sqrt{\frac{3}{2p_{n,k}}}, \frac{k\mu}{n}\right) \tag{3.33}$$

where $p_{n,k}$ is the packet loss after FEC recovery. Substituting μ in (3.32) into (3.33) gives:

$$T = \min\left(\frac{1}{RTT}\sqrt{\frac{3}{2p_{n,k}}}, \frac{k \cdot W_{max}}{n \cdot RTT}\right) \tag{3.34}$$

An experiment was executed using the iperf[100] traffic generator. TCP with AL-FEC was compared to standard TCP, and throughput on an emulated wireless channel was observed as shown in Figure 3.8.

When FEC is applied, the effective congestion window is increased as shown in Figure 3.9 and 3.10.

The additive increase, multiplicative decrease behavior of TCP is shown in Figures 3.11

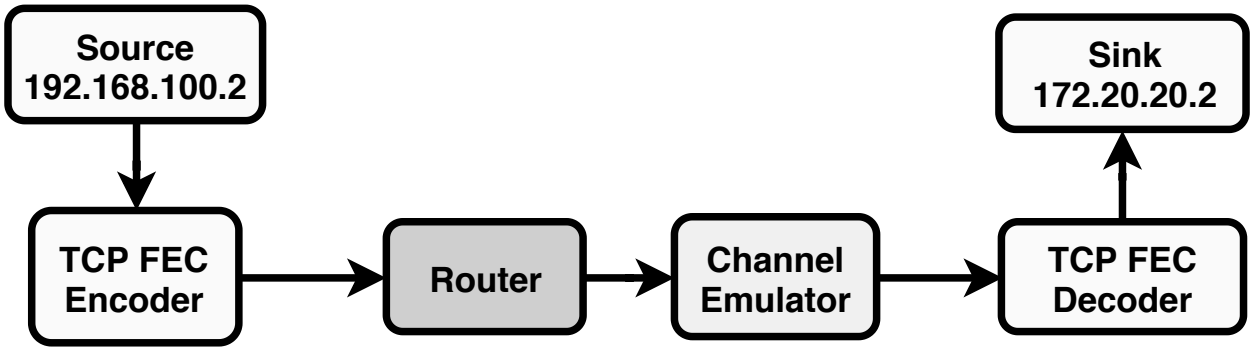

Figure 3.8: Experimental Setup for TCP throughput test

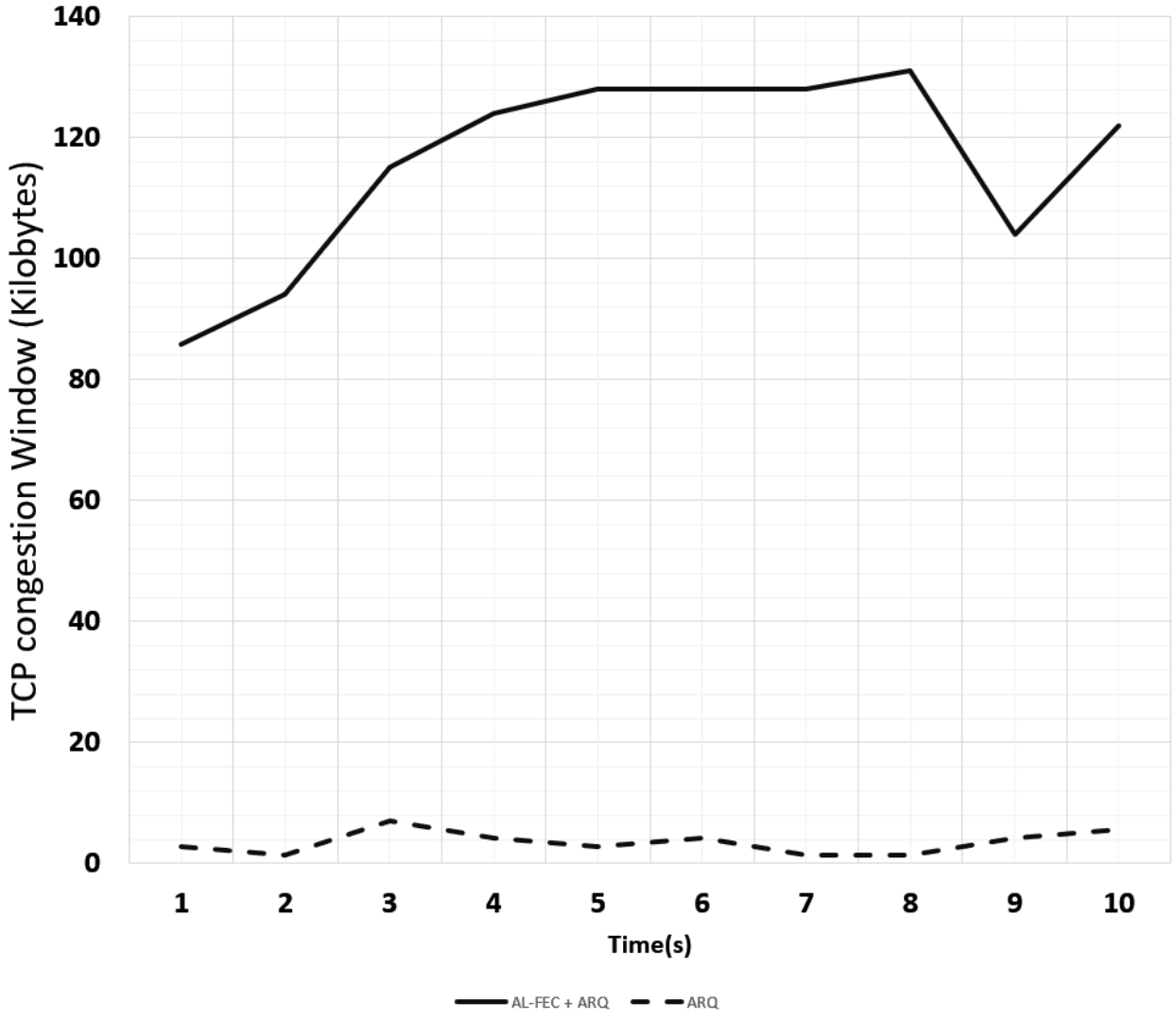

Figure 3.9: Dynamic window adjustment at 15% packet Loss With and Without AL-FEC, shows the window size is greater when FEC is applied

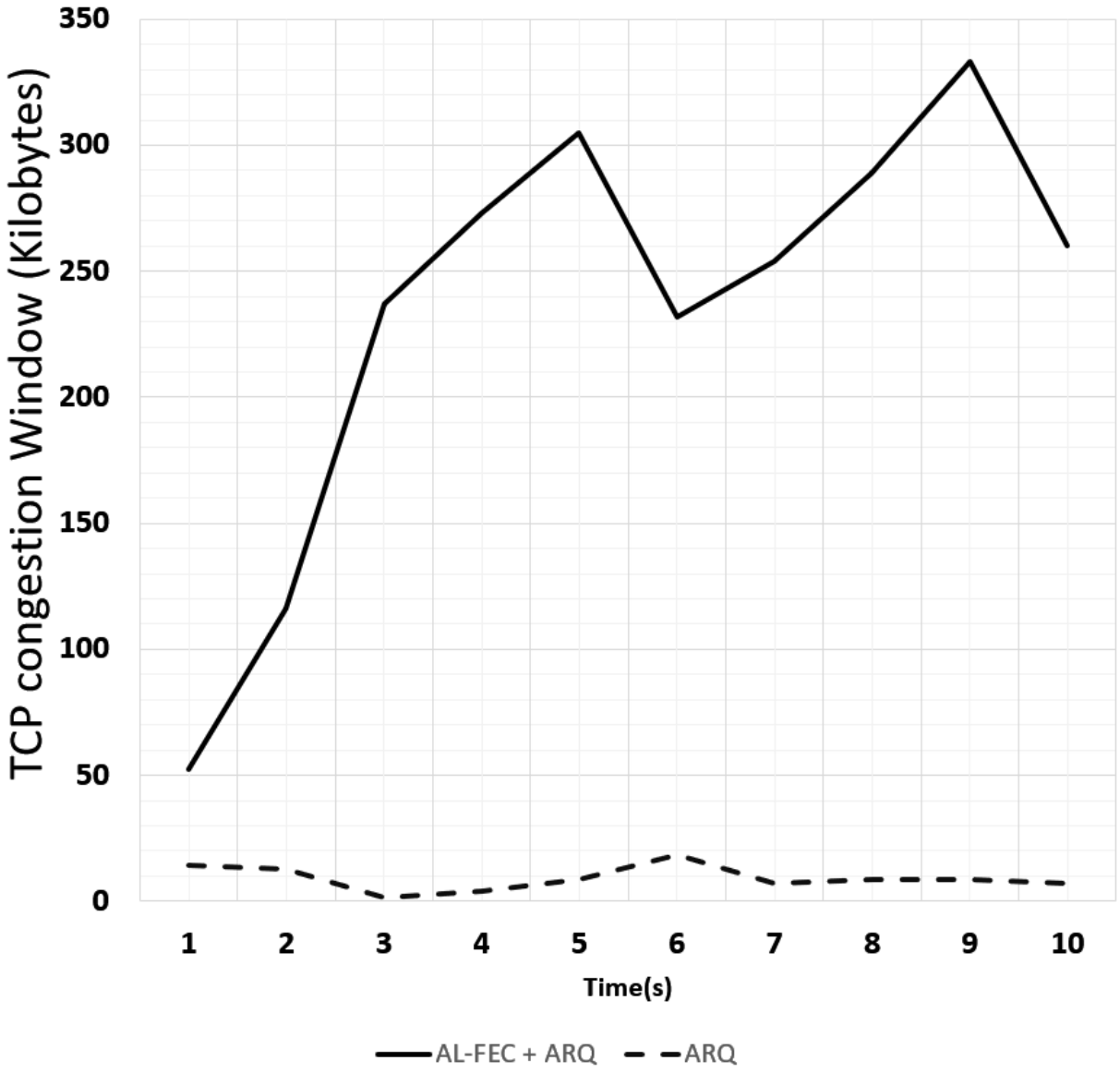

Figure 3.10: Dynamic window adjustment at 2% packet Loss With and Without AL-FEC shows the window size is greater when FEC is applied

and 3.12.

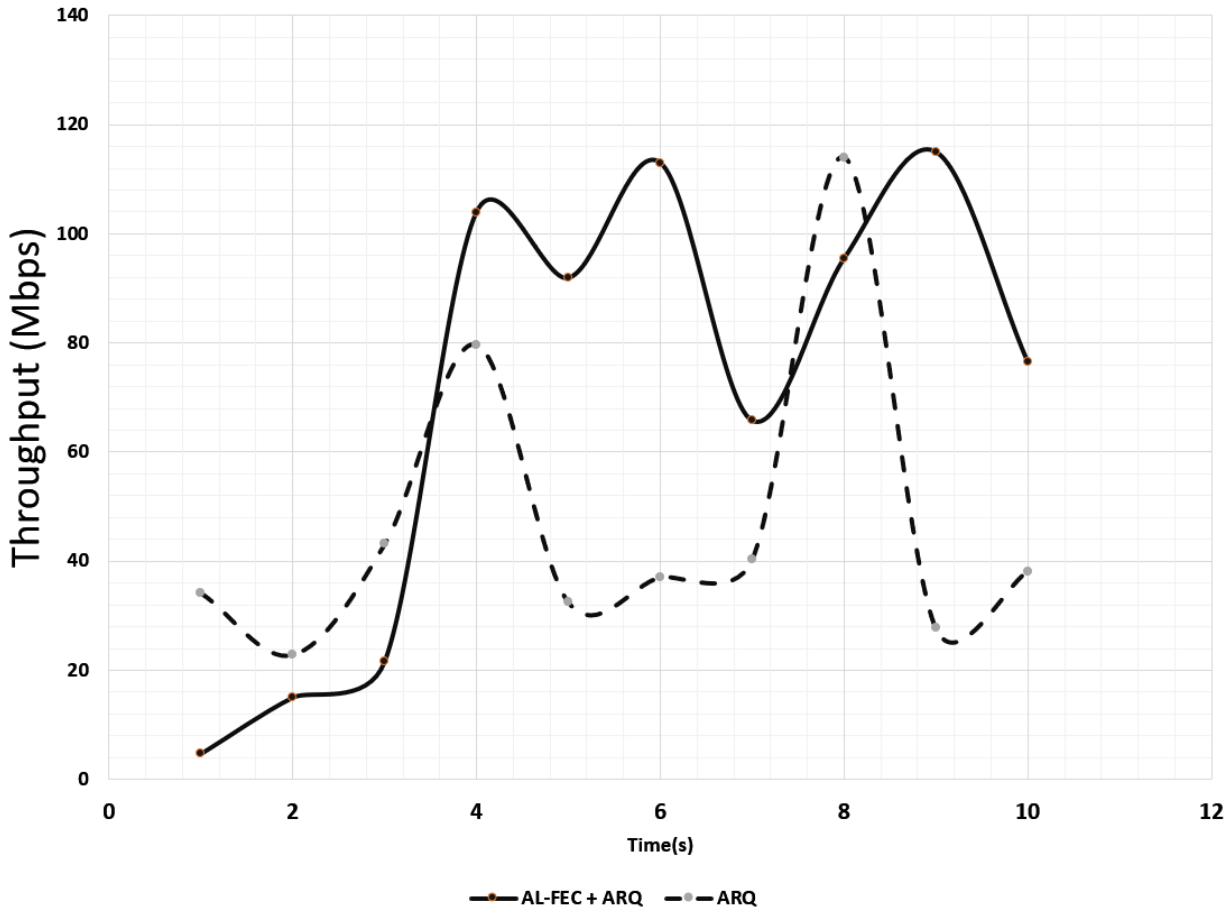

Figure 3.11: TCP Throughput experiment at 2% packet loss shows increased throughput when FEC in applied

3.9 Practical Considerations for AL-FEC

3.9.1 Protocol layer latency

There is a finite amount of time for a packet to travel from the network to the application layer. This time generally exceeds acceptable values for network signaling. Thus it is preferable to implement an application protocol which performs the reliable delivery of frames with AL-FEC. This protocol can optimize the feedback process to request frames that fail even after AL-FEC error correction. The selected protocol for reliable delivery in this thesis is

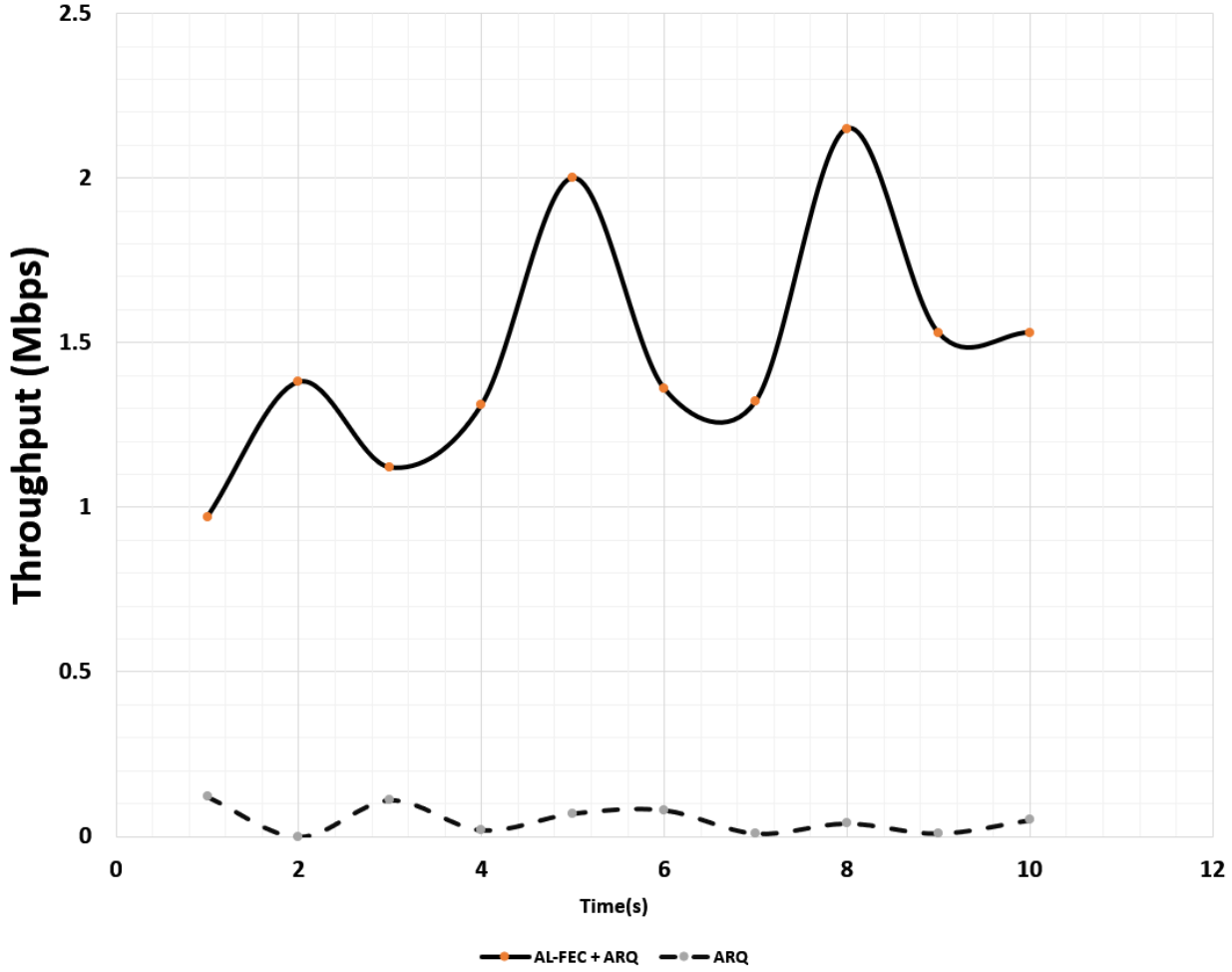

Figure 3.12: TCP Throughput experiment at 15% packet loss shows increased throughput when FEC in applied

TCP-CUBIC. As will be discussed in Chapter 5, TCP-CUBIC will fill up a playback buffer. This buffer will be of the order of 10 seconds. Thus the reliable delivery mechanism can request retransmissions, when AL-FEC is unable to recover the packet, which will minimize the risk of the video playing application being starved of input data.

3.10 Summary

In this chapter, it has been shown that it is feasible to improve air efficiency by reducing the probability of packet re-transmission when using AL-FEC, due to reduced packet errors as shown in Section 3.7 . As discussed in the wireless experiment in Section 3.7, AL-FEC can often totally recover a packet with errors, which would have otherwise been re-transmitted. On a general purpose CPU, recovery was achieved within a deadline of 40 milliseconds for video streaming applications. Complete packet recovery without any residual errors was achieved under several MCS schemes. Reed-Solomon FEC was used as an application layer error recovery scheme, in addition to packet interleaving. The coding rate used by Reed-Solomon is constrained by the decoding complexity. Simulation results show that when the SNR is above 30dB, there is an high probability of complete packet recovery under multiple MCS combinations. It is also seen that using TCP with AL-FEC increases the size of the congestion window, which can improve the overall throughput.

Chapter 4

Rate Adaptation

4.1 Introduction

Wireless Rate Adaptation is the mechanism whereby two, or multiple communicating devices, dynamically modify the physical signaling rate, depending on the wireless channel conditions. Rate adaptation enables wireless devices to optimize the modulation and coding parameters. It is possible that the SINR of a wireless channel is of a level whereby the decode error rate for high order modulation formats such as 64QAM is really high. In such a scenario, problems occur such as inability for the receiver to detect the start of a frame. Thus mobile wireless receivers can adapt to the changing channel conditions. The IEEE802.11 standards require a transmitting device to use the lowest order modulation at the beginning of the frame. The beginning of the frame contains information about modulation of the subsequent payload.

Management signals are sent a lower order modulation scheme, this is MCS index 0 and the modulation format is BPSK at BCC rate $\frac{1}{2}$. The transmitter in a WiFi network determines the rate to use based on its estimate of the wireless channel conditions. The determination is controlled by the Rate Adaptation (RA) algorithm.

4.2 IEEE 802.11 Throughput Analysis

Advances in wireless and semiconductor technology has enabled mobile devices the ability to display high bit rate streaming video with high quality. With IEEE 802.11 wireless networks, the physical channel is shared with a listen before talk mechanism, carrier sense multiple access with collision avoidance (CSMA/CA). Each user adheres to the channel access protocol such as the Distributed Coordination Function (DCF) or Enhanced Distributed Channel Access (EDCA) which results in a fair channel resource access to each user. In addition to protocol overhead, imperfections in the channel or receive processing errors, reduce the effective throughput over the air interface. The reduction in WiFi throughput is also dependent on the number of users simultaneously active on the wireless channel. Improvements on throughput have been achieved by techniques such as increase in physical parameters modulation complexity, Multiple Input Multiple Output (MIMO), and increase in channel bandwidth. Protocol optimizations such as aggregation and block acknowledgments also increase the effective throughput, by reducing the protocol overhead.

The saturation throughput of IEEE 802.11 networks can be estimated using the Markov Model as proposed by Bianchi *et al.* [25], and further refined by Tinirello *et al.*[101]. The proposed method by Bianchi accounts only for packet collisions. Thus further works such as [102] include the effects of errors on frame transmission. Further refinements to the Markov model has been presented by [103].

These studies present the throughput of the wireless channel, at a specific MCS, as a fraction of the total time slot, for which users are able to use the channel. The descriptions of symbols used in the Markov based model are shown in Table 4.1. The throughput expression is based on the probability of a busy channel P_b and the probability that a successful

Table 4.1: Symbols used in the Bianchi model [25]

Symbol	Description
τ	Probability that at a single station transmits in a generic slot time
n	Number of stations
$\overline{E(P)}$	Average payload size in bits
S	Throughput, in bits per second
P_s	Probability that a successful transmission occurs in a slot time
P_b	Probability that the channel is busy
$\overline{T_s}$	Average time channel is sensed busy
$\overline{T_c}$	Average time there is a collision on the channel
δ	Duration of empty slot time

transmission occurs P_s [101]:

$$P_b = \quad 1 - (1-\tau)^n \tag{4.1}$$

$$P_s = \quad n\tau(1-\tau)^{n-1} \tag{4.2}$$

Since τ is the probability that one station is transmitting, and there are n stations, then Equation (4.1) is the probability that at least one station in transmitting. While Equation (4.2) is the probability that exactly one station transmits on the channel.

$$S = \frac{P_s\overline{E(P)}}{(1-P_b)\delta + P_s\overline{T_s} + [P_b - P_s]\overline{T_c}} \tag{4.3}$$

From Equation (4.3), it can be seen that the methods of improving the throughput include: (a) Increasing the probability of a successful transmission, and (b) Reducing the probability of collisions.

Another option to increase throughput, is to increase the MCS. However, this must be performed considering physical channel parameters, for example a MCS combination must be selected such that the maximum error-rate post link layer FEC should be 10% according to the IEEE802.11 [7] specifications. Thus one can infer that if the current MCS combination

gives a 1% error rate post link layer FEC, then it may be possible to make a switch to a more complex MCS that possibly increases the error rate to 10%. The AL-FEC algorithm selection in this research attempts to opportunistically utilize such channel error gaps. This can be performed at the application layer, with Application Layer Forward Error Correction (AL-FEC).

4.3 Cross Layer Rate Adaptation

4.3.1 Rate Adaptation

IEEE802.11 specifies discrete rates as shown in Figure 4.1 which may be used by for transmission. Receivers detect the rate and decode the packets accordingly. The algorithm for selecting the rate is not specified by the IEEE 802.11 standard, however, algorithms such as Minstrel [55] and Auto Rate Fallback (ARF) [52] have been described in literature. This thesis applies AL-FEC to a system utilizing ARF, however the achieved gains will apply to other rate adaptation algorithms. ARF was selected because a tractable mathematical model, based on Markov models, can be used to directly model ARF operation.

4.4 Auto Rate Fallback Algorithm

The Auto Rate Fallback Algorithm (ARF) [52] initializes with a random MCS, and increase the MCS number after x successful transmissions. ARF steps down the MCS after y failures.

4.5 Rate Adaptation Parameters

4.5.0.1 Rate Adaptation Gaps

For a given channel condition, the optimum rate adaptation parameters, for example could be in between the discrete rate adaptation values specified by the IEEE802.11 standards.

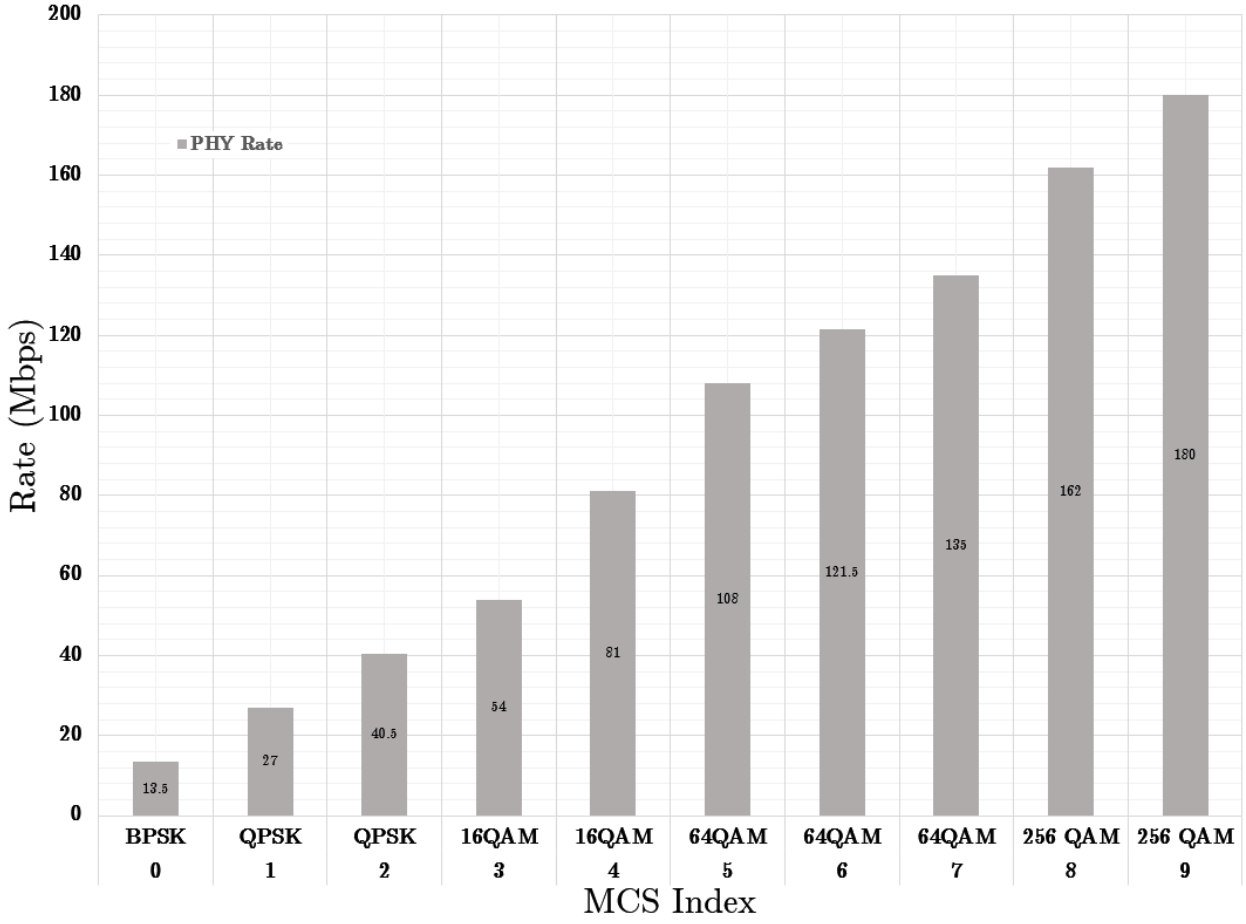

Figure 4.1: Data Rates for IEEE 802.11ac MCS index values, 800ns GI, 40MHz channel [7]

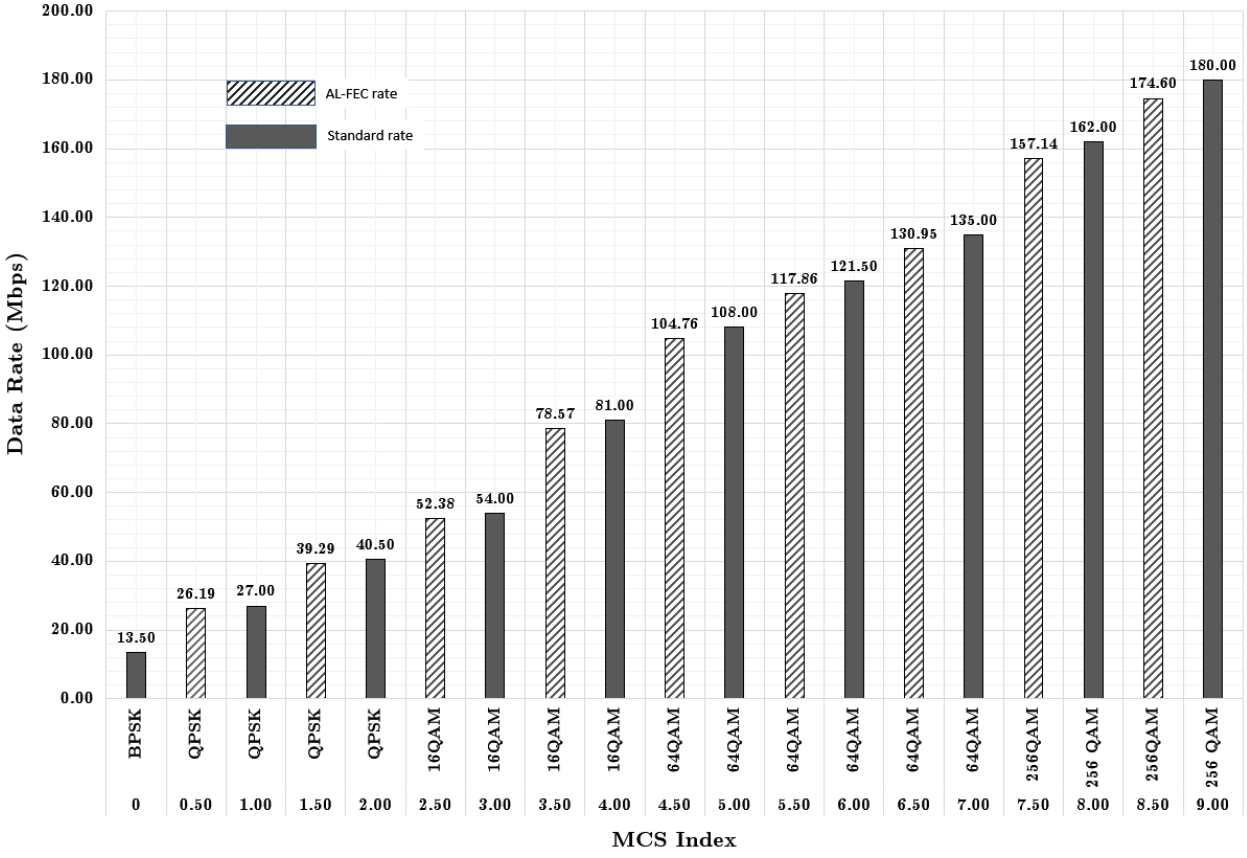

Figure 4.2: Data Rates showing AL-FEC Rates for IEEE 802.11ac MCS index values, 800ns GI, 40MHz channel, AL-FEC

Table 4.2: Data Rates and Speed Gain with MCS step-up

MCS	Modulation	PHY Rate	Rate Gain with AL-FEC
0	BPSK	13.50	
0.50	QPSK	26.19	1.94
1.00	QPSK	27.00	
1.50	QPSK	39.29	1.46
2.00	QPSK	40.50	
2.50	16QAM	52.38	1.29
3.00	16QAM	54.00	
3.50	16QAM	78.57	1.46
4.00	16QAM	81.00	
4.50	64QAM	104.76	1.29
5.00	64QAM	108.00	
5.50	64QAM	117.86	1.09
6.00	64QAM	121.50	
6.50	64QAM	130.95	1.08
7.00	64QAM	135.00	
7.50	256QAM	157.14	1.16
8.00	256 QAM	162.00	
8.50	256QAM	174.60	1.08
9.00	256 QAM	180.00	

Thus a rate adaptation algorithm must select the next lower rate for transmission. With AL-FEC, the data rate will be the overall system rate when the AL-FEC overhead is considered. Thus there exists the flexibility to select a finer grained rate adaptation at the application layer. Shown in Figure 4.2 are the effective throughput when using AL-FEC with a step-up to the next MCS value. This opportunistic step-up can be performed when AL-FEC is able to recover from all errors. Also, the relative throughput gain when AL-FEC is active, with a step-up MCS is shown in Table 4.2. From Figure 4.2 and Table 4.2, it can be seen that:

1. The effective throughput when using AL-FEC is increased, even though the AL-FEC mechanism adds an overhead to the data stream.

2. The more frequent that AL-FEC with RA can select the higher complexity MCS, the long term throughput delivered to the higher OSI layers will be increased.

3. Because of the increased reliability with FEC, AL-FEC can reduce re-transmissions, which will increase the air efficiency, and will improve the data throughput for all users

in the network, including those that do not use AL-FEC.

4.5.0.2 Rate Adaptation Speed

The responsiveness of a rate adaptation algorithm can be described by its rate of change of its modulation and coding scheme parameters. This can be regarded as the rate adaptation speed. Too slow a speed will delay the time for the MCS to adapt to the current channel conditions. When the rate adaptation speed is too fast, the user device may select non-optimal MCS values, which will cause retransmissions.

4.5.0.3 Cross Layer Rate Adaptation

When using AL-FEC, an opportunity exists to enhance the rate adaptation algorithm by decisions made at the application layer. Thus working in conjunction with the link layer rate adaptation controller, the AL-FEC application can set a desired rate adaptation which will be suitable for the combination of link layer and application layer forward error correction. To achieve cross layer rate adaptation in this thesis, the receiver signals to the video server to encode and use a step-up MCS. The receiver is aware of its channel conditions, and is aware of the current MCS used by inspecting its rate adaptation table.

4.5.0.4 AL-FEC protected bytes

With AL-FEC, additional parity bytes are added to the packet, before the IP header and link layer FEC. This is shown in Figure 4.3. The default behavior of the WiFi stack is to discard packets which fail error recovery at the link layer. However, with AL-FEC, such packets have to be sent to the application layer. This implies that, even though the packet has errors, the WiFi stack still has enough information from the packet to determine the correct application on the host, to which the packets are destined.

4.6 Application Layer Forward Error Correction (AL-FEC)

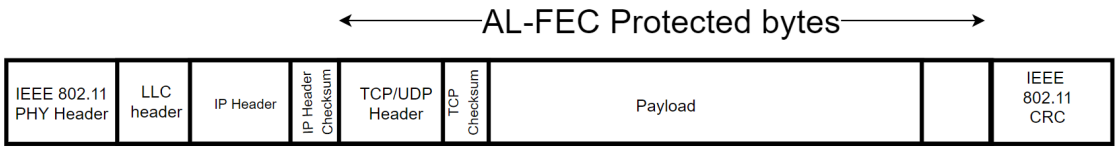

Figure 4.3: Proposed AL-FEC protected bytes

4.6.1 MCS Rate Adaptation with AL-FEC

The rate adaptation algorithms such as Auto Rate Fall-back and Minstrel will normally select the estimated best performing MCS for the current SINR and channel collision probability, however, this MCS selection may not be optimum for a concatenated FEC scheme. Traditionally, the MCS selection is completely controlled at the link layer, however, this research proposes MCS selection at the application layer. MCS selection at the application layer will provide an opportunity to increase the air efficiency, at instances in time whereby the AL-FEC decoder determines it can handle a higher error rate, while gaining channel throughput. WiFi's hybrid autorepeat request is driven by the transmitter, thus the AL-FEC application will need to signal to the transmitter that it requires a higher MCS when it is determined that additional errors introduced at this higher MCS can be error-corrected at the application layer.

The channel is assumed to be slowly changing, otherwise, the AL-FEC adaptation may be unable to respond fast enough to channel conditions. A slowly changing channel condition can often be observed when a user is in a static location while watching a video on a mobile device. A slow changing channel can also occur when the user is moving at a low speed, for example < 30 km/hr.

Such a scheme is shown in Figure 4.4. It is noteworthy that the MCS used for each

transmission when using WiFi must be specified. Thus other applications, which do not have AL-FEC support, can continue to operate on the host without major changes to the IEEE 802.11 standard.

4.6.2 Proposed IEEE 802.11 PHY modification

Previous work on AL-FEC rate adaptation was presented in [104], whereby the multicast channel was used for realization of AL-FEC advantages. This is possible because multicast packets are not acknowledged in the IEEE802.11 standards. However, using the multicast channel has disadvantages, for example all the clients in radio range will inspect the multicast packet to determine if the packet is of interest. Thus, this research work proposes modifying the IEEE 802.11 receiver to send identified unicast packets with CRC errors to the user's network stack. Thus the video server sends signaling information for the packet to the AP. The AP acts on this signaling information to perform a MCS step-up for the specific packet, which carries a video stream payload.

The proposed modification to the ACK process is shown in Figure 4.5 [7], where packets, which have failed CRC at check will still be sent to the application layer.

4.7 Frame Error Rate Estimation for IEEE 802.11

The IEEE802.11 wireless channel can be modeled as a flat fading channel with Jake spectrum. Thus multipath signals will cause the received signal power level to randomly dip below the minimum level for error free decoding. This dip is termed as fading. The time in-between power dips is termed inter-fading state. if we let R_{req} represent the minimum power level required for error free decode, and R_{rms} be the mean received power, then [105][106]:

$$\rho = \frac{R_{req}}{R_{rms}} \tag{4.4}$$

If a random variable t_i represents the inter-fading interval, with a mean of T_i, and t_f

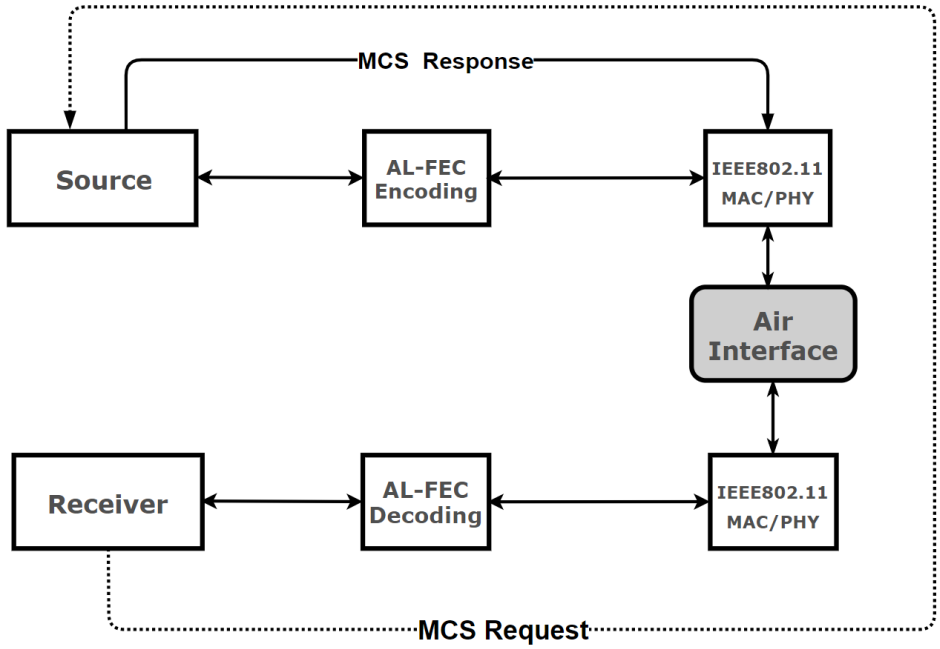

Figure 4.4: Proposed AL-FEC Architecture

represents a random variable representing the fading duration, whose mean value is T_f, then the Frame Error Rate (FER) can be given by [105]:

$$FER = 1 - \frac{T_i}{T_i + T_f} P(t_i > T_p) \tag{4.5}$$

where $PP(t_i > T_p)$ is the probability that the inter-fading interval lasts longer than the frame duration T_p.

If an exponential distribution is assumed for t_i then :

$$P(t_i > T_p) = \exp\left(-\frac{T_p}{T_i}\right) \tag{4.6}$$

The average fading duration for a Rayleigh fading channel is given by [107]:

$$T_i = \frac{\exp(\rho) - 1}{f_d \sqrt{2\pi\rho}} \tag{4.7}$$

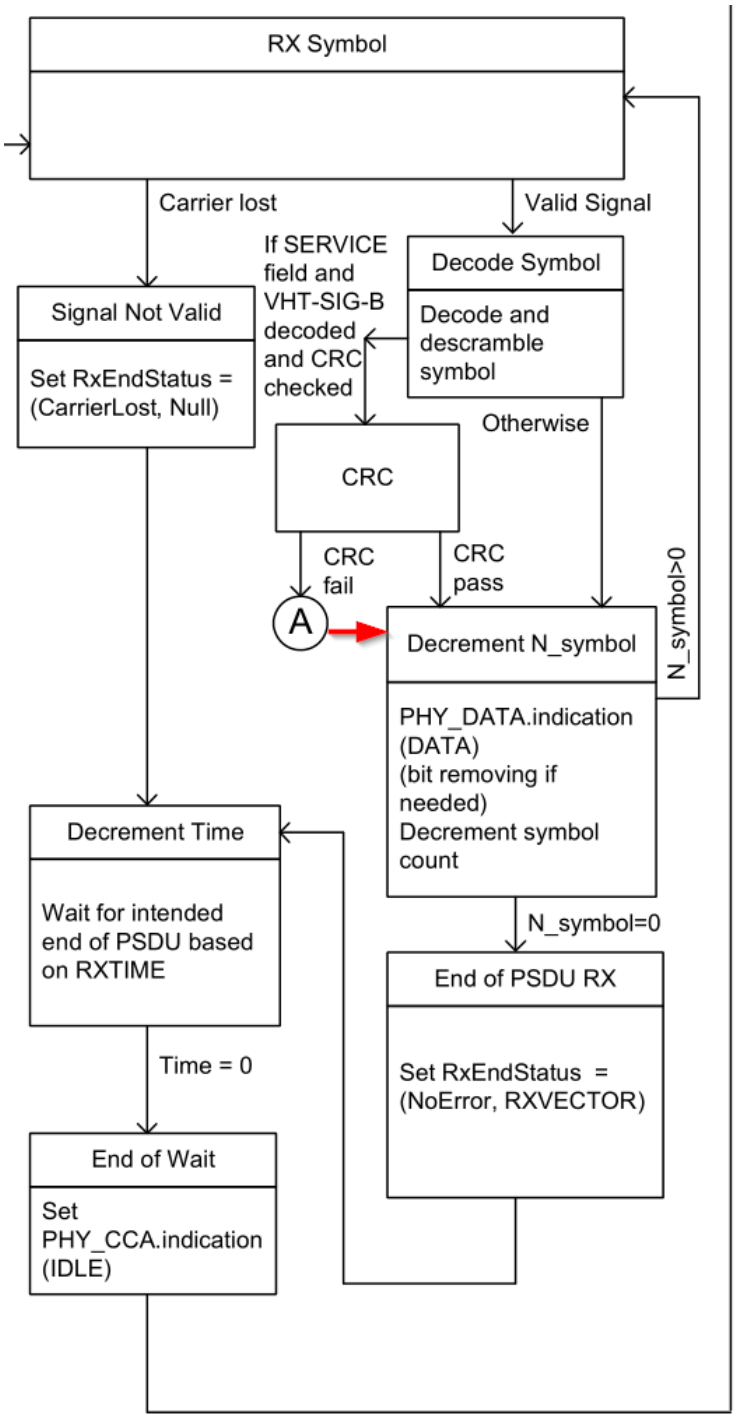

Figure 4.5: IEEE 802.11 receive path modification for AL-FEC packets, arrow shown at label (A) indicates the point at which packets which fail CRC are sent to the application layer [7]

The level crossing rate N_f is given by [105]:

$$N_f = f_d\sqrt{2\pi\rho\exp(-\rho)} \tag{4.8}$$

where f_d is the maximum Doppler frequency $f_d = \frac{v}{\lambda}$ where v is the mobile speed and λ is the wavelength. Also $\frac{1}{N_F} = T_i + T_f$, and so FER can be represented by [105]:

$$FER = 1 - \exp\left(-\rho - f_d\sqrt{2\pi\rho T_p}\right) \tag{4.9}$$

Thus when AL-FEC is active, the TCP throughput expression in Equation 3.33 can be re-written as:

$$T = \min\left(\frac{1}{RTT}\sqrt{\frac{3}{2\cdot FER_{n,k}}}, \frac{k\mu}{n}\right) \tag{4.10}$$

where $FER_{n,k}$ is the frame error rate after AL-FEC.

And $FER_{n,k}$ is:

$$FER_{n,k} = \sum_{i=0}^{k-1}\binom{n}{i}(1-FER)^i\, FER^{n-i}\frac{n-i}{n} \tag{4.11}$$

4.7.1 Rate adaptation analysis

The rate adaptation analysis will be an extension of the work by Choi *et al.* [33], whereby the proposed model incorporates the reduced error rate when AL-FEC is applied to the packet. The rate adaptation algorithm is Auto-Rate Fallback (ARF)[52]. ARF operates thus:

1. Assign each MCS rate an index from 1 ... L. These MCS rates are assigned by the IEEE802.11[7] standards. Begin with MCS value $\lfloor\frac{L}{2}\rfloor$, where L is the max MCS. The throughput at each MCS index is given by $R_1 < R_2 < ... < R_L$. For each rate R the corresponding frame error rate e is less than the next data rate error rate, thus,

$e_1 \leq e_2 \leq ... \leq e_L$. The current data rate is represented as $r(t) \in 1, 2, ..., L$.

2. Represent the collision probability with p. Similar to the Bianchi Markov Model [26], the collision probability is assumed to be independent of transmission state. Thus the conditional frame failure probability p_i, caused by collision or noise, at each MCS index i, is given by [33]:

$$p_i = 1 - (1 - p)(1 - e_i) \tag{4.12}$$

Representing each MCS index as i, the unique equilibrium probability of using each MCS can be represented as Π_i. This probability can be represented by[33]:

$$\Pi_i = \sum_{k=-\theta_{\mathrm{d}}+1}^{\theta_{\mathrm{u}}+1} r_{i,k}, \qquad 1 \leq i \leq L, \tag{4.13}$$

where $r_{i,k} = \lim_{t\to\infty} P\{r(t) = i, c(t) = k\}$

3. Set an upper threshold θ_u and a lower threshold θ_d

4. Represent the counter of consecutive successes or failures as $c(t)$. If $c(t) > 0$, then we have consecutive successes, otherwise, $c(t) < 0$ indicates we have consecutive failures at current rate $r(t)$, thus $c(t) : (-\theta_d + 1 \leq c(t) \leq \theta_u - 1)$.

5. After θ_u consecutive successful transmissions at current MCS value, increase MCS, if MCS is less than L, the maximum value.

6. After θ_d consecutive transmission failures, reduce the MCS, unless the MCS is at the minimum value.

Let $c(t) = (-\theta_d + 1 \leq c(t) \leq \theta_u - 1)$ denote the counter of transmission failures at rate $r(t)$.

Similar to Bianchi's Model [26], we define a Markov chain, which is driven by the point process of frame transmission events, with rate index $r(t)$, and a consecutive failure counter

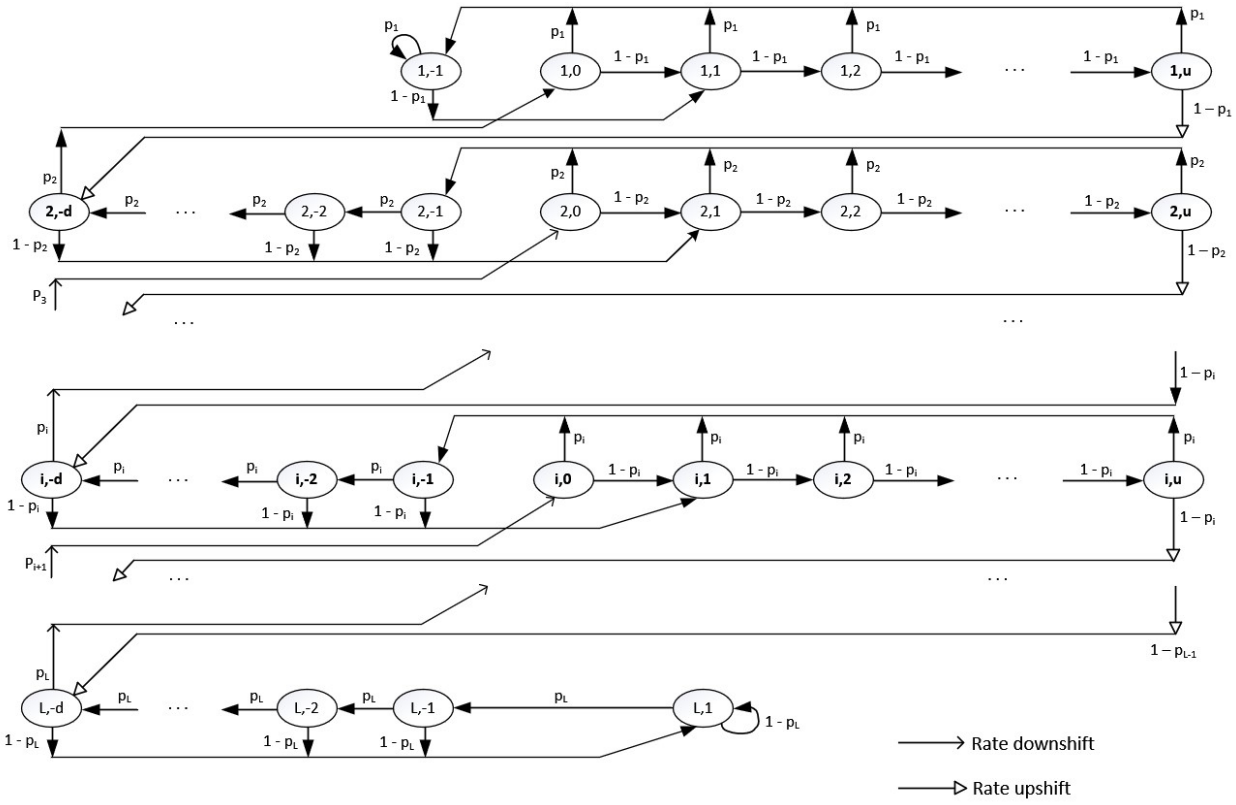

Figure 4.6: Rate Adaptation Markov Model [33]

$c(t)$. The model is discrete time and indexed by t, the end time of the t-th transmission event of a station. The ARF Markov chain $(r(t), c(t))$ is shown in Figure 4.6.

The regularities of the ARF Markov chain allows a closed form solution for Π_i, as a function of the system parameters p_i, θ_d, and θ_u. This can be done by first transforming the ARF chain to a birth-death chain. The birth-death chain consists of states which aggregate the states corresponding to $r_{i,k}$ for different counter states. These counter stages are aggregated into a single macro stage with $i : (i \in 1, ..., L)$.

The equilibrium distribution of steady-state birth-death Markov chain with birth rates λ_i $(i \in \{1, 2, ..., L-1\})$ and death rates μ_i $(i \in \{2, ..., L\})$ is given by [33][108]:

$$\Pi_1 = \frac{1}{1 + \sum_{j=1}^{L-1} (\prod_{k=1}^{j} \frac{\lambda_k}{\mu_{k+1}})} \text{ and } \Pi_i = \frac{\lambda_{i-1}}{\mu_i} \Pi_{i-1}, \tag{4.14}$$

If we denote the MCS step-up rate, and MCS step-down rate respectively as λ_i and μ_i, and inspecting the model in Figure 4.6 the transition rates are:

$$\lambda_i = \frac{r_{i,u} P\{i+1, -d | i, u\}}{P\{\text{current rate} = R_i\}} = \frac{r_{i,u}}{\Pi_i}(1 - p_i) \tag{4.15}$$

$$\mu_i = \frac{r_{i,-d} P\{i-1, 0 | i, -d\}}{P\{\text{current rate} = R_i\}} = \frac{r_{i,-d}}{\Pi_i} p_i \tag{4.16}$$

The parameters used in the model shown in Figure 4.6 obey these balance equations [33]:

$$r_{i,k} = (1 - p_i) r_{i,k-1}, \quad 1 \leq i < L, \ 2 \leq k \leq u \tag{4.17}$$

$$r_{i,k} = p_i r_{i,k+1}, \quad 1 < i \leq L, \ -d < k \leq -2 \tag{4.18}$$

where Equation 4.17 shows the state $r_{i,k}$ is the product of the probability of increasing rate state $1 - p_i$, and the previous state $r_{i,k-1}$. This product is for any of the rates $1..L$

Applying the Markov recursive multiplication property to Equation (4.17) and (4.18)

yield:

$$r_{i,k} = (1-p_i)^{k-1} r_{i,1}, \qquad 1 \le i < L,\ 1 \le k \le u \tag{4.19}$$

$$r_{i,k} = p_i^{-(k+1)} r_{i,-1}, \qquad 1 < i \le L,\ -d < k \le -1. \tag{4.20}$$

Additional Markov chain balance equations for Figure 4.6 are:

$$r_{i,1} = (1-p_i) \sum_{k=-d}^{0} r_{i,k}, \qquad 1 \le i < L \tag{4.21}$$

where $r_{i,1}$ models the transition to retransmission back-off count 1 at any MCS rate.

$$r_{i,-1} = p_i \sum_{k=0}^{u} r_{i,k} \qquad 1 \le i \le L \tag{4.22}$$

$$r_{i,0} = p_{i+1} r_{i+1,-d}, \qquad 1 \le i < L \tag{4.23}$$

$$r_{i,-d} = p_i r_{i,-d+1} + (1-p_{i-1}) r_{i-1,u}, \qquad 1 < i \le L \tag{4.24}$$

Splitting Π_i into two parts, so as to apply substitutions from Equations (4.19) and (4.21)

$$\Pi_i = \sum_{k=-d}^{u} r_{i,k} = \sum_{k=-d}^{0} r_{i,k} + \sum_{k=1}^{u} r_{i,k}. \tag{4.25}$$

$$\Pi_i = \frac{r_{i,1}}{1-p_i} + r_{i,1} \sum_{k=1}^{u} (1-p_i)^{k-1}$$

$$= \frac{1-(1-p_i)^{u+1}}{p_i(1-p_i)} r_{i,1} = \frac{1-(1-p_i)^{u+1}}{p_i(1-p_i)^u} r_{i,u}. \tag{4.26}$$

Applying Equation (4.26) to Equation (4.15):

$$\lambda_i = \frac{r_{i,u}}{\Pi_i}(1-p_i) = \frac{p_i(1-p_i)^{u+1}}{1-(1-p_i)^{u+1}} = \frac{p_i(1-p_i)^{\theta_u}}{1-(1-p_i)^{\theta_u}} \tag{4.27}$$

Re-writing Π_i to enable substitutions from Equation (4.20), (4.22) and (4.18) [33]:

$$\Pi_i = \sum_{k=-d}^{u} r_{i,k} = r_{i,-d} + \sum_{k=-d+1}^{-1} r_{i,k} + \sum_{k=0}^{u} r_{i,k}. \tag{4.28}$$

$$\begin{aligned} \Pi_i &= r_{i,-d} + \frac{1-p_i^{d-1}}{1-p_i} r_{i,-1} + \frac{r_{i,-1}}{p_i} \\ &= r_{i,-d} + \frac{1-p_i^{d}}{(1-p_i)p_i} r_{i,-1} \\ &= r_{i,-d} + \frac{1-p_i^{d}}{(1-p_i)p_i^{d-1}} r_{i,-d+1}. \end{aligned} \tag{4.29}$$

Using the definition of λ_i, we have [33]:

$$(1-p_{i-1})r_{i-1,u} = \lambda_{i-1}\Pi_{i-1} \tag{4.30}$$

And the balance equation for the birth-death chain:

$$\lambda_{i-1}\Pi_{i-1} = \mu_i \Pi_i \tag{4.31}$$

Applying (4.30) and (4.31) to Equation (4.24):

$$r_{i,-d} = p_i r_{i,-d+1} + \mu_i \Pi_i = p_i r_{i,-d+1} + p_i r_{i,-d} \tag{4.32}$$

this yields:

$$r_{i,-d+1} = \frac{1-p_i}{p_i} r_{i,-d}. \tag{4.33}$$

Substituting Equations (4.33) into Equation (4.29) gives:

$$\Pi_i = r_{i,-d} + \frac{1-p_i^d}{(1-p_i)p_i^{d-1}} \frac{1-p_i}{p_i} r_{i,-d} = \frac{1}{p_i^d} r_{i,-d}. \tag{4.34}$$

$$\mu_i = \frac{r_{i,-d}}{\Pi_i} p_i = p_i^{d+1} = p_i^{\theta_d}. \tag{4.35}$$

and the step-down rate μ_i represented by

$$\mu_i = p_i^{\theta_d} \tag{4.36}$$

Using equations 4.27 and 4.36, the probabilities Π_i can be evaluated.

4.7.2 AL-FEC Aware Rate Adaptation

When AL-FEC is enabled, the probability of packet failure is reduced. Thus if p_{FEC} represents the failure probability after FEC, then $p > p_{FEC}$ and consequently the probability of transmission success $1 - p_{FEC}$ is greater than when not using FEC. Thus a system using AL-FEC can be modeled as one without AL-FEC by modifying the failure probability to include the AL-FEC gains. θ_u and θ_d remain the same value in the AL-FEC system. Thus the AL-FEC feature enables the MCS rate to go higher for AL-FEC enabled stations.

Substituting the AL-FEC related parameters to Equation (4.27) and (4.36), we get:

$$\mu_{FEC_i} = \left(p_{FEC_i}\right)^{\theta_d} \tag{4.37}$$

$$\lambda_{FEC_i} = \frac{p_{FEC_i}\left(1-p_{FEC_i}\right)^{\theta_u}}{1-\left(1-p_{FEC_i}\right)^{\theta_u}} \tag{4.38}$$

4.7.3 Rate Adaptation Performance Indicator

To compare rate adaptation of different algorithms, and also between AL-FEC systems, this thesis proposes a Rate Adaptation Performance Indicator (RPI). RPI is given by:

$$RPI = \sum_{i=1}^{L} L_i \times t_i \tag{4.39}$$

where L_i represents each MCS value, and t_i is the probability of using the MCS value L_i.

A RA algorithm with higher probability of using high MCS index will have a higher RPI, compared to a RA algorithm which underestimates the opportunity to utilize a higher MCS index. Thus for all RA algorithms, such as ARF, Minstrel and so on, RPI will be higher when AL-FEC is enabled.

The minimum value of RPI will be 1, when all transmissions are sent at the lowest MCS, and the maximum value of RPI will be L when all transmissions are sent at the highest MCS.

4.8 AL-FEC Simulation

4.8.1 Dynamic Rate Adaptation behavior

A simulation was performed to determine the dynamic selection behavior of the MCS adaptation, while ramping up and down the SINR. The experimental setup is shown in Figure 4.7. Two instances of this experiment are executed with parameters listed in Table 4.3. In the first instance, the AL-FEC blocks in Figure 4.7 are disabled, and in the second instance the AL-FEC blocks are enabled. The selected MCS in Figure 4.8 shows the result of the simulation comparing the rate adaptation algorithm with and without AL-FEC. It can be seen that when AL-FEC is enabled, the receiver will select with increasing probability, a higher order modulation MCS. This is because the MCS selection decision is based on resid-

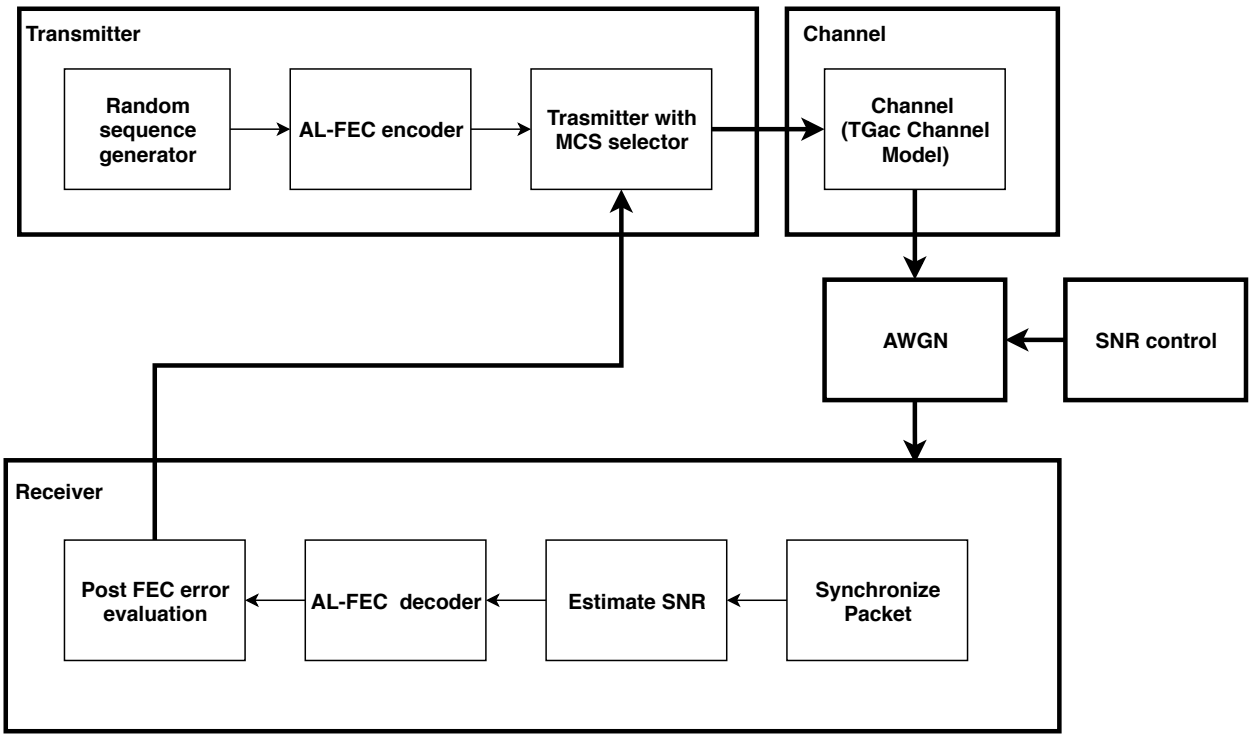

Figure 4.7: Dynamic Rate Adaptation Experiment Setup

ual error rates. When AL-FEC is turned on, the residual error rate is reduced. A reduction in the residual error rate drives a more complex MCS, which also has a higher throughput.

Table 4.3: Simulation parameters for dynamic MCS control

IEEE 802.11 Parameter	**Value**
Channel Bandwidth	40MHz
Channel Model	TGac Model-D
Minimum SNR	8dB
Max SNR	36dB
SNR increment	0.5dB

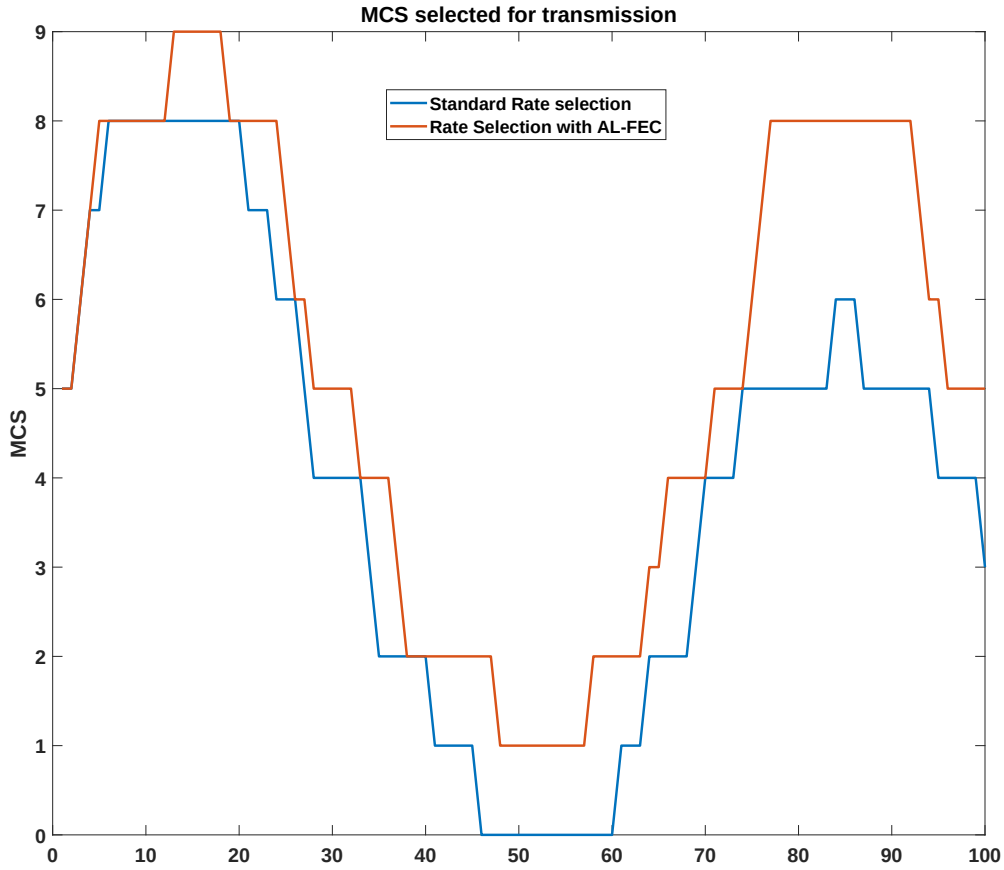

Figure 4.8: Dynamic Rate Adaptation Switching Simulation Using ARF-RA and AL-FEC/ARF

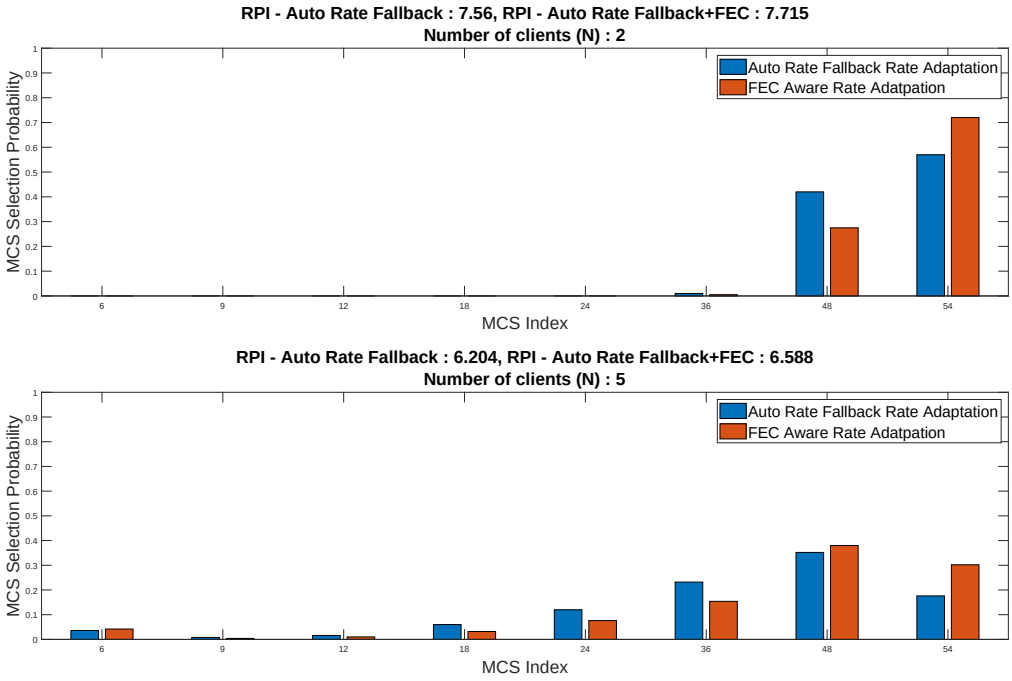

Figure 4.9: Rate Adaptation Performance Indicator, N = 2, 5

4.8.2 Rate Adaptation Performance Simulation

A rate adaptation simulation was performed to compare two systems. System A used the ARF Rate Adaptation without AL-FEC, while system B enhances ARF with AL-FEC.

As shown in Figures 4.9 and 4.10, the MCS selection behavior of ARF with AL-FEC is to, with higher probability, use more complex MCS combinations. Thus when AL-FEC is enabled, the RPI in increased. The RPI from the experimental results corresponding to Figures 4.9 and 4.10 are shown in Table 4.4.

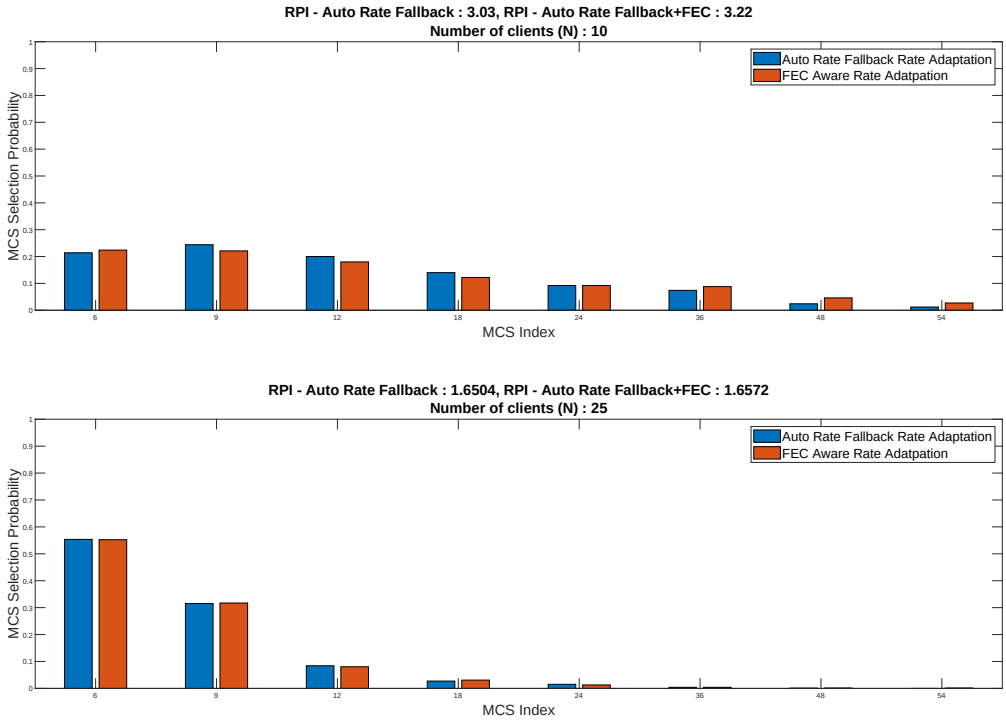

Figure 4.10: Rate Adaptation Performance Indicator, N = 10, 25

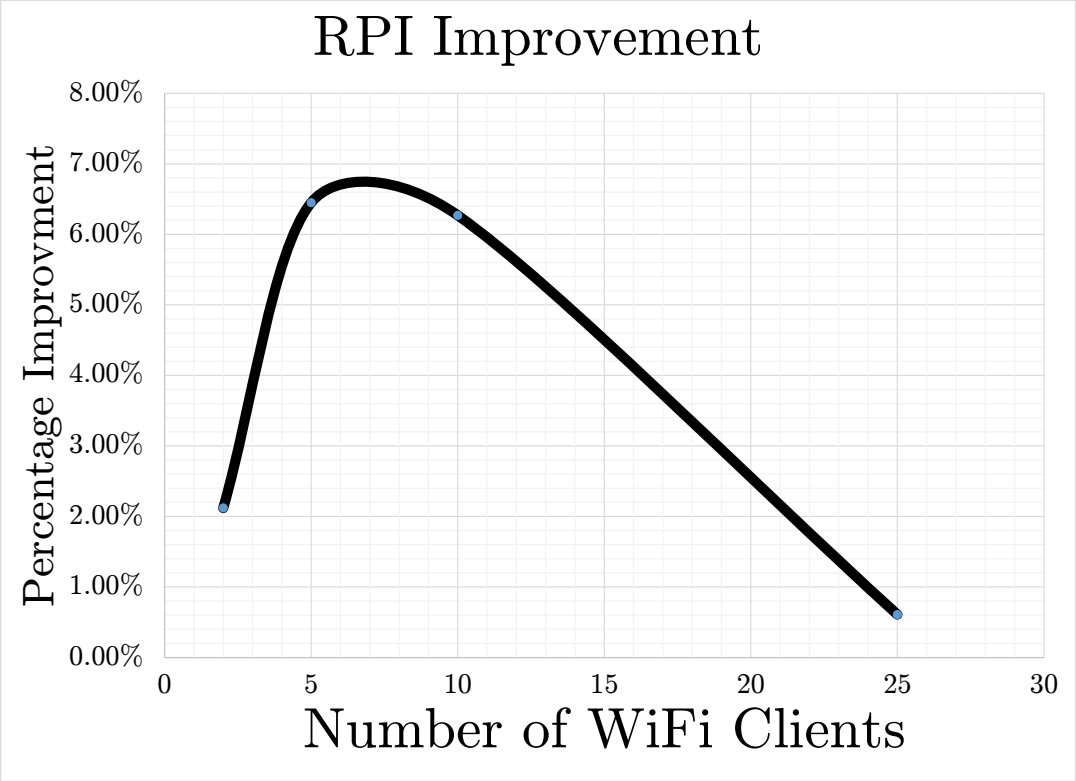

Figure 4.11: Rate Adaptation Performance Index improvement when using proposed AL-FEC system

Table 4.4: Rate Adaptation Performance Index(RPI)

Number of Clients	**ARF RPI**	**ARF+FEC RPI**	**RPI improvement**
2	7.56	7.72	2.12%
5	6.20	6.60	6.45%
10	3.03	3.22	6.27%
25	1.65	1.66	0.61%

4.9 Summary

This Chapter has proposed a AL-FEC mechanism for increasing the air efficiency of WiFi transmissions by enabling AL-FEC. To enable packet recovery at the application layer, it has been proposed in this chapter to modify the IEEE802.11 to allow packets, which have decoded the *VHT-SIG-B* field correctly, but fail *CRC* to be sent to the application layer. Thus the application layer will recover these packets with a higher probability of success. A mathematical model for ARF was extended to compare ARF+AL-FEC rate adaptation. To quantify the improvements to rate adaptation, the RPI metric was introduced. The RPI metric was used to compare standard ARF rate adaptation to ARF+AL-FEC, which showed improvements in higher complexity MCS selection probability, thus leading to higher air efficiency.

Chapter 5

Proposed Video Delivery System Architecture

5.1 Introduction

Video transport over a wireless channel, with a final presentation on mobile devices has become a pervasive method of content delivery in recent times. Because of the challenges encountered with video delivery over wireless devices, many approaches have been undertaken to provide a good user experience by service providers. These approaches include compression of the video bit-stream using protocols such as the High Efficiency Video Coding standard (H.265). Other methods include reducing the video resolution when transport bandwidth is low, and increasing the resolution on bandwidth improvement. Advances in wireless technologies regarding bit-rates have also made it possible to use ever increasing video bit rates. Thus a constant goal of a service provider is to provide a good user experience by using the highest video quality supported for the effective throughput on the wireless channel.

In this study, we consider an architecture which opportunistically increases the complexity

of the wireless channel modulation and coding scheme (MCS). Thus when the controlling entity on the wireless video display device determines that it can recover from errors residual after link-layer forward error correction, such a MCS will be selected. The more complex MCS will have a higher packet throughput, and will deliver a higher quality video stream as a consequence.

We consider a Quality of Experience index, estimated based on two objective metrics - (1) Video resolution and (2) Video stall frequency.

5.2 Proposed Video Delivery System Architecture

The proposed system architecture is as shown in Figure 5.1. The video server sends small chunks of files to the client. The video server has features to select a file resolution, based on a request from the client. The server also has capabilities to encode the selected video file. Also, based on the request from the client, the video server indicates the requested MCS to the network, and depending on the wireless exit point, the wireless access point will use the requested MCS. The MCS signaling to the access point can be achieved by setting fields in the IP/TCP header, or by a direct application programming interface, if the wireless network is under the same administrative domain. The client has knowledge of the MCS it decoded, and this is sent to the application layer of the client device. Because the MCS used for packet transmission is set on a per packet basis , the application layer for the video delivery will set the MCS of only packets for the video stream. The application layer also tracks the MCS used for other client packets, which is determined by the link layer rate adaptation algorithm (RAA). The MCS selected by the link layer RAA is determined by link layer protocols such as SoftRate [50], Minstrel[55] and AutoRate Fallback [52].

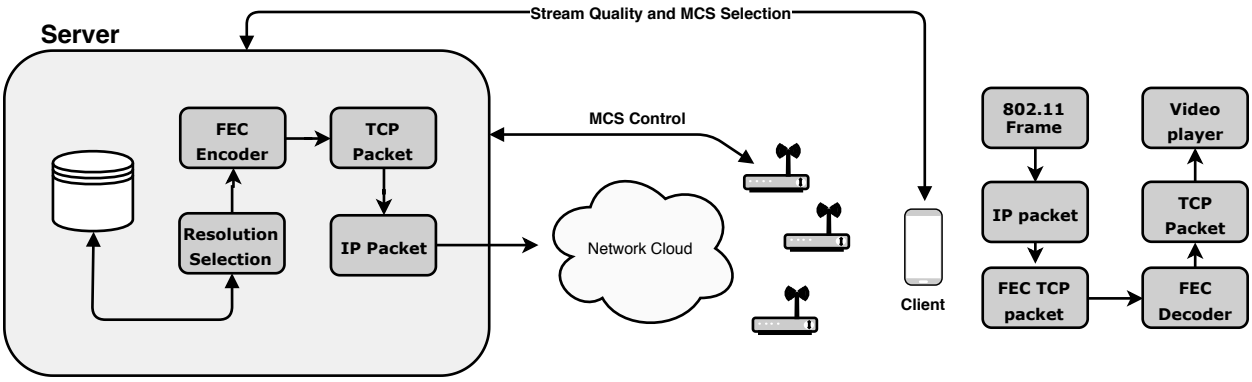

Figure 5.1: End-to-End System Architecture

5.3 Proposed Video Delivery System Architecture Compared to Standard State-of-the-Art Architectures

The key difference between the proposed video delivery architecture, and state of the art, is the feedback channel, by which stream quality and MCS selection requests can be sent. This feedback channel enables the following capabilities:

1. **Leveraging AL-FEC capabilities on a client device** - Standard video delivery architectures rely on the data link layer to ensure packet integrity. This link layer, which is normally hardware based, is usually limited in features, to reduce costs, and maintain compatibility with established IEEE802.11 standards. Thus packets which are in error will be re-transmitted with the HARQ mechanism on the datalink layer. With the proposed video architecture, the processing capability of the client device can be fully utilized to enhance error correction performance of the delivered packets.

2. **Increase air efficiency by using higher complexity MCS** - With the proposed video delivery architecture, the client is able to specify a MCS, which it has the processing capability to support. Thus higher PHY error rates could be supported due to more efficient error correction codes at the application layer.

5.4 Video Delivery Algorithm

To achieve an improved QoE using the features of AL-FEC aware rate control, two algorithms are used. One on the client side, and the other on the server side. The client algorithm inspects the current MCS selected by the data link rate control algorithm, for other data streams. Using the knowledge of the wireless channel, which is obtained from the data link MCS selection, the algorithm running on the receiver can request a higher throughput MCS, if the conditions permit. This algorithm is shown as Algorithm 1.

Algorithm 1 - Video delivery Algorithm - Client side:

Input: Current Link Layer MCS (LLMCS), Current BER from Link layer RA process, MCS_{min} from Link Layer Rate Adaptation table;

Output: Next MCS for current stream

1: **while** *More packets to be sent* **do**
2: Buffer Current Packet;
3: Decode Current Packet;
4: **if** *No Packet Errors* **then**
5: Pass packet to video layer;
6: **if** $BER < BER_{Threshold}$ and $MCS < MCS_{max}$ **then**
7: $MCS = MCS + 1$
8: **end**
9: **else**
10: **if** $MCS > MCS_{min}$ and $MCS > LLMCS$ **then**
11: $MCS = MCS - 1$;
12: **end**
13: **if** $MCS > MCS_{min}$ and $MCS \leq LLMCS$ **then**
14: $MCS = LLMCS$;
15: **end**
16: **end**
17: **end**

Algorithm 1, which operates at the client, accepts as input, the current MCS, and bit error rate from the host's rate adaptation data table. Then in line 2, the algorithm accepts the packet, and decodes the packet in line 3. If after FEC decode, there are no errors, then the video is passed to the video application in line 4. If the BER is very low at the current MCS, such that it is below a set threshold, whereby AL-FEC can recover much greater

amounts of errors, then there is step-up in MCS on line 7, otherwise the MCS is kept the same. If the algorithm does not execute the steps 4 - 9, it means that there were packet errors after decoding, and the MCS may need to be stepped down. On line 10, the algorithm checks if the MCS is greater than the minimum, and also greater than the link layer MCS. If both conditions are satisfied, the MCS is reduced. Otherwise, in line 13, the algorithm tests to see if the current MCS is the Link layer MCS, if this is the case the AL-FEC algorithm does not step down the MCS. Algorithms 1 is invoked when the AL-FEC aware client wants to receive video packets, while Algorithm 2 is always running and listening for client MCS packet indication from Algorithm 1.

Algorithm 2 - Video Delivery Algorithm - Server Side:

Input: Requested MCS

Output: Next Packet with MCS tag

1: **while** *More packets to be sent* **do**
2: Listen for packet request;
3: Accept incoming packet request;
4: Tag packet for MCS selection;
5: **end**

The server side algorithm is shown in Algorithm 2, which accepts MCS recommendations from the client, and then tags the packet with the requested MCS step up.

5.4.1 Video QoE

Video quality metrics such as stalling frequency, and resolution, can be used to estimate a subscriber's Quality of Experience when consuming video services. The Quality of Experience criteria will be determined based on the video delivery format. For reliable protocol based delivery, such as HTTP Live stream and Dynamic Streaming over HTTP (DASH),

which fill up buffers before presenting the video content, the Quality of Experience at a specific video resolution is effectively based on the buffer run out probability, for each video resolution. Streaming protocols are usually implemented with multiple resolutions such as 240 progressive lines (240p), 360p, commonly up to 2160p resolution. Thus in a user session, based on the current wireless channel throughput, the following events can occur:

1. Video quality which can be supported can adapt to increase or decrease display resolution

2. Video resolution stepping can result in a buffer underflow, which results in video stalling

Because current video streaming mechanisms use discrete resolutions, we can represent a video quality drop with an integer representing the distance from the original resolution.

Modern video streaming protocols utilize reliable protocols as the transport mechanism. The most widely used reliable protocol is TCP. Thus Quality of experience can be estimated with two parameters:

1. **Source referenced video frame resolution**. If an index is assigned to the source with increasing numbers as the resolution is increased, then, on video playback, if the streaming algorithm selects a lower bit rate stream, the video metric can be represented as the difference between the index of the source X and that of the play back resolution R.

2. **Frame stalling frequency** - This metric tracks the frequency that the video playback stalls. Stream adaptation algorithms select a lower quality bit-stream when it is determined that the network bit rate cannot support the current video resolution. When the playback buffer fills up significantly faster than real-time playback, streaming protocols will select a higher rate bit stream, which will provide a better video resolution.

Table 5.1: Example Video Streaming Resolution Table

Format Name	**Video Resolution** (pixels)	**Video Bitrate** (Mbps)	**Quality Weight** (P_n)
2160p	3840x2160	35	7
1440p	2560x1440	16	6
1080p	1920x1080	8	5
720p	1280x720	5	4
480p	854x480	2.5	3
360p	640x360	1	2
240p	426x240	0.3	1

5.5 Video QoE Estimation

As stated in section 5.4.1, the estimated QoE is a combination of the per frame quality, and the annoyance from stalling videos. Video quality assessment algorithms operate on a frame by frame basis. Thus the video quality estimation process compares individual decoded images after receiving the video stream. The presentation quality per frame can be represented as P_n, which estimates each frame quality R_n with reference to the highest frame quality X_n in the discrete set of resolutions.

$$P_n = V(X_n, R_n) \tag{5.1}$$

where X_n represents the maximum video resolution of frame n at the source, and R_n the resolution of the received video.

For each video stall event the quality at stall will be that of the last video frame.

$$P_n = P_{n-1}. \tag{5.2}$$

This thesis proposes using a set of increasing integer values P_n.

The intuition in using integer values derives from the quantitative measures obtained

Figure 5.2: 4K reference image [109]

Figure 5.3: 4K image scaled to 240p [109]

when using state-of-the-art video image quality analysis. Experimental results using SSIM[110], MSSIM [65], and other image quality analysis methods produce results depending on the specific image being evaluated. When comparing two different video resolutions of the same content, using state-of-the-art methods, the higher resolution will in general, have a higher quality metric. However, the numerical value of the image quality metric per scene is dependent on the specific image, and thus the metric value of the image quality varies, although the quality has remained constant. Using a single numerical integer for a video quality at a specific resolution is thus reasonable approach.

For example, Figure 5.2 is of 2160p resolution and Figure 5.3 is a 240p resolution reproduction of the same image. Comparing the 2160p image and the 240p image, the SSIM is 0.93. Also, as shown in Figures 5.5-5.8 and Tables 5.2-5.3, the subjective quality indicator (SQI) of image quality algorithms, have different numerical ranges, which will require a transformation to map into a mean opinion score (MOS) scale.

Thus a step down in video quality because of stalling can be represented by the difference in index weights, this difference is scaled accordingly. An example video quality set is shown in Table 5.1.

The QoE dissatisfaction of each stall event can be modeled using the Ebbinghaus forgetting curve [111][112]:

$$M = \exp\left\{-\frac{t}{T}\right\} \tag{5.3}$$

where M is the memory retention, T is the relative strength of memory, and t is the time instance.

If the k-th stalling event is at $[i_k, i_k + l_k]$, where l_k is the length of k-th stalling event, and i_k is the time interval denoting the beginning of the stalling event, a piecewise model is

constructed to estimate the impact of each stalling event on the QoE [113]:

$$S^k(t) = \begin{cases} P_{i_k-1}\left(-1+\exp\left\{-\left(\dfrac{tf-i_k}{T_0}\right)\right\}\right) & \frac{i_k}{f} \le t \le \frac{i_k+l_k}{f} \\ P_{i_k-1}\left(-1+\exp\left\{-\left(\dfrac{l_k}{T_0}\right)\right\}\right) & \\ \cdot\left(\exp\left\{-\left(\dfrac{tf-i_k-l_k}{T_1}\right)\right\}\right) & t > \frac{i_k+l_k}{f} \\ 0 & \text{otherwise} \end{cases} \tag{5.4}$$

where f is the frame rate in frames/second, and T_0, T_1 and $S^k(t)$ represent the rate of dissatisfaction, the relative strength of memory and the experience of the k-th stalling event at time t, where $k = 1, 2, ..., N$ and N is the number of stalling events.

QoE drop due to stalling events is computed by aggregating the QoE drop caused by each stalling event and is given by [34]

$$S(t) = \sum_{k=1}^{N} S^k(t) \tag{5.5}$$

N is the upper limit of total dissatisfaction, which is equivalent to the number of stalls, and it depends on the total length of the video stream. And the cumulative QoE drop over all time is given by:

$$G(N) = \int_{-\infty}^{\infty} S(t)dt, \text{ for } l_k = \frac{L}{N}, k = 1, 2, ..., N \tag{5.6}$$

where L is the total length of stalling and, if equal stall durations are assumed, $\frac{L}{N}$ will represent the length of each individual stall. Equation 5.6 decreases monotonically with respect to N. Thus the higher the number of stalls, the lower the QoE because of the annoyance effect of video stalling. By substituting Equations (5.4) and (5.5) to its terms, can be simplified as follows: If the quality loss at each stall is assumed to be a constant $P_n = C$,

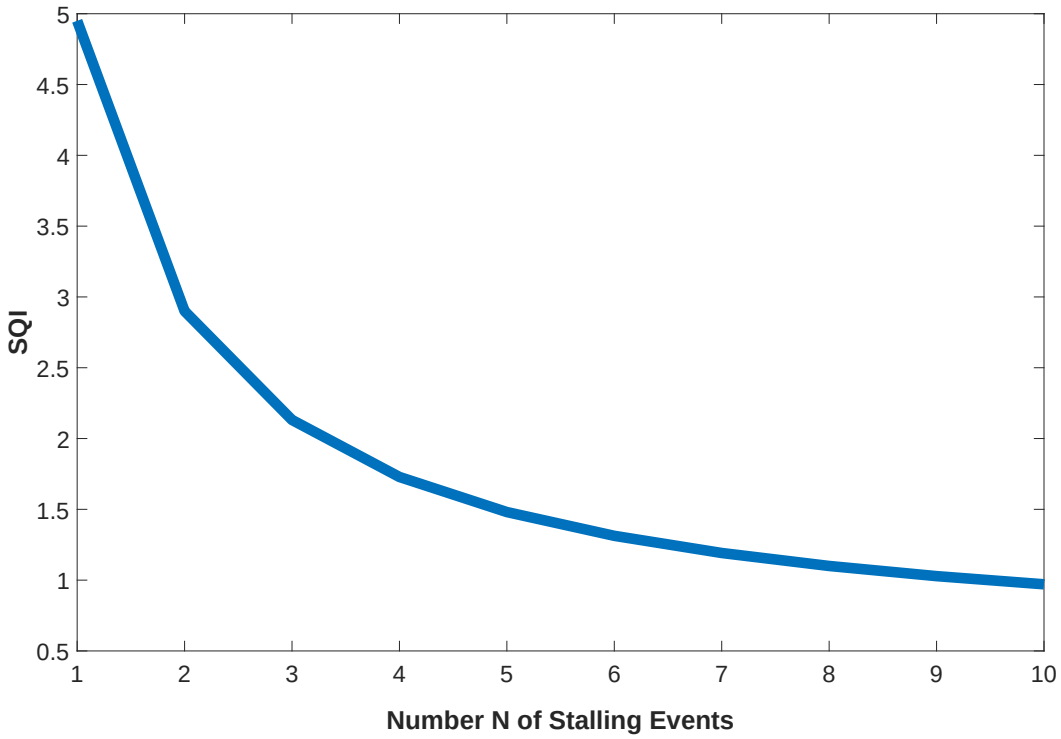

Figure 5.4: SQI reduction with number of stalls - This shows the Subjective Quality Indicator drop as the number of stalling events increases in a time interval

Figure 5.5: 4K Reference image - Horses [114]

Figure 5.6: 4K Reference image - Loader [115]

Figure 5.7: 4K Reference image - Locomotive [116]

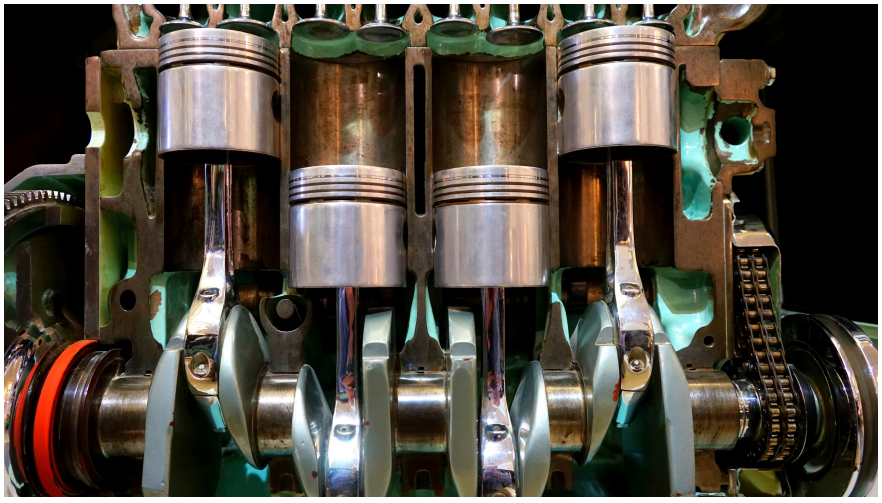

Figure 5.8: 4K Reference image - Pistons [117]

a) SSIM

Resolution	Horses	Loader	Locomotive	Pistons
2560x1440	0.98	0.90	0.94	0.96
1920x1080	0.96	0.85	0.91	0.95
1280x720	0.94	0.77	0.86	0.92
854x480	0.89	0.68	0.78	0.87
640x360	0.85	0.62	0.71	0.82
426x240	0.78	0.56	0.62	0.74

b) PSNR

Resolution	Horses	Loader	Locomotive	Pistons
2560x1440	37.22	31.20	34.64	35.63
1920x1080	34.76	28.42	31.73	33.56
1280x720	31.71	25.63	28.24	30.99
854x480	28.58	23.74	25.38	28.58
640x360	27.23	22.81	23.81	27.01
426x240	25.04	21.82	21.95	25.02

Table 5.2: QoE metrics **a**) Structural Similarity (**SSIM**) **b**) Peak Signal to Noise Ratio (**PSNR**)

a) MSE

Resolution	Horses	Loader	Locomotive	Pistons
2560x1440	12.35	49.28	22.34	17.79
1920x1080	21.72	93.55	43.71	28.64
1280x720	43.87	177.95	97.58	51.76
854x480	90.09	275.11	188.46	90.10
640x360	123.05	340.67	270.44	129.41
426x240	203.69	427.88	414.99	204.66

b) MSSSIM

Resolution	Horses	Loader	Locomotive	Pistons
2560x1440	1.00	0.98	0.99	0.99
1920x1080	0.99	0.97	0.98	0.99
1280x720	0.98	0.94	0.96	0.98
854x480	0.96	0.89	0.92	0.96
640x360	0.94	0.84	0.88	0.93
426x240	0.89	0.78	0.81	0.89

Table 5.3: QoE metrics **a**) Mean Squared Error **MSE b**) Multiscale Structural Similarity **MSSSIM**

Figure 5.9: SSIM Image quality metrics - For the same resolution drop, the SSIM is different depending on image. Image resolution index 1 corresponds to 1 step down from maximum resolution, index 2 represents a 2 level drop and so on

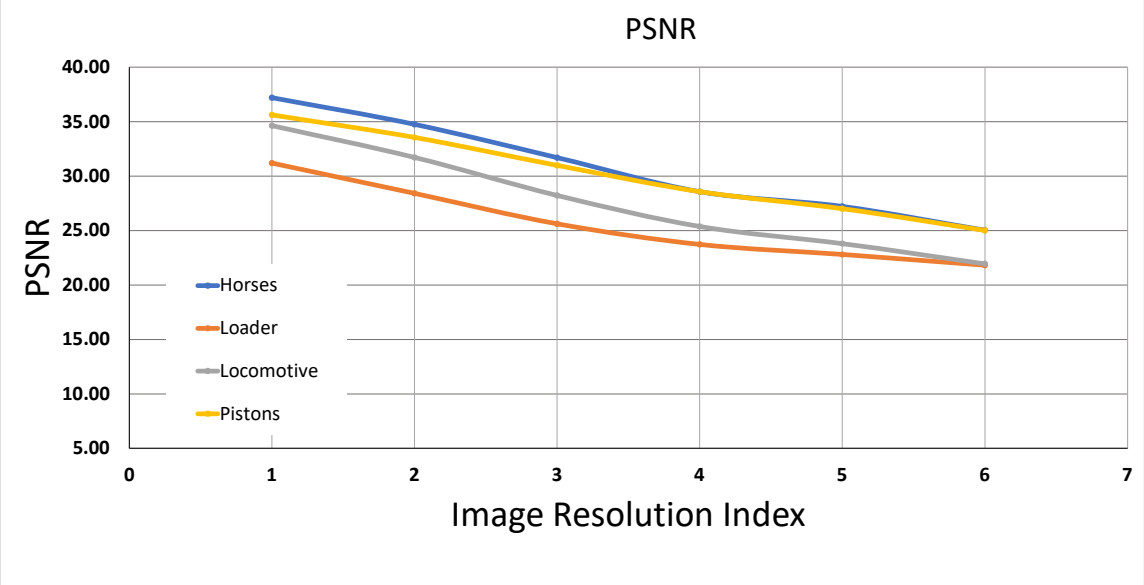

Figure 5.10: PSNR Image quality metric for different images, at the same resolutions

Figure 5.11: MSE Image quality metrics for the same resolution range using different images

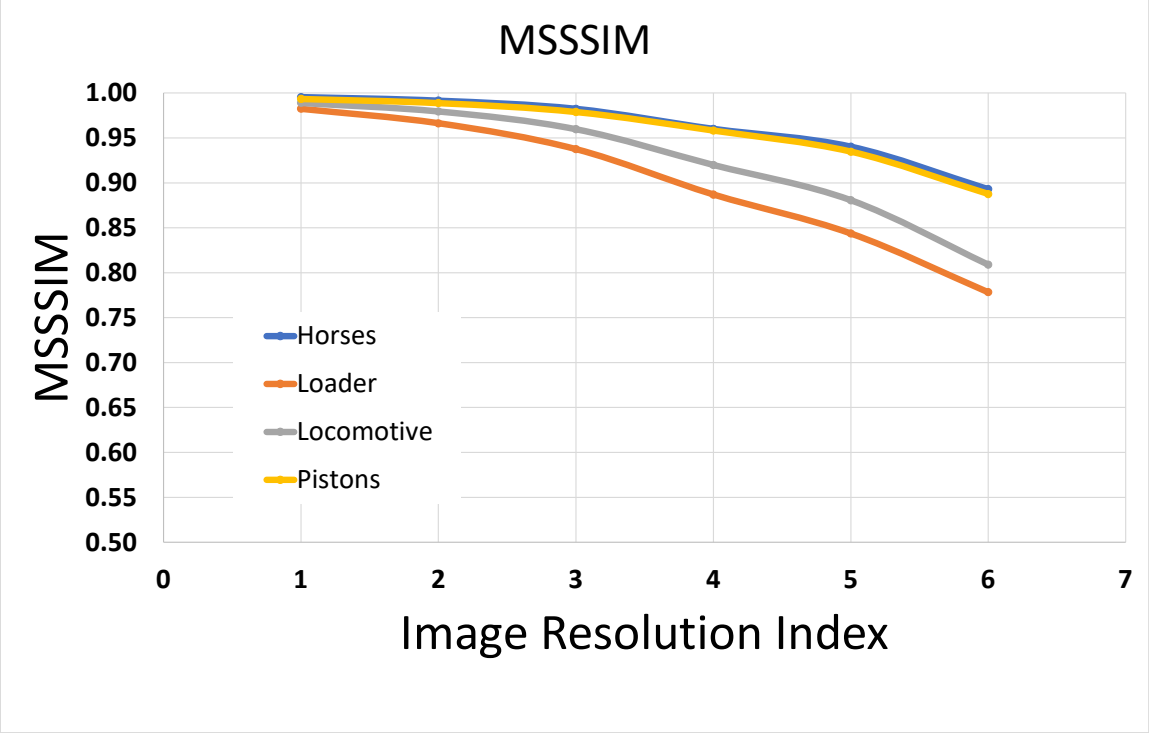

Figure 5.12: MSSSIM Image quality metrics

and the total length of stalling L is fixed, then the length of each stall is $\frac{L}{N}$. Thus the stalling frequency is inversely proportional to the total number of stalls N, and the cumulative QoE drop over the video viewing period can be written as [34]:

$$G(N) = C(T_1 - T_0)\left\{N \exp\left[-\left(\frac{\mathrm{L}}{\mathrm{NT_0}}\right)\right]\right\} - CL \tag{5.7}$$

for $N \geq 1, T_0 > 0, T_1 > 0, L > 0$

If overall QoE is represented by Q, with the constant quality setting, $P_n = P, \forall n \in [0, T]$ to $P, \forall n \in [0, T + NT_s]$, then the overall stalling experience will be [34]:

$$NS^k\left(T_s\right), \forall k \in [1, N] \tag{5.8}$$

and the overall QoE can be represented using a Subjective Quality Index (SQI) Q as [34]:

$$Q = \frac{\left(T + NT_s\right)P + NS_k(T_s)}{T + NT_s} \tag{5.9}$$

This SQI representation Q is plotted in Figure 5.4, using the absolute category rating (ACR) scale, to give the subjective quality index (SQI).The drop in QoE represents the annoyance experienced by the subscriber when the video stalls.

5.5.1 Overall QoE

For each time unit, the overall QoE can be represented as the combination of QoE effects due to: 1) Image quality degradation P_n, and 2) QoE drop due to annoyance effect of video stalling, S_n. To determine the stalling QoE degradation:

$$Q_n = P_n + S_n \tag{5.10}$$

where Q_n represents the QoE at the nth time interval, as a combination of the static image quality P_n and the annoyance effect of video stalling S_n

5.5.2 Proposed Indexed Image Quality Metric compared to state-of-the-art Metrics

The proposed Indexed Image Quality uses sequential numbers to represent the image quality, which gives a consistent quality evaluation. The functionality of this index depends on the assumption that the image is transported over a reliable protocol, thus for every index, the image is a scaled down version of the source, without any image artifacts, such as error blocks. With state-of-the-art image quality estimation methods, images can be compared even when the images have artifacts.

To determine SQI using state-of-the-art methods, a reference image f is compared with a test image g. The dimensions of this test image are $M \times N$. The SQI methods include:

5.5.2.1 Structural Similarity (SSIM)

SSIM is determined as the product of three component metrics: luminance l, contrast c, and structure s.

$$SSIM(f,g) = l(f,g)c(f,g)s(f,g) \tag{5.11}$$

where:

$$\begin{cases} l(f,g) = \frac{2\mu_f\mu_g+C_1}{\mu_f^2+\mu_g^2+C_1} \\ c(f,g) = \frac{2\sigma_f\sigma_g+C_2}{\sigma_f^2+\sigma_g^2+C_2} \\ s(f,g) = \frac{\sigma_{fg}+C_3}{\sigma_f\sigma_g+C_3} \end{cases} \tag{5.12}$$

and μ_f and μ_g are the mean luminance of f and g, σ_f and σ_g are the standard deviations of f and g, C_1, C_2 and C_3 are constants to avoid a zero denominator. The range of values for SSIM are [0,1].

5.5.2.2 Multiscale Structural Similarity (MSSIM)

MSSIM iteratively applies the SSIM method to multiple down samples of the reference image. D iterations of the scaling operation are performed.

$$\text{MSSIM}(\mathbf{x}, \mathbf{y}) = [l_m(\mathbf{x}, \mathbf{y})]^{\alpha D} \cdot \prod_{j=1}^{D} [\text{c}_j(\mathbf{x}, \mathbf{y})]^{\beta_j} [s_j(\mathbf{x}, \mathbf{y})]^{\gamma_j} \tag{5.13}$$

where the exponents α_D, β_j and γ_j are used to control the relative importance of different components.

5.5.2.3 Peak Signal to Noise Ratio (PSNR)

$$PSNR(f, g) = 10 \log_{10} \left(\frac{255^2}{MSE(f, g)} \right) \tag{5.14}$$

PSNR as defined can attain unbounded numerical values when the mean square error (MSE) tends to zero.

5.5.2.4 Mean Squared Error (MSE)

$$MSE(f, g) = \frac{1}{MN} \sum_{i=1}^{M} \sum_{j=1}^{N} (f_{ij} - g_{ij})^2 \tag{5.15}$$

Where $f_{ij} - g_{ij}$ is the difference error in luminance between pixels in the same position coordinates on the reference and test image.

5.5.3 Mapping State-of-the art Image Quality Metrics to Indexed Quality Metric

These state-of-the-art image quality metrics were calculated for the images in Figures 5.5-5.8. The results are shown in Tables 5.2-5.3 and Figures 5.10 to 5.12. Considering two different images of scaled resolution, such as the Horses in Figure 5.5, to Figure 5.8, the state-of-the-art image quality methods described in this section can give different values. Comparing system performance with existing studies will require a mapping of the indexed (Subjective Quality Index) SQI to a state-of-the-art metric. For example, the index values 1...6 were mapped to the SSIM values for "Horses" in Table 5.2. Using a quadratic polynomial curve fit, we obtain:

$$f(x) = -0.005893x^2 + 0.08068x + 0.707 \tag{5.16}$$

where x is the index quality metric, and f is the SSIM.

Video consumption can also be classified into one of two categories: (1) Realtime, and (2) Non-Realtime. Realtime video delivery is required for applications such as video conferencing, and Non-Realtime video is better suited for streaming media. Realtime video delivery for conferencing is often bidirectional. A key difference between these two categories is the size of the buffer at the receiver. Conferencing applications should have buffers which are less than 1 second. However, streaming applications typically have buffers of the order of 10 seconds or more depending on the streaming client application, available buffer size, and service provider policy.

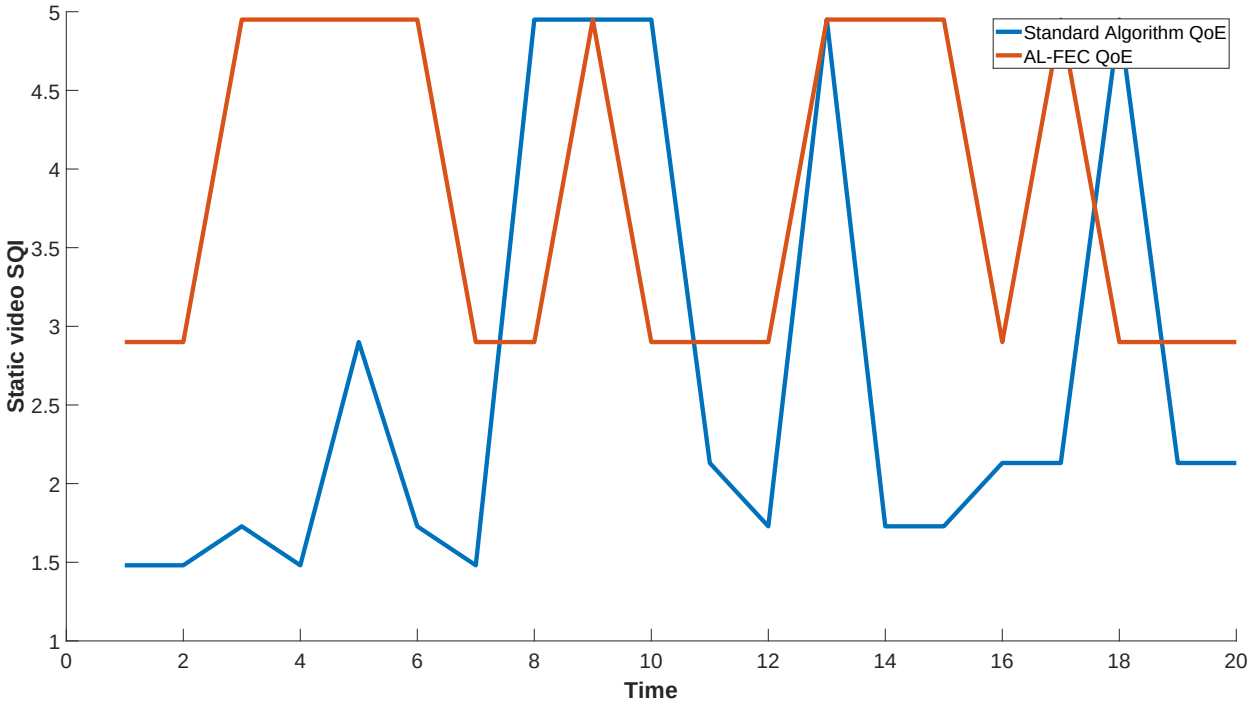

Figure 5.13: Simulated Instantaneous QoE measure

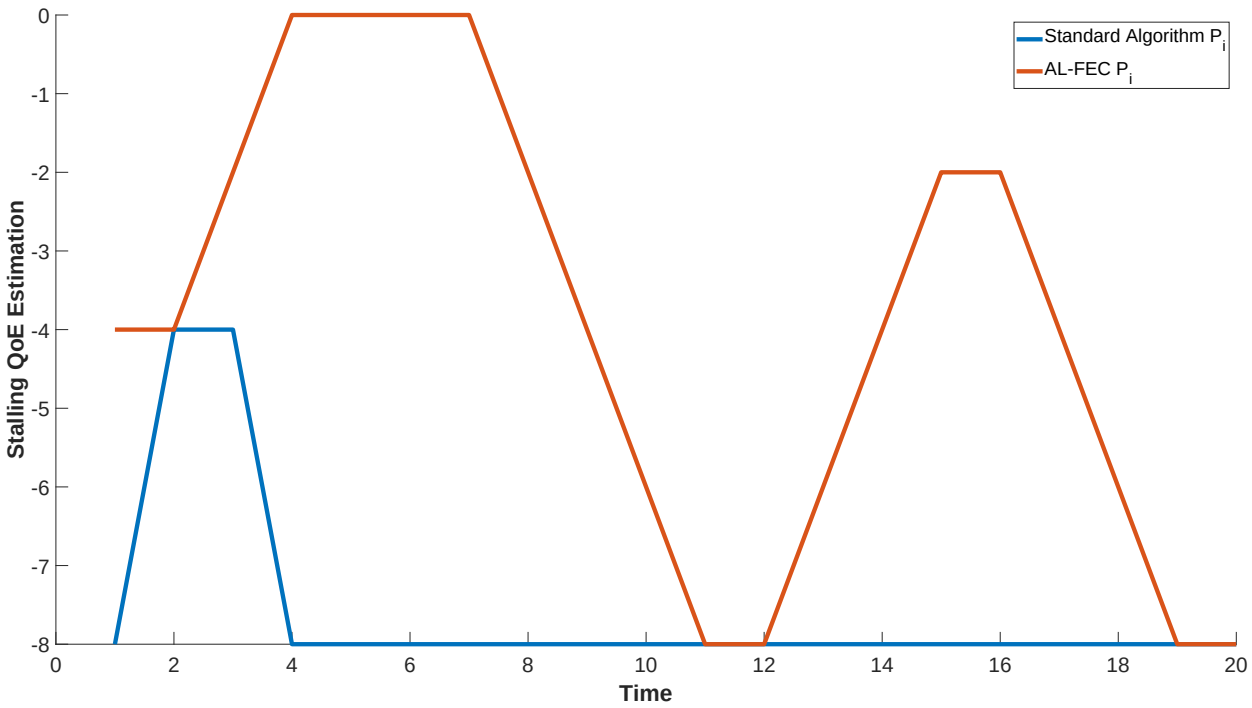

Figure 5.14: Simulated QoE drop measure

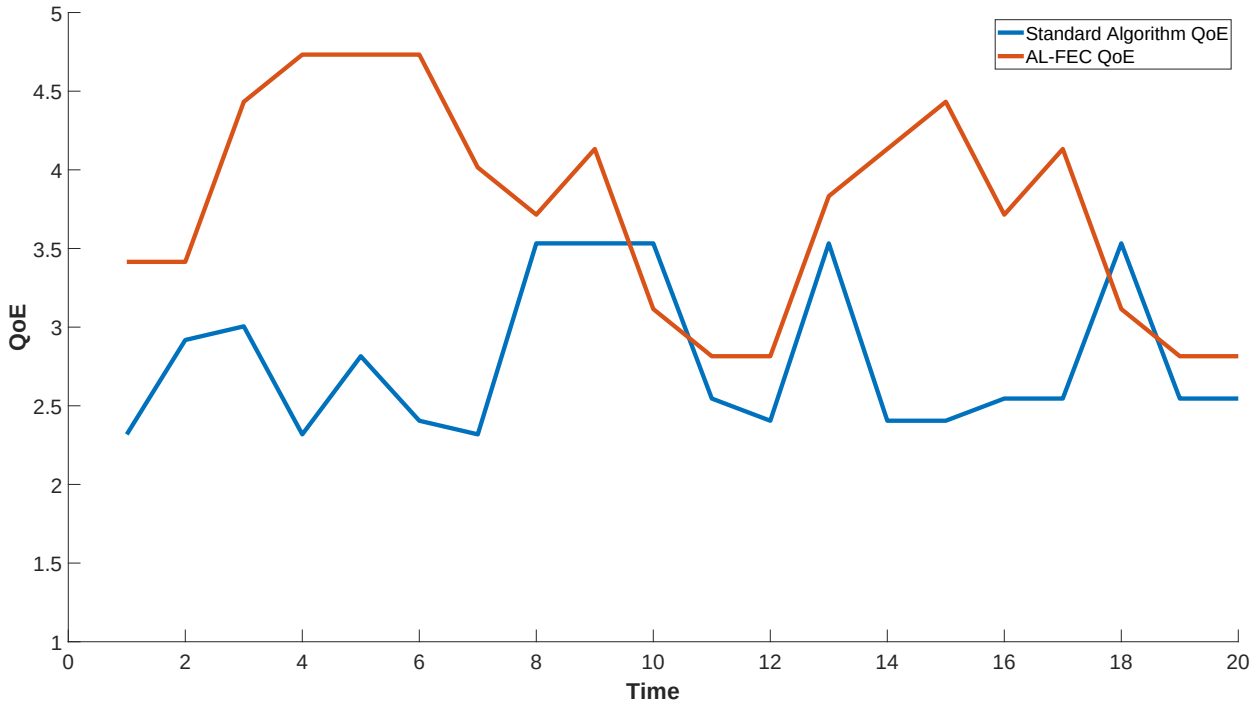

Figure 5.15: Simulated Composite QoE measure which includes the static SQI drop due to video quality degradation, and annoyance effects due to video stalling

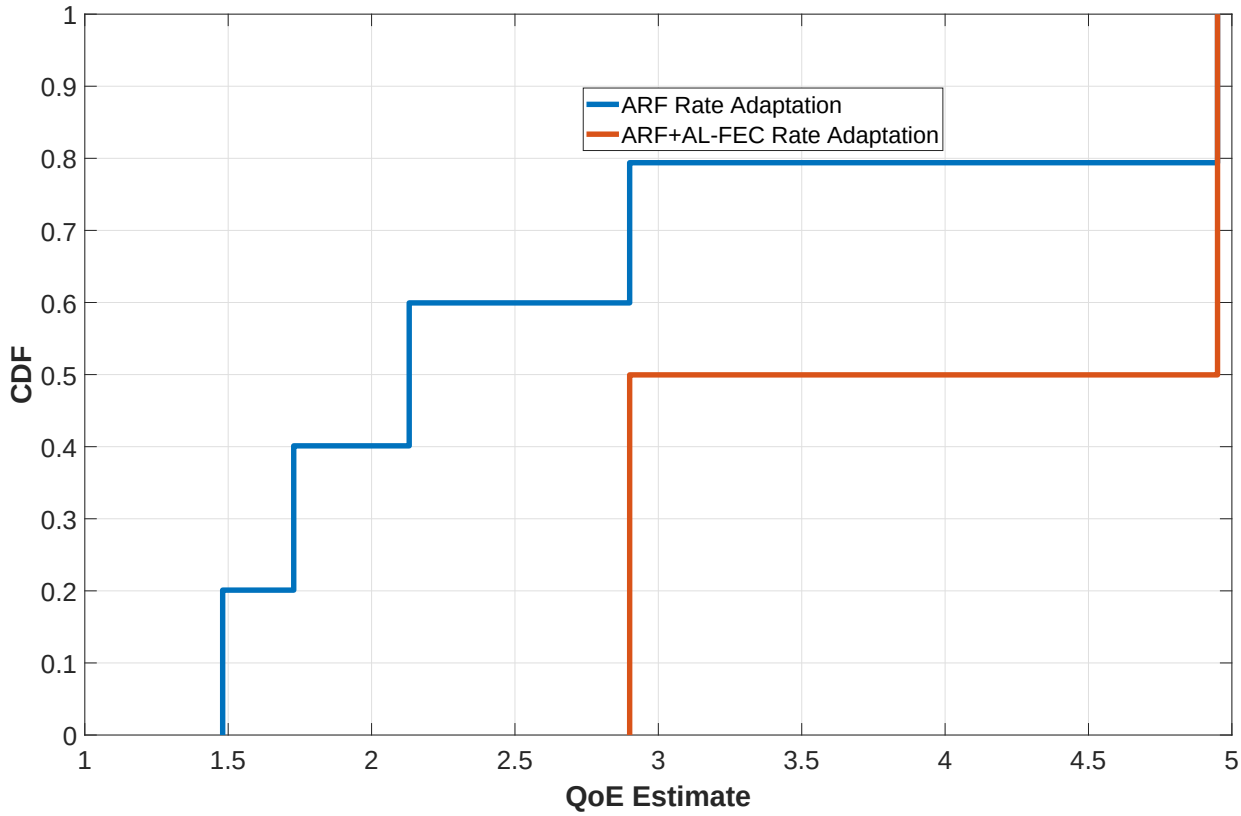

Figure 5.16: Simulated End-to-End QoE CDF

5.6 End-to-End QoE simulation Results

The stalling video QoE change for a client was simulated, with the results shown in Figure 5.13.

The WiFi parameters for the simulation are shown in Table 4.3.

The rate adaptation process was tracked, and the corresponding data rate which was used, enabled the video play out buffers to remain full for a longer period. Simulated effects of frame quality P_i drop are shown in Figure 5.14, and the overall combined QoE is shown in Figure 5.15. Figure 5.15 shows that the AL-FEC enabled rate adaptation will provide, with a high degree of probability, a better delivered QoE. In a few instances, the AL-FEC system over-estimates the higher MCS, which will result in the AL-FEC decoder to fail, thus momentarily reducing the delivered QoE to that lower than that of the standard rate adaptation system.

Running the simulation over 1000 instances produced the empirical cumulative distribution function (CDF) shown in Figure 5.16. The empirical CDF shows that under the same average channel conditions, 50% of the time, the QoE for clients will be close to a SQI of 3 for AL-FEC enabled clients, while it will vary between 2.0 and 2.5 for standard rate adaption clients. This shows that AL-FEC enabled clients are able to deliver a better QoE, due to the better efficient use of the air interface, leading to an effective increased throughput.

5.7 Summary

In this chapter we have determined the performance of video delivery over a WiFi system, which utilizes cross layer knowledge of the wireless channel. The wireless channel information comes from the link layer rate adaptation values, and the current BER on the PHY layer. These wireless channel information is used to guide the behavior of the AL-FEC rate adaptation algorithm.

A SQI metric Q is proposed, which quantifies the improved QoE. The improved QoE is based on the reduced probability of packet failure, and higher throughput MCS selection using the joint AL-FEC and MCS selection algorithm. It has been shown that QoE gains can be achieved by using AL-FEC with application layer control of the link layer MCS.

Chapter 6

Conclusion

6.1 Major Research Findings

This thesis has addressed multiple areas with the common goal to improve the video quality of experience by users, who are consuming video services. Using Forward Error Correction at the application layer (AL-FEC), interacting with cross layer rate adaptation for reliable delivery of video packets, it has been shown that measurable improvements can be achieved depending on channel conditions. The research findings are in the following categories:

6.1.1 AL-FEC video packet delivery

Protecting video packets over WiFi using FEC was investigated in Chapter 3. Reed-Solomon codes in $GF(2^{16})$ are applied to an existing WiFi superchannel, creating a concatenated FEC system. An interleaver is also introduced in order to achieve improvements in FEC performance. The performance was evaluated over the IEEE 802.11 Standard MCS combination for a SISO channel. A general purpose processor was used for the AL-FEC error correction, which was able to deliver video packets at low error rates.

6.1.2 AL-FEC Aware Rate Adaptation

It was shown in Chapter 4, that AL-FEC combined with rate adaptation, can enable the selection of a higher throughput MCS for WiFi delivery. Thus extra bandwidth is available for video delivery. The higher error rate with the higher MCS is offset by the AL-FEC error correction. This will reduce the time used to transfer packets to a subscriber, yielding a better air efficiency.

6.1.3 Quality of Experience estimation

This thesis proposes an algorithm for Quality of Experience estimation for streaming video over reliable protocols. The algorithm simplifies the estimation of video quality by assigning QoE weights to each video quality available. This algorithm is suitable for streaming video services with reliable delivery. In such systems, the video is available in multiple resolutions. Resolutions are of increasing size, which requires a corresponding increase in bandwidth. The live streaming application such as Dynamic Streaming Over Hypertext Transport Protocol (DASH), will select different video quality files based on its measured network throughput. The estimation utilizes two main parameters: (1) Video quality and (2) Stall frequency. The video resolution table, with an example shown in Table 5.1 is a priori information for the QoE estimator. And using the additional number of stalls, a QoE estimate can be obtained.

6.2 Thesis Conclusion

In current times, the processing units of mobile devices have increased greatly in capability. At the same time more users are requesting the use of wireless channels. Using the processing capabilities of these devices, a better video QoE can be served to subscribers.

This thesis analyzes the theoretical air efficiency improvements, and validates the resultant QoE improvement through simulations. Chapter 3 outlines the reduction in BER which

is possible when using AL-FEC. With the reduced BER, it is possible to use increased orders of modulation for transmission, which can increase throughput. Chapter 4 investigated the AL-FEC aware rate adaptation algorithm. AL-FEC is used in conjunction with the ARF rate adaptation algorithm. The AL-FEC step-up event frequency is measured using the metric G_{FEC}, which compares the frequency with which the AL-FEC rate adaptation process steps up the MCS compared to the standard rate adaptation process.

Chapter 5 shows the end-to-end system, and illustrates the mechanism by which the AL-FEC rate adaptation process on a device requests a MCS step-up. Also based on a QoE model shown, a QoE improvement from 1.5 to 3 can be achieved during simulations.

6.3 Engineering Significance of Findings and Recommendations

This thesis proposes an alternative approach to improve the air efficiency for WiFi transmission. Using the proposed RPI metric, up to 14% improvement was observed in simulations. Although concatenated code systems have been proposed, they have mostly been for broadcast type of transmissions. A concatenated code system for unicast transmissions will help to recover some of the packets lost due to collisions or noise on the wireless channel. Thus, using the combination of AL-FEC and rate adaptation, air efficiency will be improved. For service providers, the improved air efficiency will enable a better streaming video QoE compared to standard systems. The AL-FEC enabled rate adaptation is an opportunity for video content service providers, who have a control of the network, and can thus enable signaling between the video server and client devices, to improve the subscriber QoE.

6.3.1 WiFi Hybrid ARQ

The current specification for WiFi requires the sender to automatically retransmit when a recipient does not respond, i.e. positive acknowledgment. Thus this thesis suggests a

recommendation to the IEEE 802.11 working groups to include a requirement for passing control to the application layer such that the sender does not automatically re-send unacknowledged packets. To get around this issue in experiments, the broadcast mode was used.

6.3.2 AL-FEC Schemes

Although AL-FEC mechanisms have been proposed, such as FEC-FRAME, further provisions can be added to the IEEE 802.11 specifications for AL-FEC, and the performance of different FEC codes need to be investigated. Two FEC codes were candidates for the application layer in this study - (1) Low Density Parity Check (LDPC), and (2) Reed-Solomon codes. LDPC was not suitable for use because of the error-floor phenomenon. Also, newer Reed-Solomon decoding algorithms are available, such as list-decoding. Investigating these other codes require further work.

6.4 Thesis limitations and Future Directions

This thesis has presented a method to improve streaming video QoE for subscribers, using WiFi. Simulated performance shows approximately a QoE improvement of 1 unit on the MOS scale, compared to a standard WiFi implementation. The improvement is based on increased air efficiency, due higher MCS selections. Using the proposed Rate Analysis Performance Index (RPI), it has been shown that AL-FEC enabled transmissions have a higher probability of selecting higher MCS. For example with 5 simulated clients, there is a 6% increase in the RPI. This increase in RPI enables QoE to be approximately 3 for ARF+AL-FEC enabled clients, while staying between 2 and 2.5 for standard ARF clients. The limitations which can be addressed in the future include:

1. **Improved support for AL-FEC operation by the IEEE802.11 protocol**: Currently the link layer FEC discards packets that fail CRC as shown in Figure 4.5. These

packets have a valid signal, and possibly the SERVICE field, and VHT-SIG-B have been decoded correctly, thus they are good candidates for AL-FEC recovery.

2. **Further study of concatenated FEC scheme for WiFi**: Research on additional FEC schemes to use for the concatenated FEC has the potential to provide further gains in air efficiency. For example, using Polar Codes [118], Raptor Codes [119] or some alternative FEC scheme can be compared to optimize criteria such as power efficiency, which is not considered in this thesis.

Bibliography

[1] Desktop vs Mobile Internet Traffic Share. https://gs.statcounter.com/platform-market-share/desktop-mobile-tablet/worldwide/#monthly-201001-201907. Accessed: 2019-08-14.

[2] Gary J Sullivan, Jens-Rainer Ohm, Woo-Jin Han, and Thomas Wiegand. Overview of the high efficiency video coding (hevc) standard. *IEEE Transactions on circuits and systems for video technology*, 22(12):1649–1668, 2012.

[3] Hari Kalva. The h. 264 video coding standard. *IEEE multimedia*, 13(4):86–90, 2006.

[4] Humberto de Jesus Ochoa Dominguez, Osslan Osiris Vergara Villegas, Vianey Guadalupe Cruz Sanchez, Efren David Gutierrez Casas, and KR Rao. The h. 264 video coding standard. *IEEE Potentials*, 33(2):32–38, 2014.

[5] HTTP Live Streaming Architecture. https://developer.apple.com/documentation/http_live_streaming/understanding_the_http_live_streaming_architecture. Accessed: 2019-08-14.

[6] IEEE Standard for Ethernet. *IEEE Std 802.3-2018 (Revision of IEEE Std 802.3-2015)*, pages 1–5600, Aug 2018.

[7] IEEE Standard for Information technology—Telecommunications and information exchange between systems Local and metropolitan area networks—Specific requirements - Part 11: Wireless LAN Medium Access Control (MAC) and Physical Layer (PHY)

Specifications. *IEEE Std 802.11-2016 (Revision of IEEE Std 802.11-2012)*, pages 1–3534, Dec 2016.

[8] Yan Chen, Yang Hu, Oscar C Au, Houqiang Li, and Chang Wen Chen. Video error concealment using spatio-temporal boundary matching and partial differential equation. *IEEE Transactions on Multimedia*, 10(1):2–15, 2007.

[9] Susanna Aign and Khaled Fazel. Temporal and spatial error concealment techniques for hierarchical MPEG-2 video codec. In *Proceedings IEEE International Conference on Communications ICC'95*, volume 3, pages 1778–1783. IEEE, 1995.

[10] Mounira Ebdelli, Olivier Le Meur, and Christine Guillemot. Video inpainting with short-term windows: application to object removal and error concealment. *IEEE Transactions on Image Processing*, 24(10):3034–3047, 2015.

[11] S. Aign and K. Fazel. Temporal and spatial error concealment techniques for hierarchical MPEG-2 video codec. In *Proceedings IEEE International Conference on Communications ICC '95*, volume 3, pages 1778–1783 vol.3, June 1995.

[12] Shoaib Khan, Yang Peng, Eckehard Steinbach, Marco Sgroi, and Wolfgang Kellerer. Application-driven cross-layer optimization for video streaming over wireless networks. *IEEE communications Magazine*, 44(1):122–130, 2006.

[13] Haiyan Luo, Song Ci, Dalei Wu, Jianjun Wu, and Hui Tang. Quality-driven cross-layer optimized video delivery over LTE. *IEEE Communications Magazine*, 48(2):102–109, 2010.

[14] M Watson et al. Forward Error Correction (FEC) Framework draft-ietf-fecframe-framework-11. 2011.

[15] D. Wu, S. Ci, H. Luo, W. Zhang, and J. Zhang. Cross-layer rate adaptation for video

communications over LTE networks. In *2012 IEEE Global Communications Conference (GLOBECOM)*, pages 4834–4839, Dec 2012.

[16] Y. Wu, S. Kumar, F. Hu, Y. Zhu, and J. D. Matyjas. Cross-layer forward error correction scheme using raptor and rcpc codes for prioritized video transmission over wireless channels. *IEEE Transactions on Circuits and Systems for Video Technology*, 24(6):1047–1060, June 2014.

[17] Z. Chen and D. Wu. Rate-Distortion Optimized Cross-Layer Rate Control in Wireless Video Communication. *IEEE Transactions on Circuits and Systems for Video Technology*, 22(3):352–365, March 2012.

[18] G David Forney Jr. Concatenated codes. research monograph no. 37, 1966.

[19] Ieee standard for information technology– local and metropolitan area networks– specific requirements– part 11: Wireless lan medium access control (mac)and physical layer (phy) specifications amendment 5: Enhancements for higher throughput. *IEEE Std 802.11n-2009 (Amendment to IEEE Std 802.11-2007 as amended by IEEE Std 802.11k-2008, IEEE Std 802.11r-2008, IEEE Std 802.11y-2008, and IEEE Std 802.11w-2009)*, pages 1–565, Oct 2009.

[20] M Salehi and J Proakis. Digital communications. *McGraw-Hill Education*, 31:366, 2007.

[21] Erik Dahlman, Stefan Parkvall, and Johan Skold. *4G: LTE/LTE-advanced for mobile broadband*. Academic press, 2013.

[22] Eng Hwee Ong, J. Kneckt, O. Alanen, Z. Chang, T. Huovinen, and T. Nihtilä. IEEE 802.11ac: Enhancements for very high throughput WLANs. In *2011 IEEE 22nd International Symposium on Personal, Indoor and Mobile Radio Communications*, pages 849–853, Sep. 2011.

[23] Timo Vanhatupa. Wi-fi capacity analysis for 802.11 ac and 802.11 n: Theory & practice.

[24] IEEE Standard for Information technology– Telecommunications and information exchange between systemsLocal and metropolitan area networks– Specific requirements– Part 11: Wireless LAN Medium Access Control (MAC) and Physical Layer (PHY) Specifications–Amendment 4: Enhancements for Very High Throughput for Operation in Bands below 6 GHz. *IEEE Std 802.11ac-2013 (Amendment to IEEE Std 802.11-2012, as amended by IEEE Std 802.11ae-2012, IEEE Std 802.11aa-2012, and IEEE Std 802.11ad-2012)*, pages 1–425, Dec 2013.

[25] Giuseppe Bianchi. IEEE 802.11-saturation throughput analysis. *IEEE communications letters*, 2(12):318–320, 1998.

[26] Giuseppe Bianchi. Performance analysis of the IEEE 802.11 distributed coordination function. *IEEE Journal on selected areas in communications*, 18(3):535–547, 2000.

[27] P. S. Swamy, R. K. Ganti, and K. Jagannathan. Adaptive csma under the sinr model: Fast convergence through local gibbs optimization. In *2015 53rd Annual Allerton Conference on Communication, Control, and Computing (Allerton)*, pages 271–278, Sep. 2015.

[28] Pierre Brémaud. *Markov chains: Gibbs fields, Monte Carlo simulation, and queues*, volume 31. Springer Science & Business Media, 2013.

[29] Sergio D Servetto and Guillermo Barrenechea. Constrained random walks on random graphs: routing algorithms for large scale wireless sensor networks. In *Proceedings of the 1st ACM international workshop on Wireless sensor networks and applications*, pages 12–21. ACM, 2002.

[30] Barry D Hughes. Random walks and random environments. 1996.

[31] C. Lee and D. Y. Eun. On the efficiency-optimal markov chains for distributed networking applications. In *2015 IEEE Conference on Computer Communications (INFOCOM)*, pages 1840–1848, April 2015.

[32] David Applebaum. *Lévy processes and stochastic calculus*. Cambridge university press, 2009.

[33] J. Choi, K. Park, and C. k. Kim. Cross-Layer Analysis of Rate Adaptation, DCF and TCP in Multi-Rate WLANs. In *IEEE INFOCOM 2007 - 26th IEEE International Conference on Computer Communications*, pages 1055–1063, May 2007.

[34] Z. Duanmu, A. Rehman, K. Zeng, and Z. Wang. Quality-of-experience prediction for streaming video. In *2016 IEEE International Conference on Multimedia and Expo (ICME)*, pages 1–6, July 2016.

[35] ITU-TG 1080. G. 1080: Quality of Experience Requirements for IPTV Services. 2008.

[36] R ITU. Recommendation BT. 500-11. *methodology for the subjective assesment of the quality of televission pictures, tech. rep., International telecommunication union, Geneva, Switzerland*, 2002.

[37] Introducing Consistent Quality - measuring more than just speed. `https://www.tutela.com/blog/introducing-consistent-quality-measuring-more-than-speed`. Accessed: 2019-11-17.

[38] Scott Stemberger Michael Sherman, Maikel Wilms. Uncovering Real Mobile Data Usage and the Drivers of Customer Satisfaction. `https://www.bcg.com/publications/2015/telecommunications-customer-insight-uncovering-real-mobile-data-usage-drivers-custo aspx`. Accessed: 2019-11-17.

[39] H Series. Audiovisual and Multimedia Systems; Infrastructure of audiovisual services—Coding of moving video. H. 264. Advanced video coding for generic audiovisual services. *International Telecommunication Union. Version*, 12, 2007.

[40] Ricky KP Mok, Edmond WW Chan, and Rocky KC Chang. Measuring the quality of experience of HTTP video streaming. In *Integrated Network Management*, pages 485–492, 2011.

[41] Shu Lin and Daniel J Costello. *Error control coding*. Pearson Education Inc, 2001.

[42] Xiaomin Chen. *Coding in 802.11 WLANs*. PhD thesis, National University of Ireland Maynooth, 2012.

[43] Christian R Berger, Shengli Zhou, Yonggang Wen, Peter Willett, and Krishna Pattipati. Optimizing joint erasure-and error-correction coding for wireless packet transmissions. *IEEE Transactions on Wireless Communications*, 7(11):4586–4595, 2008.

[44] I. Sodagar. The MPEG-DASH Standard for Multimedia Streaming Over the Internet. *IEEE MultiMedia*, 18(4):62–67, April 2011.

[45] A. Eslami and H. Pishro-Nik. On finite-length performance of polar codes: Stopping sets, error floor, and concatenated design. *IEEE Transactions on Communications*, 61(3):919–929, March 2013.

[46] X. Zhang and S. Chen. A two-stage decoding algorithm to lower the error-floors for ldpc codes. *IEEE Communications Letters*, 19(4):517–520, April 2015.

[47] Robert J McEliece. The guruswami-sudan decoding algorithm for reed-solomon codes. *IPN progress report*, 42(153), 2003.

[48] TA Gulliver, M Jorgenson, and WK Moreland. Performance of reed-solomon codes with dependent symbol errors. *IEE Proceedings-Communications*, 143(3):117–121, 1996.

[49] J. Camp and E. Knightly. Modulation rate adaptation in urban and vehicular environments: Cross-layer implementation and experimental evaluation. *IEEE/ACM Transactions on Networking*, 18(6):1949–1962, Dec 2010.

[50] Mythili Vutukuru, Hari Balakrishnan, and Kyle Jamieson. Cross-layer wireless bit rate adaptation. *SIGCOMM Comput. Commun. Rev.*, 39(4):3–14, August 2009.

[51] Starsky H. Y. Wong, Hao Yang, Songwu Lu, and Vaduvur Bharghavan. Robust rate adaptation for 802.11 wireless networks. In *Proceedings of the 12th Annual International Conference on Mobile Computing and Networking*, MobiCom '06, pages 146–157, New York, NY, USA, 2006. ACM.

[52] A. Kamerman and L. Monteban. WaveLAN®-II: A high-performance wireless LAN for the unlicensed band. *Bell Labs Technical Journal*, 2(3):118–133, Summer 1997.

[53] Daji Qiao, Sunghyun Choi, Amit Jain, and Kang G Shin. MiSer: an optimal low-energy transmission strategy for IEEE 802.11 a/h. In *Proceedings of the 9th annual international conference on Mobile computing and networking*, pages 161–175. ACM, 2003.

[54] Robert T Morris and John C Bicket. Bit-rate selection in wireless networks. In *Master's thesis, MIT*. Citeseer, 2005.

[55] Thomas Huehn and Cigdem Sengul. Practical power and rate control for wifi. In *2012 21st International Conference on Computer Communications and Networks (ICCCN)*, pages 1–7. IEEE, 2012.

[56] C. Bouras, N. Kanakis, V. Kokkinos, and A. Papazois. Al-fec for streaming services over lte systems. In *2011 The 14th International Symposium on Wireless Personal Multimedia Communications (WPMC)*, pages 1–5, Oct 2011.

[57] Amin Shokrollahi. Raptor codes. *IEEE/ACM Trans. Netw.*, 14(SI):2551–2567, June 2006.

[58] J. Wu, C. Yuen, N. Cheung, J. Chen, and C. W. Chen. Streaming mobile cloud gaming video over tcp with adaptive source–fec coding. *IEEE Transactions on Circuits and Systems for Video Technology*, 27(1):32–48, Jan 2017.

[59] S. Fan and H. Zhao. Delay-based cross-layer QoS scheme for video streaming in wireless ad hoc networks. *China Communications*, 15(9):215–234, Sep. 2018.

[60] S. Ullah, K. Thar, M. G. R. Alam, Jae Hyeok Son, Jin Won Lee, and C. S. Hong. Delivering scalable video streaming in icn enabled long term evolution networks. In *2016 18th Asia-Pacific Network Operations and Management Symposium (APNOMS)*, pages 1–4, Oct 2016.

[61] Srisakul Thakolsri, Wolfgang Kellerer, and Eckehard Steinbach. QoE-based cross-layer optimization of wireless video with unperceivable temporal video quality fluctuation. In *2011 IEEE international conference on communications (ICC)*, pages 1–6. IEEE, 2011.

[62] Mohammed Shehada, Srisakul Thakolsri, Zoran Despotovic, and Wolfgang Kellerer. QoE-based cross-layer optimization for video delivery in long term evolution mobile networks. In *2011 The 14th International Symposium on Wireless Personal Multimedia Communications (WPMC)*, pages 1–5. IEEE, 2011.

[63] Srisakul Thakolsri, Shoaib Khan, Eckehard G Steinbach, and Wolfgang Kellerer. QoE-Driven Cross-Layer Optimization for High Speed Downlink Packet Access. *JCM*, 4(9):669–680, 2009.

[64] Rakesh Radhakrishnan and Amiya Nayak. Cross layer design for efficient video streaming over LTE using scalable video coding. In *2012 IEEE international conference on communications (ICC)*, pages 6509–6513. IEEE, 2012.

[65] Z. Wang, E. P. Simoncelli, and A. C. Bovik. Multiscale structural similarity for image quality assessment. In *The Thrity-Seventh Asilomar Conference on Signals, Systems Computers, 2003*, volume 2, pages 1398–1402 Vol.2, Nov 2003.

[66] A. M. Eskicioglu and P. S. Fisher. Image quality measures and their performance. *IEEE Transactions on Communications*, 43(12):2959–2965, Dec 1995.

[67] Zhou Wang and A. C. Bovik. A universal image quality index. *IEEE Signal Processing Letters*, 9(3):81–84, March 2002.

[68] H. Zimmermann. Osi reference model - the iso model of architecture for open systems interconnection. *IEEE Transactions on Communications*, 28(4):425–432, April 1980.

[69] John M. Cioffi. John M Coiffi Book.

[70] Irving S Reed and Gustave Solomon. Polynomial codes over certain finite fields. *Journal of the society for industrial and applied mathematics*, 8(2):300–304, 1960.

[71] Stephen B Wicker and Vijay K Bhargava. *Reed-Solomon codes and their applications*. John Wiley & Sons, 1999.

[72] D. Torrieri. Information-bit, information-symbol, and decoded-symbol error rates for linear block codes. *IEEE Transactions on Communications*, 36(5):613–617, May 1988.

[73] Stephen B Wicker. Reed-solomon error control coding for rayleigh fading channels with feedback. *IEEE transactions on Vehicular Technology*, 41(2):124–133, 1992.

[74] William Wesley Peterson and Edward J Weldon. *Error-correcting codes*. MIT press, 1972.

[75] James Massey. Shift-register synthesis and bch decoding. *IEEE transactions on Information Theory*, 15(1):122–127, 1969.

[76] Lloyd R Welch and Elwyn R Berlekamp. Error correction for algebraic block codes, December 30 1986. US Patent 4,633,470.

[77] Venkatesan Guruswami and Madhu Sudan. Improved decoding of reed-solomon and algebraic-geometric codes. In *Proceedings 39th Annual Symposium on Foundations of Computer Science (Cat. No. 98CB36280)*, pages 28–37. IEEE, 1998.

[78] Richard E Blahut. *Algebraic codes for data transmission*. Cambridge university press, 2003.

[79] J. Ramsey. Realization of optimum interleavers. *IEEE Transactions on Information Theory*, 16(3):338–345, May 1970.

[80] Matthew S Gast. *802.11 ac: A survival guide*. " O'Reilly Media, Inc.", 2013.

[81] Shu Lin and Daniel J Costello. *Error control coding*. Pearson Education India, 2004.

[82] Sébastien Simoens, Stéphanie Rouquette-Léveil, Philippe Sartori, Yufei Blankenship, and Brian Classon. Error prediction for adaptive modulation and coding in multiple-antenna ofdm systems. *Signal Processing*, 86(8):1911–1919, 2006.

[83] Yufei W Blankenship, Philippe J Sartori, Brian K Classon, Vip Desai, and Kevin L Baum. Link error prediction methods for multicarrier systems. In *Vehicular Technology Conference, 2004. VTC2004-Fall. 2004 IEEE 60th*, volume 6, pages 4175–4179. IEEE, 2004.

[84] Ericsson. System-level evaluation of ofdm — further considerations. *Technical Report, 3GPP, TSG-RAN WG1*, 2003.

[85] IEEE Standard for Information Technology - Telecommunications and Information Exchange Between Systems - Local and Metropolitan Area Networks - Specific Requirements - Part 11: Wireless LAN Medium Access Control (MAC) and Physical

Layer (PHY) Specifications. *IEEE Std 802.11-2007 (Revision of IEEE Std 802.11-1999)*, pages 1–1076, June 2007.

[86] Reed Solomon Coding. `https://www.vocal.com/wp-content/uploads/2012/05/Reed_Solomon_Implementation.pdf`. Accessed: 2019-11-15.

[87] V Erceg, L Schumacher, P Kyritsi, A Molisch, and DS Baum. Ayg et al.,". *TGn channel models," IEEE*, pages 802–11.

[88] I. Osunkunle. Improving 802.11 video transport air efficiency with al-fec. In *2017 IEEE International Conference on Wireless for Space and Extreme Environments (WiSEE)*, pages 31–36, Oct 2017.

[89] B Adamson, C Bormann, M Handley, and J Macker. Negative-acknowledgment (NACK)-oriented reliable multicast (NORM) protocol. *Internet Society Request for Comments RFC*, 3940, 2004.

[90] Jana Iyengar and Martin Thomson. Quic: A udp-based multiplexed and secure transport. *draft-ietf-quic-transport-01 (work in progress)*, 2017.

[91] Sangtae Ha, Injong Rhee, and Lisong Xu. CUBIC: a new TCP-friendly high-speed TCP variant. *ACM SIGOPS operating systems review*, 42(5):64–74, 2008.

[92] L. Baldantoni, H. Lundqvist, and G. Karlsson. Adaptive end-to-end fec for improving tcp performance over wireless links. In *2004 IEEE International Conference on Communications (IEEE Cat. No.04CH37577)*, volume 7, pages 4023–4027 Vol.7, June 2004.

[93] H. Lundqvist and G. Karlsson. Tcp with end-to-end fec. In *International Zurich Seminar on Communications, 2004*, pages 152–155, Feb 2004.

[94] Mark Allman, Vern Paxson, Wright Stevens, et al. Tcp congestion control. 1999.

[95] Matthew Mathis, Jeffrey Semke, Jamshid Mahdavi, and Teunis Ott. The macroscopic behavior of the tcp congestion avoidance algorithm. *ACM SIGCOMM Computer Communication Review*, 27(3):67–82, 1997.

[96] Chadi Barakat and Eitan Altman. Bandwidth tradeoff between TCP and link-level FEC. *Computer networks*, 39(2):133–150, 2002.

[97] MinJi Kim, Muriel Médard, and João Barros. Modeling network coded tcp throughput: A simple model and its validation. *arXiv preprint arXiv:1008.0420*, 2010.

[98] Jitendra Padhye, Victor Firoiu, Don Towsley, and Jim Kurose. Modeling TCP throughput: A simple model and its empirical validation. In *Proceedings of the ACM SIGCOMM'98 conference on Applications, technologies, architectures, and protocols for computer communication*, pages 303–314, 1998.

[99] Luca Baldantoni, Henrik Lundqvist, and Gunnar Karlsson. Adaptive end-to-end FEC for improving TCP performance over wireless links. In *2004 IEEE International Conference on Communications (IEEE Cat. No. 04CH37577)*, volume 7, pages 4023–4027. IEEE, 2004.

[100] Chung-Hsing Hsu and Ulrich Kremer. IPERF: A framework for automatic construction of performance prediction models. In *Workshop on Profile and Feedback-Directed Compilation (PFDC), Paris, France*. Citeseer, 1998.

[101] I. Tinnirello, G. Bianchi, and Y. Xiao. Refinements on ieee 802.11 distributed coordination function modeling approaches. *IEEE Transactions on Vehicular Technology*, 59(3):1055–1067, March 2010.

[102] Vladimir Vishnevsky and Andrey Lyakhov. Lans: Saturation throughput in the presence of noise. In *Proceedings of the Second International IFIP-TC6 Networking Conference on Networking Technologies, Services, and Protocols*, pages 1008–1019, 1.

[103] H. Chen. Revisit of the markov model of ieee 802.11 dcf for an error-prone channel. *IEEE Communications Letters*, 15(12):1278–1280, December 2011.

[104] I. Osunkunle. AL-FEC Wireless Rate Adaptation for WiFi Multicast. In *2018 IEEE Canadian Conference on Electrical Computer Engineering (CCECE)*, pages 1–5, May 2018.

[105] Xi Yong, Wei Ji-Bo, and Zhuang Zhao-Wen. Throughput analysis of IEEE 802.11 DCF over correlated fading channel in MANET. In *Proceedings. 2005 International Conference on Wireless Communications, Networking and Mobile Computing, 2005.*, volume 2, pages 694–697. IEEE, 2005.

[106] JS DaSilva. Optimal packet length for fading land mobile data channels. In *ICC'80*, pages 61–3, 1980.

[107] William C Jakes and Donald C Cox. *Microwave mobile communications*. Wiley-IEEE Press, 1994.

[108] Leonard Kleinrock. Queueing systems. volume i: theory. 1975.

[109] Nasa free image library. `images-assets.nasa.gov/image/KSC-20190225-PH_SPX01_0001/KSC-20190225-PH_SPX01_0001~orig.jpg`. Accessed: 2020-04-15.

[110] Zhou Wang, A. C. Bovik, H. R. Sheikh, and E. P. Simoncelli. Image quality assessment: from error visibility to structural similarity. *IEEE Transactions on Image Processing*, 13(4):600–612, April 2004.

[111] Jaap M. J. Murre and Joeri Dros. Replication and analysis of ebbinghaus' forgetting curve. *PLOS ONE*, 10(7):1–23, 07 2015.

[112] Zhengfang Duanmu, Kai Zeng, Kede Ma, Abdul Rehman, and Zhou Wang. A quality-of-experience index for streaming video. *IEEE Journal of Selected Topics in Signal Processing*, 11(1):154–166, 2016.

[113] Pedro Casas, Raimund Schatz, Florian Wamser, Michael Seufert, and Ralf Irmer. Exploring qoe in cellular networks: How much bandwidth do you need for popular smartphone apps? In *Proceedings of the 5th Workshop on All Things Cellular: Operations, Applications and Challenges*, pages 13–18. ACM, 2015.

[114] Pexels free image library. `https://www.pexels.com/photo/two-horses-2216086/`. Accessed: 2020-04-15.

[115] Pexels free image library. `https://www.pexels.com/photo/sky-vehicle-technology-power-129544/`. Accessed: 2020-04-15.

[116] Pexels free image library. `https://www.pexels.com/photo/locomotive-engine-258347/`. Accessed: 2020-04-15.

[117] Pexels free image library. `https://www.pexels.com/photo/equipment-machine-machinery-metal-190539/`. Accessed: 2020-04-15.

[118] Erdal Arikan. Channel polarization: A method for constructing capacity-achieving codes for symmetric binary-input memoryless channels. *CoRR*, abs/0807.3917, 2008.

[119] Michael Luby, Mark Watson, Tiago Gasiba, Thomas Stockhammer, and Wen Xu. Raptor codes for reliable download delivery in wireless broadcast systems. In *CCNC 2006. 2006 3rd IEEE Consumer Communications and Networking Conference, 2006.*, volume 1, pages 192–197. IEEE, 2006.